Epigenetic transcriptional regulation in Friedreich's Ataxia

Sathiji Nageshwaran

Ph.D. Thesis

Imperial College London

2017

Abstract

The Frataxin gene is pathologically partially silenced causing the neurodegenerative disorder, Friedreich's Ataxia (FRDA). The occurrence of the GAA trinucleotide expansion within intron 1 has been shown to invoke several epigenetic mechanisms associated with gene silencing. In this thesis I have investigated the effect on the pathological silencing of frataxin through alteration of potential key regulators of gene expression.

The occurrence of stochastic silencing of eye colour within the Drosophila eye following translocation of the *white* gene, which encodes eye colour, near a region of silent chromatin (heterochromatin) led to the description of position effect variegation (PEV). The ability to induce PEV of transgene expression in a mammalian system through the addition of GAA repeats to the 3' end of the transgene was the first insight that PEV may be implicated in frataxin gene silencing. Furthermore, several regulators of PEV were identified in Drosophila screens. With the potential dynamic silencing mechanisms implicated in FRDA and the occurrence of PEV modifiers, I have assessed the effect in mammalian systems of altering the dosage of these modifiers using mouse transgenic models and human cell lines. These experiments have underlined the multifactorial and combinatorial nature of frataxin gene silencing, suggesting that the ability to concomitantly address several layers of silencing may be required to result in significant de-repression. Knockdown or knockout of the archetypal modifiers of PEV, SUV39H1, SUV39H2 (histone methyltransferases) as well as the polycomb silencing factor BMI1 did not significantly alter frataxin expression in vitro or in vivo.

The histone deacetylase, nicotinamide has been shown to upregulate frataxin expression in FRDA. As yet the specific target of nicotinamide is not known.

Knockdown of one potential target of nicotinamide, the histone deacetylase SIRT1, did not alter frataxin expression. Recent discovery of a group of proteins that modify human PEV (the HUSH complex and histone methyltransferase, SETDB1) provided further potential targets for assessment as FRDA modifiers. Knockdown of the relatively recently identified histone lysine methyltransferase, SETDB1, did show a trend towards frataxin upregulation in both stable and transient knockdowns.

Given the genome-wide effects of the knockout and knockdown methodologies, CRISPR based genome engineering technology was utilised to attempt to directly edit the frataxin epigenome with locus-specific targeting of transcriptional activators (dCas9-VPR), the histone acetyltransferase (dCas9-p300) and dominant-negative histone tail peptides (dCas9-H3KM). Downstream of the GAA repeat dCas9-VPR resulted in a trend towards upregulation. dCas9-p300 targeting the upstream region of the GAA resulted in a trend towards upregulation in both disease and control lines. Transient overexpression of H3.3 and H3K27M upregulated frataxin expression.

I will carry this work forward to further establish the effect of several targeted epigenome modifiers at the frataxin locus during my postdoctoral fellowship.

Ethics
Ethical approval for animal experiments was provided by the UK Home Office.

Clinical kinematic studies were undertaken within ‘Effect of Nicotinamide in Friedreich's Ataxia’ study (Clintrials.gov identifier NCT01589809).

Epigenetic transcriptional regulation in Friedreich's Ataxia

Sathiji Nageshwaran

MBBS (University College London)
BSc (Hons) (University College London)
MRCP

A thesis submitted in partial fulfilment of the requirement for the Degree of Doctor of Philosophy at Imperial College London

July 2017

Supervised by
Prof. Richard Festenstein

Declaration

I declare that this thesis represents my own work, except where due acknowledgement is made, and that it has not been previously included in a thesis, dissertation or report submitted to this University or to any other institution for a degree, diploma or other qualifications.

Signed ……..

List of publications

Transcriptional Activation of Pericentromeric Satellite Repeats and Disruption of Centromeric Clustering upon Proteasome Inhibition. Natisvili T, Yandim C, Silva R, Emanuelli G, Krueger F, **Nageshwaran S**, et al. (2016) PLoS ONE 11(11): e0165873. http://journals.plos.org/plosone/article?id=10.1371/journal.pone.0165873

Epigenetics and triplet repeat neurological diseases. **S Nageshwaran**, R Festenstein. Front. Neurol., 21 December 2015 | http://dx.doi.org/10.3389/fneur.2015.00262

Kinematic body sensor networks and behaviourmetrics for objective efficacy measurements in neurodegenerative disease drug trials. Gavriel, C, Thomik, A.A.C, Lourencco, P.R., **Nageshwaran, S**. Athanasopoulos, S. Sylaidi, A, Festenstein, R, Faisal, A.A.
http://ieeexplore.ieee.org/stamp/stamp.jsp?tp=&arnumber=7299426

f2MOVE: fMRI-compatible haptic object manipulation system for closed-loop motor control studies. A Sylaidi, P Lourenco, **S Nageshwaran**, C Lin, M Rodriguez, R Festenstein, A Faisal. Neural Engineering (NER), 2015 7th International IEEE/EMBS Conference. 22-24 April 2015. 1104 – 1107. doi: 10.1109/NER.2015.7146821 http://ieeexplore.ieee.org/xpl/articleDetails.jsp?arnumber=7146821

Acknowledgements

"The fool who persists in his folly will become wise." – William Blake.

"This is how the entire course of a life can be changed: by doing nothing."
— Ian McEwan, On Chesil Beach.

"You'll have bad times, but it'll always wake you up to the good stuff you weren't paying attention to." – Sean, Good Will Hunting.

"That rabbit hole goes deep." – A patient I once looked after who shall remain nameless.

I will not say much, but I will say this. Amma and Appa I love you, you are the foundation on which I am built. Niraj and Vaithu, you are my guardians.

To the beautiful souls I came to know within the MRC CSC you showed me through your example what is required of excellent scientists. I owe a great debt of gratitude to all the friends I made, were it not for you I would not be writing this (or anything for that matter).

The 2nd floor peeps - Eleanor (*Jane*), Tim, Kyoko, Holly, Lucy, Leila, Michelle, Bea – thank you for keeping me sane.

Giulia – My treble clef. I cherished every moment with you.

Helen – You were my voice of reason (although I rarely listened).

Cihan – Thank you for your honesty.

Theona – Your ability to see the good and to let go will forever stand you in good stead. (Alfredo – I never met you, but you're a lucky man.)

Raquel – Your intelligence is only matched by your beauty.

Lorenzo – Your intelligence is only matched by Raquel's beauty.

Pui – You are, and will continue to be an excellent scientist.

Suchira – You are my brother. There is no greater compliment I can bestow. You guided me through darkness, showed me resilience and strengthen me with every word.

There should always be flowers on your birthday.
Cu drag,
Sath.

Contents

List of figures

Abbreviations

18S	18S ribosomal RNA
ATF7IP	Activating Transcription Factor 7 Interacting Protein
BAC	Bacterial Artificial Chromosome
BMI1	BMI1 Proto-Oncogene, Polycomb Ring Finger
CD2	CD2 Antigen
Cpf1	Clustered Regularly Interspaced Short Palindromic Repeats from Prevotella and Francisella 1
Cre-lox	Cre-Lox recombination
CRISPR	Clustered Regularly Interspaced Short Palindromic Repeats
CTCF	CCCTC-binding factor
DAPI	4',6-diamidino-2-phenylindole
dCas9	dead CRISPR associated protein 9
DM1	Myotonic Dystrophy type 1
DMPK	dystrophia myotonica protein kinase
DNA	Deoxyribonucleic acid
FAM208A	Family With Sequence Similarity 208 Member A
FAST-1	FXNAntisense Transcript - 1
FRDA	Friedreich's Ataxoa
FXG-GAA-Luc	HEK-293 Disease Line
FXN	Frataxin
FXN-Luc	HEK-293 Control Line
G9a	Euchromatic histone-lysine N-methyltransferase 2
GAPDH	Glyceraldehyde 3-phosphate dehydrogenase
GFP	Green fluorescent protein
gRNA	guide RNA
H3F3A	Histone 3.3A
H3F3B	Histone 3.3B
HAT	Histone Acetyltransferase
HDAC	Histone Deacetylase
HEK-293	Human Embryonic Kidney - 293 cell line
Het	Heterozygote
HKMT	Histone Lysine Methyltransferase
HOX	Homeotic genes
hTERT	Telomerase reverse transcriptase
HUSH	Human Silencing Hub
Inr/DPE	Initiator motif (Inr), and downstream promoter element (DPE),
MPP8	M-Phase Phosphoprotein 8
mRNA	Messenger RNA
MS2	Bacteriophage MS2
n20	20 nucleotide target DNA sequence
NAD+	Nicotinamide adenine dinucleotide
OCT1	Organic Cation Transporter 1
ORF	Open reading frame
P300	E1A binding protein p300

PAM	Protospacer adjacent motif
PEV	Position-effect variegation
PPHLN1	Periphilin-1
PRC1	Polycomb repressive complex 1
qRT-PCR	Quantitative Reverse transcription polymerase chain reaction
RNA	Ribonucleic acid
RNA Pol II	RNA polymerase II
ROS	Reactive oxygen species
SEM	Standard error mean
SETDB1	Histone-lysine N-methyltransferase SETDB1
shRNA	short hairpin RNA
siRNA	small interfering RNA
SIRT1	Sirtuin 1
SpCas9	Streptococcus pyogenes Cas9
SRF	Serum Response Factor
STDEV	Standard deviation
SUV39H1	Suppressor Of Variegation 3-9 Homolog 1
SUV39H2	Suppressor Of Variegation 3-9 Homolog 2
TALEN	Transcription activator-like effector nucleases
TATA	Goldberg-Hogness box
TFAP2	Transcriptional regulation by the AP-2
TSS	Transcription Start Site
tTag	T Antigen
UTR	Untranslated region
VPR	VP64-p65-Rta
WT	Wild type
YG8R	Human FXN YAC transgenic mouse model

Introduction

Epigenetics and transcriptional regulation in Friedreich's Ataxia

Friedreich's ataxia (FRDA) is a neurodegenerative disorder resulting from a mutation in the frataxin (FXN) gene. It is inherited in an autosomal recessive fashion with a majority of cases resulting from a non-coding trinucleotide expansion (GAA) within intron 1.[1] This results in a transcriptional defect with a reduction of primary and mature FXN transcripts.[2] Splicing defects have not been noted from mutant alleles. Carriers of the mutation are asymptomatic, although have up to a 50% reduction in frataxin levels.[3] The ability to translate transcripts from mutant alleles to functional frataxin and the relatively broad range of frataxin levels required for health make up-regulation of endogenous transcription an enticing therapeutic target.

Friedreich's ataxia (FRDA) is a progressive neurodegenerative disorder that affects 1 in 50 000 people.[70,71] It is inherited in an autosomal recessive fashion, being the commonest of the inherited ataxias. Most often symptoms begin in childhood with patients describing poor coordination. As the disease progresses patients develop clearer signs of cerebellar dysfunction (e.g. dysarthria, ataxia, nystagmus and intention tremor), peripheral neuropathy, cardiac dysfunction and often diabetes. Optic atrophy and sensorineural deafness are late features. The disease places great physical and psychological stress on patients and their families, and is as yet incurable.[71]

The large majority of FRDA cases are caused by an abnormal GAA trinucleotide repeat expansion within intron 1 of the frataxin (FXN) gene that encodes the mitochondrial protein frataxin.[1] In unaffected individuals there are often between 10 and 66 GAA repeats, while FRDA patients may have as many as 1700 repeats.[1,2]

Unlike other triplet repeat disorders (e.g. Huntington's disease), the GAA repeat expansion has been shown to result in reduced expression of the FXN gene. Carriers of the expansion are asymptomatic however have lower frataxin levels than unaffected individuals. As frataxin appears integral to the disease process in FRDA, and levels are quantifiable in peripheral blood, increasing frataxin has become a key end point in recent clinical trials of therapeutic agents. In addition to frataxin levels several clinical scales are in use (SARA, SCAFI and FARS), which have been validated to detect change in FRDA related movement disorder and effect on activities of daily living (ADL).[73] As FRDA is a slowly progressive disorder novel assessment strategies and biomarkers are needed to highlight treatment efficacy and quantify subjective rating measures.

To date there have been several therapeutic trials for FRDA. Agents aimed to increase frataxin expression or boost mitochondrial respiratory function. To address the disorder at an epigenetic level, recent studies, including our own,

have investigated the effect of histone deacetylase inhibitors (HDACi) on FRDA with promising results.[17]

A number of therapeutic avenues have been investigated for FRDA.[74] Most have aimed to increase endogenous frataxin expression. Additionally gene therapy (both targeting the nervous system and specifically cardiac tissue) and protein replacement therapy are under investigation.[74]

Frataxin

Frataxin is a highly conserved protein found in most organisms.[75] Human frataxin is synthesized as a 210 amino acid precursor and then transported to the mitochondria where it undergoes maturation to forma a 14kDa protein. Despite its integral role to health, its physiological function is still poorly defined. There are two hypotheses put forward for the function of frataxin, both originating from its iron-binding capacity. The iron chaperone hypothesis suggests that frataxin acts to scavenge iron or store iron, such that it is maintained in a bioavailable form.[75] Ferritin supplementation was shown to partially relieve an absence of frataxin and its function as an iron scavenger is thought to likely be redundant in mammals.[76] It has also been shown to be important in iron-sulphur cluster biogenesis, an important group of cofactors involved in a number of cellular processes (e.g. electron transport, gene regulation and DNA repair). A potential role in protecting against excessive oxidative stress has been shown in Drosophila, where overexpression of frataxin provided resistance to oxidative stress and improved lifespan.[77]

CRISPR

Clustered regulatory interspersed palindromic repeats (CRISPR) are short sequences of DNA found within bacterial genomes following viral attack. Associated with CRISPR associated system (Cas) genes they form a bacterial acquired immune mechanism against viral infection.[78] Cas proteins contain nuclease regions which in association with CRISPR RNAs can target and excise regions of viral DNA. This system was subsequently repurposed by the synthetic biology community to undertake facile genome engineering through co-expression of CRISPR associated protein 9 (Cas9) alongside a guide RNA (gRNA) towards a specific 20 nucleotide sequence of DNA associated with a protospacer motif (PAM – 3' NGG).[79] This technology has allowed for accurate genome edits for knockout (through indel formation) and knockin.[78] Further modification through deactivation of the nuclease domains (RUVC and HNH) in Cas9 created a targeting protein without the ability to cut DNA.[80] It is now possible to fuse various proteins to Cas9 to assess their function at a locus of interest. Altering the state of chromatin using this technology is known as epigenome engineering.[80]

Gene regulation of frataxin

There are several mechanisms implicated in the silencing of the frataxin gene. A directly causal relationship of the GAA repeat to gene silencing was recently highlighted, whereby zinc finger mediated excision of the pathological repeat expansion within patient derived cell lines resulted in correction of frataxin expression to that of carrier levels. There was also correction of other biochemical hallmarks, such as decreased aconitase activity and increased ATP. The epigenetic signature seen in FRDA was also corrected. Frataxin reactivation was maintained through reprogramming of somatic cells into induced pluripotent stem cells.[4]

A brief description of the DNA elements within the frataxin gene is required before embarking on its regulatory features.

The frataxin gene is comprised of 5 exons and is located at 9q13-q21.1.
The minimal frataxin promoter has been shown in transient reporter assays to consist of the region 1255bp upstream of the open reading frame (ORF).[5] The transcription start site (TSS) is located 220bp upstream of the ORF.[1] Another TSS named TSS2 was suggested through primer extension experiments at 62bp upstream of the ORF.[6] Interestingly a 64bp region alone upstream of the ORF was shown to promote transcription in the earlier reporter assay experiments by the same group, but to a lesser extent (20% of that with the entire minimal promoter). The 100nt upstream of TSS2, which contains an L2-like element, when included in the reporter assay inhibited transcription. The combinatorial function of these two TSS may have importance in frataxin regulation. Unlike many human genes, the frataxin promoter lacks a TATA box and instead has an initiator motif and downstream promoter element (Inr/DPE) 24 bp downstream of TSS1. These alternative promoter elements are frequently found regulating Drosophila genes, such as the *white* gene.[7] Binding sites for Serum response factor 2 (SRF2), transcription factor AP2 (TFAP2) and Octamer binding protein (OCT1) have been shown and computationally predicted.[8,9]

Frataxin expression

Frataxin is ubiquitously expressed in humans, but at a relatively low level. In the presence of a pathological GAA expansion, causing FRDA, this level is significantly lowered. Importantly asymptomatic carriers have levels approximately 50% of healthy individuals. The length of the GAA expansion, and in particular the shorter expansion (referred to as GAA1) is known to correlate with disease severity and inversely with frataxin levels.[10,11] The expansion has also been shown to exhibit somatic instability and undergoes expansions and contractions through DNA damage-repair mechanisms, the former possibly implicated in disease progression.[12,13] Limiting expansion is being investigated as one avenue of therapy.[14]

Alu elements

The GAA expansion is found within an Alu element. These are short repetitive sequences and thought to be the result of retrotransposon integration, with

approximately 1 million found within the human genome.[15,16] The Alu element harbouring the expansion was sub-classified with the AluSx family, which have an estimated age of 37 million years.[16] This repetitive sequence may provide an environment that promotes polymerase slippage during DNA replication, which can lead to small expansions of the GAA sequence. Larger expansions may possibly be due to strand displacement during DNA replication and the formation of secondary structures, resulting in reiterative synthesis and triplet expansion. [15,16]

Downregulation of frataxin expression

Pathological downregulation of FXN expression is postulated to be the result of inhibited passage of RNA polymerase through atypical DNA structures (non-B DNA) and through local action of silencing machinery and heterochromatin formation.[17] It is likely that variations in the extent of these mechanisms dictate the overall level of gene repression.

Atypical DNA structures

'Sticky DNA' was discovered when assessing (GAA.TTC)n repeat sequences, whereby long purine tracts (>59 repeats) were shown to form triplex structures that impede transcription in vitro and in vivo.[18] Here an intermediate R-loop structure formed between the interaction of nascent RNA and the template single-strand DNA, permit the association of freed polypyrimidine tract with the non-template strand.[18] Whether these interactions are more likely to occur within the same allele (intramolecular) or both alleles (intermolecular) is unclear. Experimentation on haploid cell lines with a (GAA)n expansion would help to elucidate this.

R-Loops

R-loops themselves outside the context of sticky DNA have also recently been implicated in frataxin downregulation.[19] These structures are known to form in G-rich sequences, whereby the nascent RNA adheres to the template strand, which can impede further transcription.

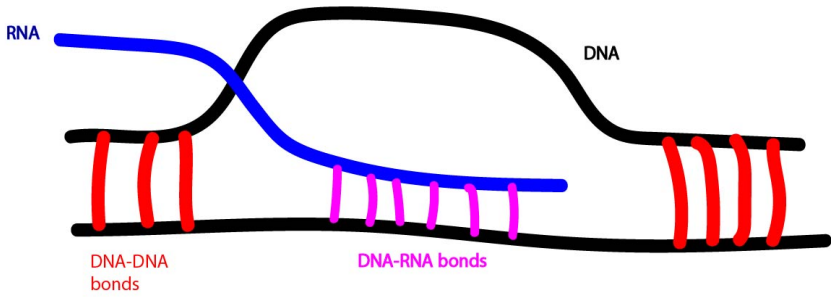

Figure I1: Drawing of an R-loop structure. Nascent RNA is able to bind the free DNA strand.

Here, the co-localisation of the repressive histone modification (H3K9me2) and R-loops was noted at the expanded GAA region within patient cells and correlated with the length of expansion. Isolated reduction of H3K9me2, through inhibition of the lysine methyltransferase G9a that catalyses the formation of this modification, however did not reduce the presence of R-loops or increase FXN transcription. While, increasing the presence of R-loops with the DNA topoisomerase inhibitor camptothecin was able to reduce FXN transcription. Nascent transcription was shown to be decreased upstream of the expansion and may be the result of abnormal transcriptional termination and/or inhibition of RNA Polymerase II (RNA Pol II) elongation. [19]

Heterochromatin mediated gene silencing

DNA is packaged in distinct compartments within the nucleus. If considered in a basic bimodal state, these can be classified as regions of open and closed chromatin. 'Open' dictating ease of access to transcriptional machinery and the opposite for 'closed' chromatin. The latter is also known as heterochromatin, which was initially morphologically described by its dense staining which can now be visualised with 4',6-diamidino-2-phenylindole (DAPI), a fluorescent stain that binds A-T rich regions.[20] Superimposed on this are more intricate layers of compartmentalisation dictated by several regulatory phenomena that have been regarded as the epigenome.

Heterochromatic regions of DNA are frequently highly repetitive and devoid of actively transcribed genes.[21] Here, DNA is woven around an octamer of histone proteins to form a nucleosome. Histone proteins undergo posttranslational modifications along their N-terminal tails, which further dictate and/or imply the state in which local chromatin is found.[21] A variety of histone modifications (or 'marks') exist, with multiple functions. Those of greatest importance, and most studied with respect to frataxin gene regulation, are acetylation and methylation of histone 3 at position 9 (H3K9) and position 27 (H3K27) of their N-terminal tails. H3K9me3 is a highly conserved modification, which is most often associated with silenced regions of the genome, these are often repressed in all cells and define these regions as constitutive heterochromatin. H3K27me3 is also found at developmentally regulated regions of the genome, such as the HOX gene cluster.[22]

As posttranslational modifications of histone proteins and other chromatin associated factors are dynamic, this provides the potential to alter gene expression. This epigenetic gene regulation is an enticing avenue of therapeutic potential, where genes regulated in this manner are implicated in disease. As the frataxin gene is regulated in such a fashion, my doctoral work has involved investigating the result of perturbation of this dynamic system on frataxin expression.

The epigenetic architecture of the frataxin locus

As a result of the (GAA)n expansion within the FXN gene a number of epigenetic alterations have been found at the locus.

DNA methylation

DNA methylation is the molecular basis of a regulatory phenomenon thought to have evolved to silence exogenous DNA integrants, such as transposons.[23] Several studies have shown an increase in DNA methylation in FRDA cells compared to cells from unaffected individuals. This is found at CpG sites upstream and downstream of the expansion. Of the 15 CpGs upstream of the GAA repeat, 3 sites were noted to be protected from methylation in unaffected controls.[24] In another study the upstream methylation was inversely correlated to the level of FXN expression and the downstream methylation to age of disease onset.[25] Methylation was highest nearest the repeat and gradually declined towards the 5' end of the gene. The promoter regions of both FRDA and unaffected cells were found to be unmethylated.[24] Targeted methylation of the 13th CpG upstream of the GAA, through use of a bacterial sequence specific DNA methyltransferase, within a reporter construct assessing transcriptional output showed no effect, indicating this site to be not heavily implicated in FXN silencing.[25]

Antisense transcription

Whereas RNA that is transcribed from the template DNA strand, the sense strand, will be processed and translated into protein, transcription from the opposite strand, the antisense strand, is implicated to have a role in gene regulation. This is through its complementary binding to template strand RNA, preventing its processing and translation. Recently an antisense transcript was implicated in FRDA named FAST-1, with its discovery in patient derived fibroblast lines. The model put forward in this study is one whereby depletion of CTCF, an insulator protein within the 5' UTR of frataxin, permitted antisense transcription and reduced frataxin expression.[26]

Histone modification

Several studies have shown the presence of the silencing histone post-translational modifications H3K9me3 and H3K27me3 along the affected loci.[27] The co-existence of these marks is interesting, as they are frequently found in distinct chromatin compartments.[62] As yet the causal relationship between the existence of these marks and the expansion is yet to be elucidated, in particular the requirement for either or both marks to maintain silencing.

Genome editing

Until recent years the process of altering DNA sequence was a labour intensive process, however a number of sequence specific nucleases have now been described and used to modify genomic DNA in a large number of species, including human embryos.[28] One such group of nucleases, transcription activator-like effector nucleases (TALENs) have been used in the context of the frataxin gene to excise the pathological repeats and restore the chromatin architecture of the gene to one similar to euchromatic genes, as well as relieve frataxin silencing. This study provides direct evidence to the causality of the GAA expansion in gene silencing.[29]

A more versatile tool that has arguably revolutionised the molecular biology toolkit is the discovery of the clustered regularly interspaced short palindromic repeats (CRISPR) in prokaryotic DNA and their association with the Cas9 endonuclease.[30] A protective mechanism harnessed by prokaryotes to find and remove exogenous phage DNA.[30] This immunity system has been adopted by those in the field of synthetic biology and modified in a number of ways to both edit DNA and RNA, image genomic loci and alter gene expression, with considerable accuracy and minimal off-target effects.[31] This loci specific effect allows questions relating to particular genomic regions to be investigated without altering genome-wide factors, which can result with techniques such as interfering RNA techniques. Specific regions of the genome can be targeted through introduction of an 18-20 nucleotide (n20) guide RNA (gRNA) that is complementary to the region of interest.[30] Almost all genomic regions can be targeted where a protospacer associated motif (PAM) sequence is found next to a target sequence of 20 nucleotides (n20).[30] The canonical PAM sequence is NGG associated with Cas9 from Streptococcus Pyogenes (SpCas9). Recent directed evolution techniques have allowed for the discovery of Cas9 proteins with alternative PAM specificities, broadening the potential targetable genome by CRISPR/Cas9, including a GAA PAM.[32,33]

Epigenome editing

Building on the targeting function of these endonucleases, fusion of effector proteins with inactive Cas9, made through mutation of amino acids D10A and H840A, (dead Cas9 or dCas9) has allowed a new field to develop assessing the effect, and providing support towards the causality and local function of various chromatin-altering proteins and chromatin states on gene expression. The current state of this field of investigation was recently comprehensively reviewed in a review that emphasised that epigenomic screens are a next potential area of growth within the field.[34] In brief, experiments harnessing this technique are undertaken by fusion of proteins of interest (e.g. histone acetyl transferases – HATs) to dCas9 and targeted to regions of interest. Assessment is then undertaken of changes in gene expression, local chromatin signature and genome-wide effects. This

technology has been taken further through multiplexing gRNAs and genome-wide gRNA libraries.[35]

Aims

To investigate the effect of alteration in levels of modifiers of heterochromatin mediated silencing on frataxin expression in FRDA.

To investigate the potential for targeted epigenome editing to relieve heterochromatin mediated silencing in FRDA.

Hypotheses

The archetypal modifier of position effect variegation and lysine methyltransferase SUV39H1 is important in maintenance of pathological frataxin gene silencing.

SUV39H2, an isoform of SUV39H1, is important in maintenance of pathological frataxin gene silencing.

A core component of PRC1, BMI1, is important in maintenance of pathological frataxin gene silencing in YG8R mice.

The human silencing hub complex (HUSH) and its binding partner SETDB1, a lysine methyltransferase, are important in pathological frataxin gene silencing.

Local alteration of the epigenome at the pathologically silenced frataxin locus through targeting dCas9-VPR and dCas9-p300 will relieve silencing with minimal off-target effects.

Local alteration of the epigenome and inhibition of lysine methyltransferases with dCas9-H3.3K9M and dCas9-H3.3K27M will identify a hierarchy of histone modifications and relieve frataxin gene silencing.

Methods

Cell Culture

HEK-293 FXN

Human Dermal Fibroblasts – GM04078, GM07492, GM03665, GM03816, GM04503 acquired from Coriell Biorepository

Cells were cultured in DMEM with 10% FBS, 1% Penicillin/Streptomycin and 1% Glutamax and experiments conducted in early passage. Lines were tested for Mycoplasma infection regularly and, where required, treated with Plasmocure (Invivogen) 50ug/ml for 2 weeks. Experiments were undertaken in early passage (<9). GAA expansions in human dermal fibroblasts have been shown to be stable when assessed up to 13 weeks in one study.[82]

Plasmid Transfection in HEK-293T FXN-Luc and FXN-GAA-Luc lines

2ul of lipofectamine 2000 was mixed with 50ul of Optimem per transfection (per well in a 24-well plate) and was then added to 200ng of dCas9-P300 or dCas9-VPR and 10ng of gRNA. The mixture was allowed to equilibrate at room temperature for 20 minutes. Fresh media was added to each transfected well. 50ul of the DNA-lipofectamine mixture was added drop-wise to each well. When using pooled gRNAs a total of 10ng of DNA was used (e.g. in a pool of 5 gRNAs, 2ng of each gRNA were used). Outside of preliminary experiments, 3 biological replicates were undertaken.

Fibroblast

Lentiviral knockdown
pGIPZ shRNA (GE Dharmacon) constructs were used to knockdown chromatin modifiers. Cultures were grown overnight in LB with Ampicillin (100ug/ml) and DNA extracted using Qiagen Maxi- or Midiprep kits and Sanger sequence verified.

Day 0: 1 confluent 10cm dish of HEK 293T cells is split 1:4.
Day 1: 1 plate is used per shRNA transfection.
The following transfection mixture was made and allowed to incubate at RT for 20 mins.

1. pMD2.G – 2ug
2. psPAX2 – 8ug
3. pGIPZ shRNA – 20ug
4. Poly-ethyleneimine (PEI) – 90ug
5. PBS – made up to a volume of 1ml
6. Replace media and add mixture to plate drop-wise.

Day 2: Replace media of HEK293T. Plate 2x10^5 human fibroblasts per well in a 6-well plate.
Day 3: Lentiviral transduction: Aspirate and filter media from HEK293Ts with 0.45um cellulose acetate filter. Dilute 1:1 with DMEM. Add polybrene (Sigma) to a final concentration of 8ug/ml. Replace media of HEK293Ts. Aspirate media from human fibroblasts and add 3ml of polybrene treated viral supernatant. Repeat this process after 3 hrs.
Day 4: Repeat lentiviral transduction. When cells are confluent expand into 10cm dish and begin puromycin selection (2ug/ml).
Day 11: Select until untransduced cells dead (kill-well).

shRNA sequences
(shRNAs in bold were a gift from Prof Giunti's Lab, UCL)

Gene	Clone identifier	shRNA label	Sequence (5'-3')

SUV39H1	**V3LHS_327225**	**shRNA1**	**CAAGTGTGTGCGTATCCTCAATA**
	V3LHS_403672	**shRNA2**	**ACGCATCACTGTAGAGAATGATA**
	V3LHS_327224	**shRNA3**	**CACCTGCTCCTACCTGCTCTATA**
SUV39H2	**V3LHS_353036**	**shRNA1**	**CTGGACTATGAGTCTGATGAATA**
	V3LHS_407457	**shRNA2**	**CTCAATGATAAAGAAATTTAATA**
	V3LHS_407455	**shRNA3**	**AAGCGTTAAGCTGATAATGTATA**
	V2LHS_262274	**shRNA4**	**GCTTAGTATATGTGTACTTAATA**
SIRT1	**V2LHS_20109**	**shRNA1**	**CGATGTTTGATATTGAATA**
	V3LHS_389163	**shRNA2**	**AAGTTGACTGTGAAGCTGT**
	V3LHS_389161	**shRNA3**	**AGACTCAAGTTCACCAGAA**
	V3LHS_412846	**shRNA4**	**AGGAACTTTAGCATGTCAA**
	V2LHS_20111	**shRNA5**	**CAGCTAAGAGTAATGATGA**
	V2LHS_20110	**shRNA6**	**GTGATGAAATTATCACTAA**
MPP8	V3LHS_361717	shRNA1	AGGGTGAAATAAGAGATTT
	V3LHS_361716	shRNA2	GGAATCAAGACAGAAGCAA
	V3LHS_361713	shRNA3	CCGACAGCAGAGAAGAGAA
	V2LHS_200399	shRNA4	CCTGTTGCAGGTCCCAATA
	V2LHS_200650	shRNA5	CTGTAGTTCTGAATGATAA
	V2LHS_163067	shRNA6	CATGGACCTGCAGTTGGAA
PPHLN1	V3LHS_385874	shRNA1	TCATCAAAGGTGTTAGACA
	V3LHS_385877	shRNA2	AGCTAGAGAAATCAGATGA
	V3LHS_385875	shRNA3	GGGACGATATGAATATGAA
	V3LHS_349404	shRNA4	CGGTGTGTTGAAGAACTCA
	V2LHS_116069	shRNA5	CTCTAAAGCAATAGCATCA
FAM208A	V3LHS_365717	shRNA1	AGGAGAGAACAGCAATTCA
	V3LHS_355057	shRNA2	ACGATTCTGGTGCTAAGAT
	V3LHS_355058	shRNA3	TGGATGATGTTAAAAATCA
	V2LHS_81789	shRNA4	GGCTTTAACTGAAGTAGAA
	V2LHS_81717	shRNA5	CCGGGAACCAGTAGAAGAA
SETDB1	V2LHS_43632	shRNA1	CTGATAGTCAGCATGCGAA
	V3LHS_388253	shRNA2	TGGAGAAGATGGATTGTGT
	V3LHS_388251	shRNA3	AGGTGAAATTTGACAACAA
Scramble	**Non-silencing**		**CTCTCGCTTGGGCGAGAGTAAGTA**

pGIPZ sequencing primer: 5' GCATTAAAGCAGCGTATC 3'

siRNA knockdown

Day 0: 50x10^3 cells are seeded in a 12-well plate.
Day 1: 2.5ul 10uM siRNA added to 97.5ul Optimem per
Materials:

- Dharmafect I (Dharmacon/Thermofisher)
- siRNA smartpools against target (Dharmacon/Thermofisher) siRNAs purchased from Dharmacon: ON-TARGETplus Human siRNA SMARTPool: SETDB1 (9869), SUV39H1 (6839) and SUV39H2 (79723).
- Optimem (Invitrogen #31985070)
- FRDA Fibroblasts GM04078, GM03816 from Coriell

Protocol (12-well plate):

- Seed 50K cells per well (1ml volume) and reverse transfect after seeding as follows:
    - 2.5ul 10uM siRNA + 97.5ul optimem
    - 2.5ul Dharmafect I + 97.5ul optimem
    - Leave 5 mins at RT
    - Combine optimem diluted siRNA and Dharmafect I
    - Leave 15-20 mins at RT
    - Apply drop-wise to wells
- 72-96h post-transfection, aspirate media and wash 1x with dPBS
- Harvest in-well in 50ul 0.5%NP40 lysis buffer supplement with protease inhibitors and scrape cells using cell lifter
- Transfer to microtube for downstream IB analysis

RNA Extraction

Dermal fibroblasts:
RNA extraction was undertaken using Trizol® reagent for human dermal fibroblasts. Briefly, 10^6 cells were lysed in Trizol reagent for 5 mins at RT. 200ul of chloroform was added and mixed thoroughly and allowed to equilibrate at RT. Centrifuge at 12000g, 4°C for 15min. The aqueous phase was trasnfered to a new tube and 500ul isopropanol was added and left for 10min at RT and centrifuge at 12000g, 4°C for 25min. 1ml 70% ethanol was added to the supernatant per 1ml Trizol. Samples were mixed by vortexing and centrifuge at 7500g, 4°C for 15min. Supernatent was removed and RNA pellets were air-dried and followed by DNase treatment with DNA free kit (Ambion®). 40µl master mix containing 33µl RNase free water, 2µl Superase, 4µl 10X DNaseI buffer and 1µl DNaseI with 10min incubation at 37°C. 4µl of inactivation reagent was then mixed with each sample, incubated at room temperature for 2min and followed by centrifugation at 10000g for 2min. 35µl supernatant which contained RNA isolated was retained for cDNA synthesis.

HEK293T: RNA extraction was undertaken using RNeasy Plus Minikit as per manufacturer protocol.

cDNA synthesis

Total RNA was reverse transcribed into complementary DNA with ThermoScript® kit following protocol provided and amplified using non-gradient cycler PCR machine. 50-250ng of random hexamer (primer) and 2µl of 10mM dNTP mix was mixed with 1.25µg of RNA and sterile water was then added to make up total volume of 12µl. Reaction mixture was then incubated at 65°C for 5min then keep at 12°C. 4µl of 5X cDNA synthesis buffer, 1µl of 0.1M DTT, 1µl of ThermoScriptTM reverse transcriptase (15U/µl) was mixed with reaction mixture. Sterile water was added to make up total volume of 20µl and incubate at 50°C for 60min. Quantitative RT-PCR was used to analyse cDNA samples generated.

cDNA synthesis for HEK293T FXN-Luc lines was undertaken using qSCRIPT cDNA synthesis kit using 500ng of RNA.

qRT-PCR for FXN mRNA expression

Initial step:
40 cycles:
2min 94°C 30sec 94°C 30sec 58°C 30sec 72°C Plate read
1sec 80°C Plate read
1sec 82°C Plate read
1 sec 85°C Plate read
(incubation) (denaturation) (annealing) (extension)
Melting curve from 70°C to 95°C, read every 0.5°C, hold 1sec

Statistics

A paired t-test was used when comparing baseline to experimental gene expression change.

CRISPR

dCas9-VPR (addgene #63800) was kindly provided by Alex Chavez). dCas9-P300 and MLM3636 gRNA expression vector was kindly provided by Anne Koeferle. See plasmid transfection (page 19).

gRNA design: Guide RNAs were designed using www.crispr.mit.edu/ to target the FXN promoter and 250bp up- and downstream of the GAA expansion.

FXN Promoter

Promoter 1 ACACCAGGCTGCTTGGCCGCCGGTAG
Promoter 2 ACACCTACACAAGGCATCCGTCTCCG
Promoter 3 ACACCCCGCTTCTAAAATTCTAAACG

Promoter 4 ACACCTTACAGCAGTTGGGTATGTGG
Promoter 5 ACACCGCAGAGTACAGATTTACACAG
Promoter 6 ACACCCTTGGGAGCTGCTGTCTTGCG
Promoter 7 ACACCATGCACGAATAGTGCTAAGCG
Promoter 8 ACACCGCAAAGCACGGAGTGCAACCG
Promoter 9 ACACCGGCCGCAGGCACTCTTCTGTG
Promoter 10 ACACCGCAGCTAGAGGTTAGACCTCG
Promoter 11 ACACCAACCAGGACCCCTGACCCAAG
Promoter 12 ACACCCCGCTCCGCCCTCCAGCGCTG
Promoter 13 ACACCCTGGGTGCTGCGGCGACCCCG

250 downstream sequence of GAA

GAA DOWN1 ACACCCAAGATCGCCCAATGCACTCG
GAA DOWN2 ACACCAATGGATTTCCCAGCATCTCG
GAA DOWN3 ACACCGCCTATTTTTCCAGAGATGCG
GAA DOWN4 ACACCAATAAAAATAAAAAATAAAAG
GAA DOWN5 ACACCAAAGAAAAGTTAGCCGGGCGG

250 upstream sequence of GAA

GAA UP1 ACACCAACTTCCCACACGTGTTATTG
GAA UP2 ACACCATGGATTTCCTGGCAGGACGG
GAA UP3 ACACCGTTGCCAGTGCTTAAAAGTTG
GAA UP4 ACACCAGTTTCTTCAAACACAATGTG
GAA UP5 ACACCTCCGGAGTTCAAGACTAACCG

Oligonucleotide annealing

Equal concentrations of forward and reverse gRNA oligonucleotides were mixed in the presence of Cutsmart® buffer (NEB). Annealing was undertaken by placing the mixture in a water bath at 95 degrees and gradual cooling at 1 degree per minute.

Cloning

Restriction-ligation
MLM3636 was cut with BsmBI, visualised on 1% agarose gel and gel extracted as per manufacturer protocol (Qiagen Gel Extraction Kit). Cut MLM3636 was mixed with annealed gRNA oligoneucleotides (diluted 1:100 with water) at a ratio of 1:4 and ligated for 2hrs at RT with T4 Ligase and T4 Ligase buffer.

pCas9d-VP64-Hygro plasmid map

Asc1, Pme1 and EcoRV unique sites highlighted

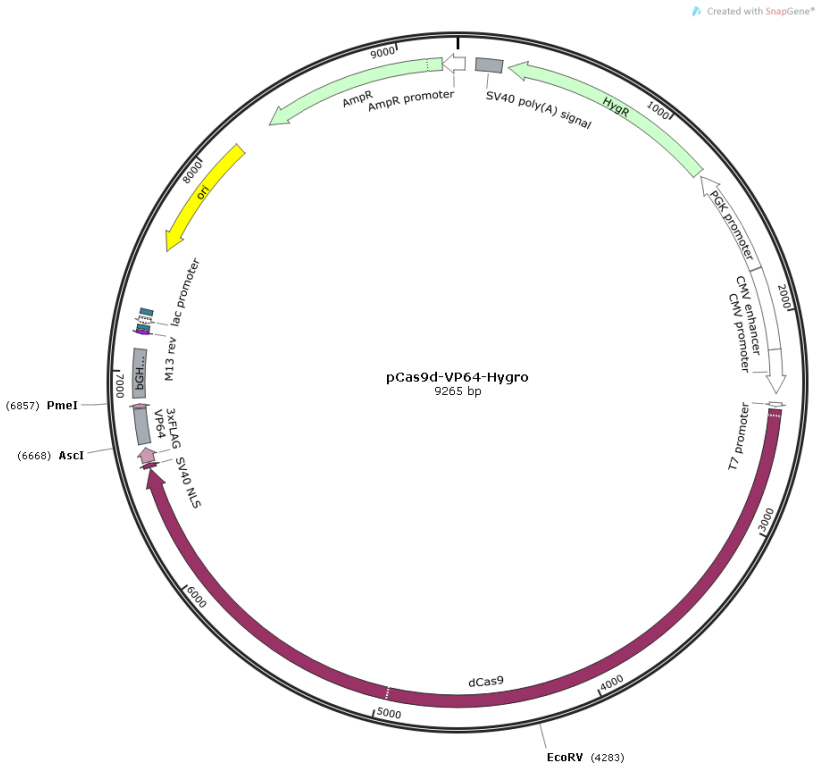

Oligonucleotides designed for Gibson isothermal assembly of lysine to methionine H3 tail to pCas9d-VP64-Hygro after restriction with AscI and PmeI.

H3 aa 1-27 1F: 5' – GGCGGTGGAAGCGGGGCCCGAACCAAGCAGACTGCTCGTAAGTCCACCGGTGGGAAA GCCCCCCGCAAACAGCTGGCCACGAAAGCCGCCAGGAAATGAAAACCCGCTGATCAG - 3'

H3 aa 1-27 1R: 5' – CTGATCAGCGGGTTTTCATTTCCTGGCGGCTTTCGTGGCCAGCTGTTTGCGGGGGGCT TTCCCACCGGTGGACTTACGAGCAGTCTGCTTGGTTCGGGCCCCGCTTCCACCGCC – 3'

H3 aa 1-27 K9M 1F: 5' - GGCGGTGGAAGCGGGgcccgaaccaagcagactgctcgt**ATG**tccaccggtgggaaagccccccgcaaa cagctggccacgaaagccgccaggaaaTGAAAACCCGCTGATCAG – 3'

H3 aa 1-27 K9M 1R: 5' – CTGATCAGCGGGTTTTCAtttcctggcggctttcgtggccagctgtttgcgggggctttcccaccggtgga **CAT**acgagcagtctgcttggttcgggcCCCGCTTCCACCGCC – 3'

H3 aa 1-27 K27M 1F: 5' - GGCGGTGGAAGCGGG gcccgaaccaagcagactgctcgtaagtccaccggtgggaaagccccccgcaaacagctggccacgaaagccgcc agg**ATG**TGA AAACCCGCTGATCAG – 3'

H3 aa 1-27 K27M 1R: 5' – CTGATCAGCGGGTTTTCA**CAT**cctggcggctttcgtggccagctgtttgcgggggctttcccaccggtgg acttacgagcagtctgcttggttcgggcCCCGCTTCCACCGCC – 3'

H3 aa 1-27 K9MK27M 1F:
5’ - GGCGGTGGAAGCGGG
gcccgaaccaagcagactgctcgt**ATG**tccaccggtgggaaagccccccgcaaacagctggccacgaaagccgc
cagg**ATG**TGAAAACCCGCTGATCAG – 3’
H3 aa 1-27 K9MK27M 1R:
CTGATCAGCGGGTTTTCA**CAT**cctggcggctttcgtggccagctgtttgcgggggctttcccaccggtgg
a**CAT**acgagcagtctgcttggttcgggcCCCGCTTCCACCGCC

Table of qRT-PCR primers

Primer name	**Sequence 5’-3’**
b-actin F	GCGGGAAATCGTGCGTGACAT
b-actin R	GATGGAGTTGAAGGTAGTTTC GTG
GAPDH F	GGAGCGAGATCCCTCCAAAAT
GAPDH R	GGCTGTTGTCATACTTCTCATGG
FXN mRNA F	ATGTCTCCTTTGGGAGTGGTGT CT
FXN mRNA R	CCCAGTCCAGTCATAACGCTTAGGT
SUV39H1 F	GCTATGACTGCCCAAATCGT
SUV39H1 R	ACACGTCCTCCACGTAGTCC
SUV39H1 (mouse) F	TGTCAACCATAGTTGTGATCC
Suv39H1 (mouse) R	ATTCGGGTACTCTCCATGTC
SUV39H2 F	GAGGCGCGAGGAGCTTG
SUV39H2 R	GCAGTAACGGGCACTTCAGA
SIRT1 F	TAGCCTTGTCAGATAAGGAAGGA
SIRT1 R	ACAGCTTCACAGTCAACTTTGT
BMI1 (mouse) F	TGTGTCCTGTGTGGAGGGTA
BMI1 (mouse) R	TGTTCAGGAGTGGTCTGGTT
BMI1 (human) F	CAGCAATGACTGTGATGC
BMI1 (human) R	AATCCAGAGGTTGATTATCG
FXN-Luc F	CGGAAAAGATGCTGGAAGTG
FXN-Luc R	AACCAGGGCGTATCTCTTCA
FAM208A F	ACATCTAGTGTGAGTGTTGTGACT

FAM208A R	GTCCTCCTGCAAGCATCTGA
MPP8 F	AGTTATTGCTCGGCTCTGTG
MPP8 R	CAGTCCCTTCTGTTTGGTCAT
PPHLN1 F	GCCAGAGTCGTGGCTTACAG
PPHLN1 R	GCCTGCTTGCAGAATGATCG
SETDB1 F	TTAACACAGGCCCTGAATTTCT
SETDB1 R	TACCCCTGTGGGTAGACACTCT
18S (F) (mouse)	ATGGTAGTCGCCGTGCCTAC
18S (R) (mouse)	CCGGAATCGAACCCTGATT
Human 18S rRNA F1	GGCCCTGTAATTGGAATGAGTC
Human 18S rRNA R1	CCAAGATCCAACTACGAGCTT

Chapter 1

Knockout of the PRC1 component BMI1 does not alter FXN gene expression in disease specific tissues from YG8R mice.

Summary

FRDA YG8R mice have been created by homozygous knockout of endogenous murine FXN, a lethal genotype, and rescued with a human FXN transgene.[13] BMI1 homozygote mice, were crossed with FRDA mice to generate BMI1 heterozygote (BMI+/-) FRDA mice (no effect on FXN expression was noted in these mice). These were subsequently crossed together to generate BMI1 (-/-) FRDA mice.[36] All mice are on a C57Bl/6 background. Heart and cerebellum tissues were taken for initial analysis. No clear change in FXN mRNA expression was noted in BMI heterozygote and homozygote mice.

Introduction

The silencing of the *FXN* gene in FRDA, is suggested to be accompanied by the spreading of both H3K9me3 and H3K27me3 heterochromatic modifications on either

side of the GAA-repeat expansion (Figure 1.0).[27] H3K9me3 is formed by several enzymes including SUV39H1 and SUV39H2 and bound by HP1. H3K27me3 is a modification found at developmentally silenced genes by constituents of the polycomb repressor complex (PRC).[33] This multiprotein complex comprises PRC1 and PRC2. PRC1 is thought to localize and promote the formation of H2AK119u1, which targets PRC2 to catalyse the formation of H3K27me3. [33] One of the core proteins in PRC1 is BMI1. In order to investigate whether disruption of this complex increases FXN expression, an in vivo approach was adopted, using transgenic mice that are heterozygote or homozygote knockouts of BMI1.[37]

YG8R mice

YG8R mice are created using the entire human frataxin within a yeast articificial chromosome (YAC), which is cloned into a mouse Fxn null background. This gave rise to YG8R (90 and 190 GAA) and YG22 (biallelic 190 GAA repeats) Through subsequent mating with mouse heterozygous knockout WT Fxn, YG8RR (rescue) mice were created with 90 and 190 GAA repeats.[81] These show reduced human mRNA in the cerebellum, skeletal muscle and a mild progressive phenotype. Cardiac aconitase deficiency was noted at 6 months compared to WT. YG8R mice showed impairments on rotarod, open field locomotor and grip strength testing. Despite the mild phenotype seen with YG8R mice, the ability to rescue the WT Fxn knockout as well as reduction in mRNA and common epigenetic signature along the transgenic allele (increased H3K9me3 and H3K27me3).[81]

H3K9me3 and H3K27me3 at the frataxin locus

The co-existence of the heterochromatic modifications H3K9me3 and H3K27me3 have been shown along the pathologically silenced FXN locus by our group and others (figure 1.0).

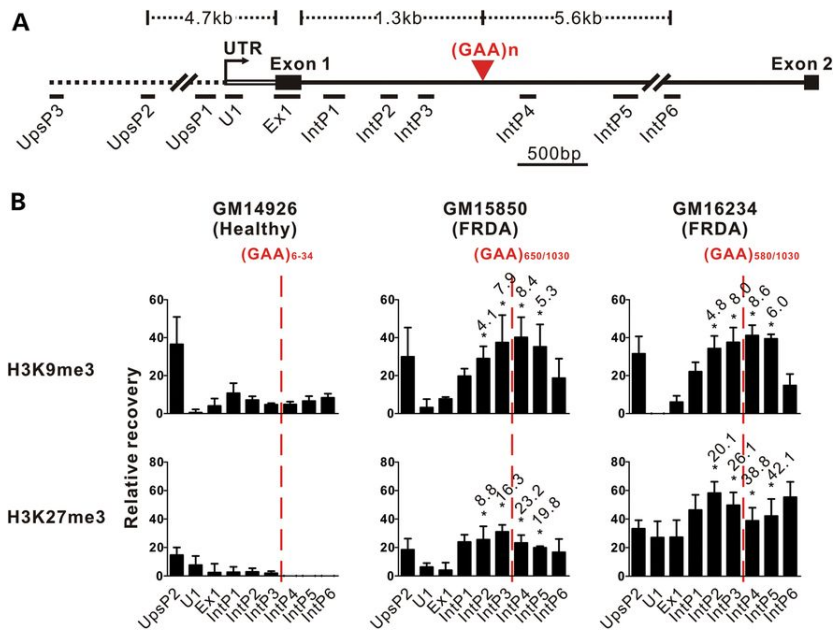

Fig 1.0: Chromatin immunoprecipitation (ChIP) of H3K9me3 and H3K27me3 along the frataxin gene. A) FXN gene locus highlighting ChIP primer regions. B) ChIP-qPCR of H3K9me3 and H3K27me3 along the FXN gene locus in unaffected lymphoblastoid line (GM14926) and 2 FRDA lines (GM15850, GM16234). An increase in H3K9me3 and H3K27me3 are found upstream and downstream of the GAA expansion in diseased lines. Figure adapted from Chan et al. Hum Mol Genet 2013.[27]

Results

BMI1 is a key component in the PRC1 complex, which is regarded as important in the recognition of H3K27me3 and thereby results in local spreading of this mark.[33,34,38] BMI1 knockout mice were first characterized by van Lohuizen and crossing a hCD2 mouse model of PEV to strongly derepressed silencing (Figure 1.1, unpublished data Santiago Uribe-Lewis).[34,83] BMI1 heterozygote mice have been shown to be less viable and exhibit changes associated with brain aging. While homozygote knockout BMI1 mice are known to be up to 50% less viable and have significant haemopoetic and lymphoid abnormalities.[37,39] Reduced viability may partly explain the reduced number of homozygote mice available for assay in figure 1.10.

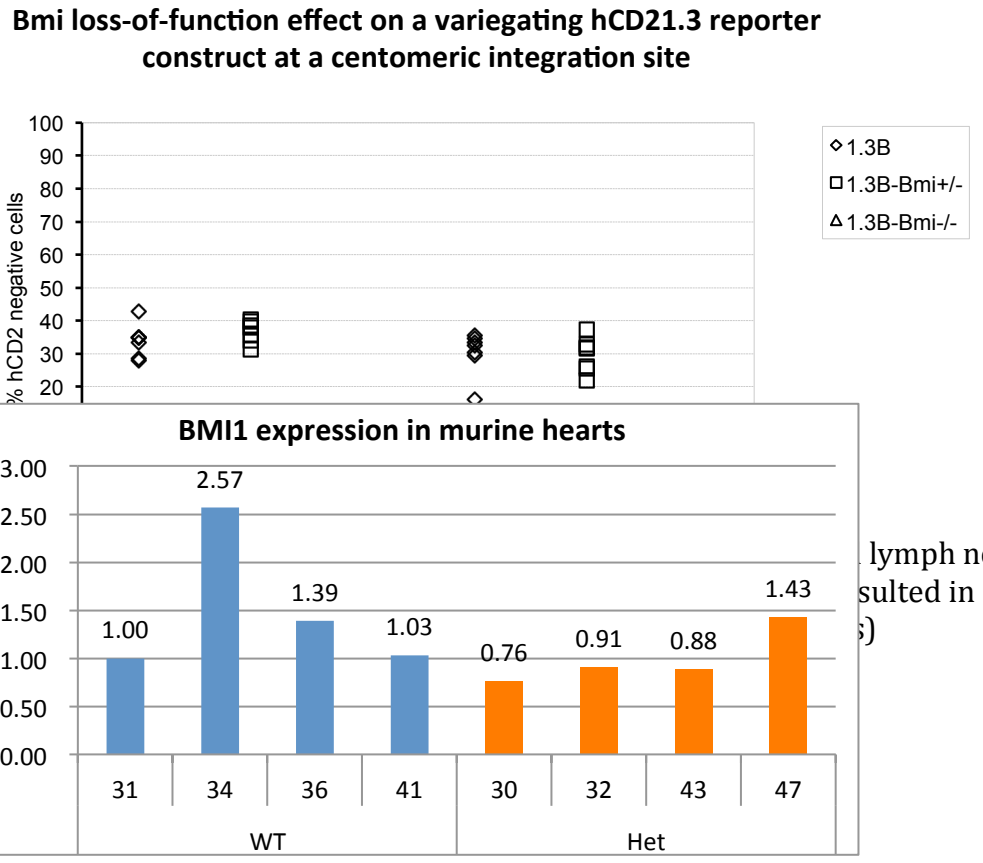

Fig. 1.1: Flu lymph node stained wit sulted in almost complete r s)

Figure 1.2: BMI expression in wild type (WT) and heterozygote YG8R mice normalised to lowest expressing WT (31).

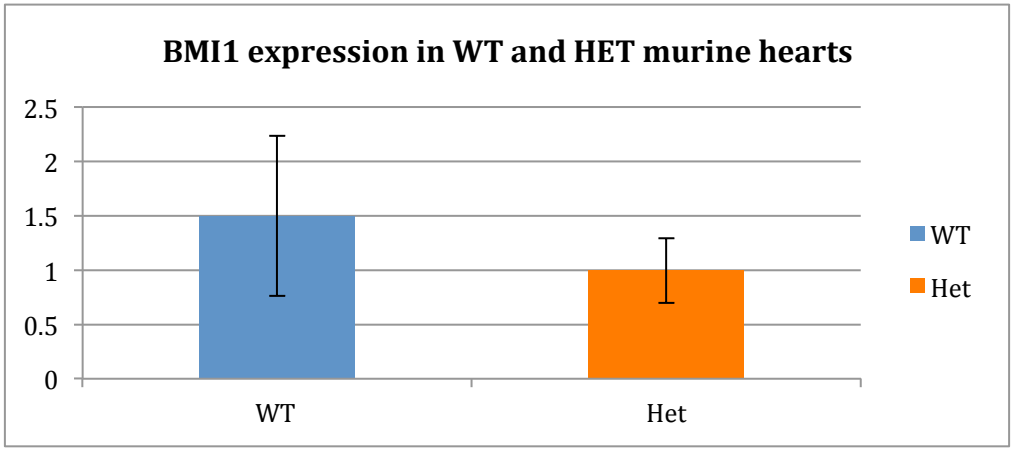

Figure 1.3: Average BMI1 expression in wild type (WT) and heterozygote YG8R mice normalised to WT. Expression relative to β-actin, normalized to WT. Error bars: STDEV.

There is a wide variation in the expression of BMI1 within both WT and heterozygote mice (figure 1.2). No significant difference was noted in reduction of BMI1 expression in heterozygote knockout YG8R mice. This may be the result of compensatory upregulation from the wild type allele or allele specific polymorphisms that alter expression.

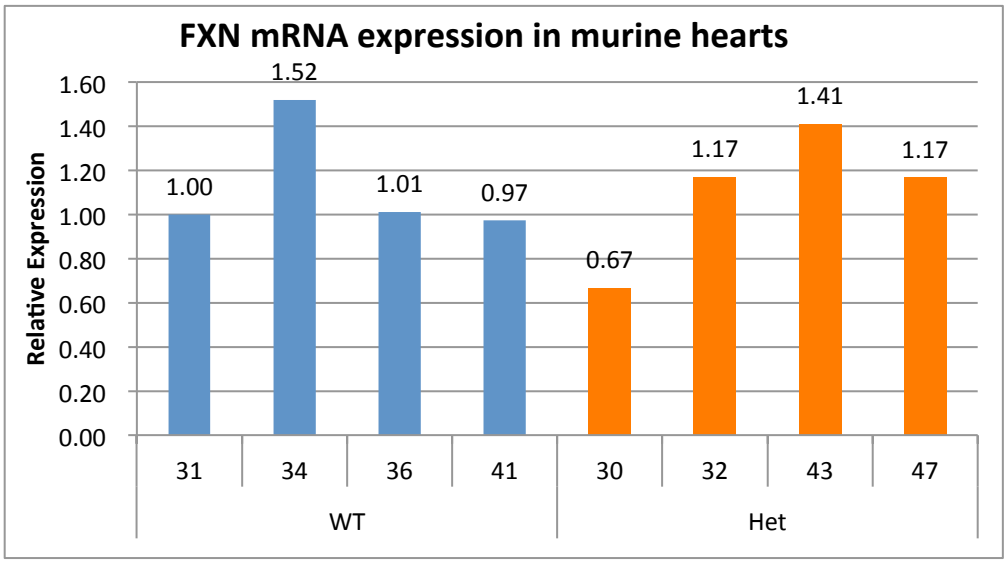

Figure 1.4: FXN mRNA expression in BMI WT YG8R mice and heterozygote mice. Expression relative to β-actin, normalized to WT.

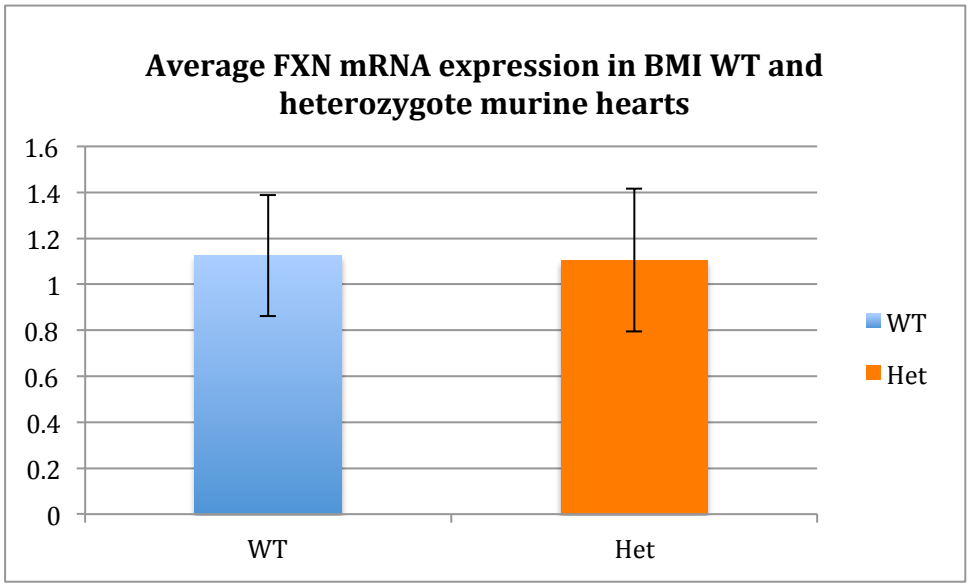

Figure 1.5: Average FXN mRNA expression in BMI WT YG8R mice and heterozygote mice. Expression relative to β-actin, normalized to WT. Error bars: STDEV.

Assessment of frataxin expression in BMI (+/-) mice showed no significant difference between WT and heterozygotes (figure 1.4 and 1.5). This was unsurprising as a clear difference in expression was not imparted between the WT and heterozygote groups. Furthermore, in the earlier PEV model, little or no relief from silencing was noted in BMI heterozygote knockout hCD2 mice (figure 1.0).

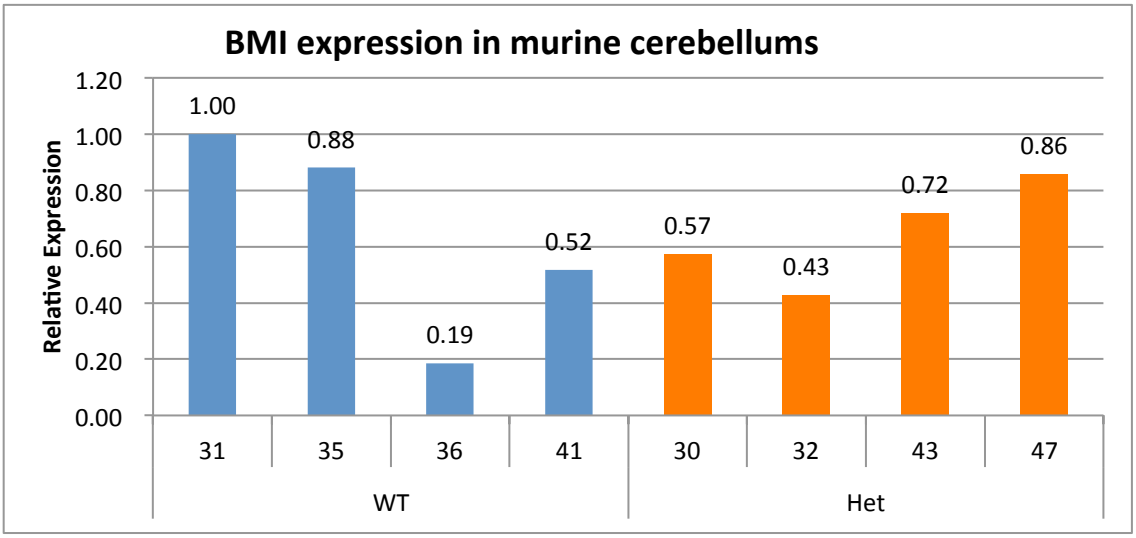

Figure 1.6: BMI1 expression in YG8R BM1 WT and heterozygote cerebellums. Expression relative to β-actin, normalized to WT.

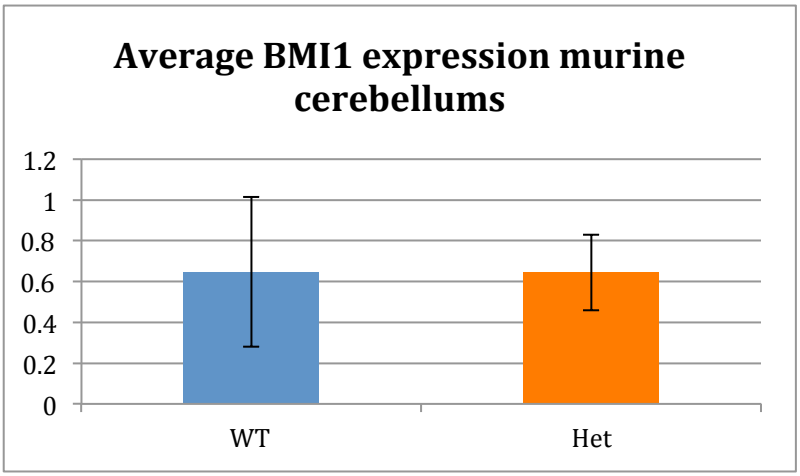

Figure 1.7: Average BMI1 expression between BMI1 WT and heterozygote mice. Expression relative to β-actin, normalized to WT. Error bars: STDEV.

As with murine hearts, no significant difference in BMI expression was noted between WT and BMI(+/-) mice with broad variation between mice cerebellums. Despite having normal expression in the heart, mouse 36 had below heterozygote expression levels in the cerebellum. This may highlight a tissue specific variation in expression as well as variation between mice. (figures 1.6 and 1.7)

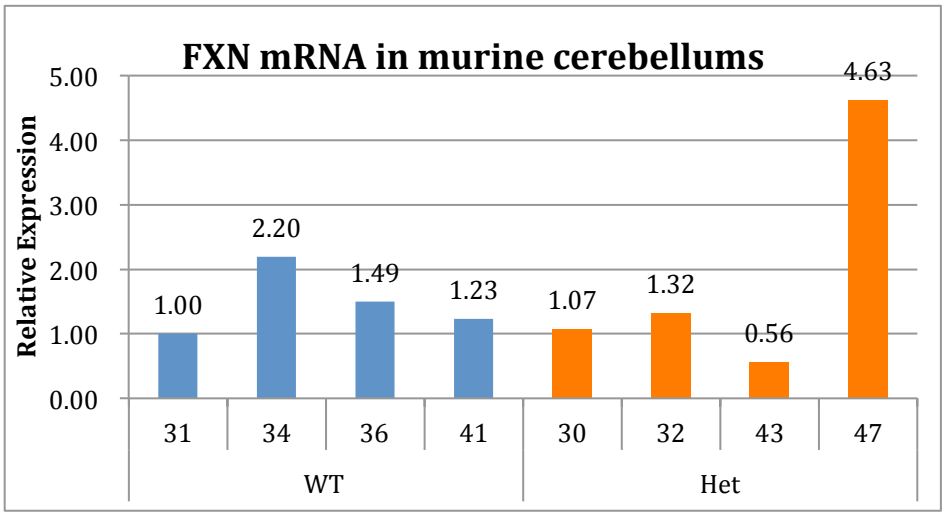

Figure 1.8: FXN expression in BMI WT and heterozygote mouse cerebellums. Expression relative to b-actin, normalized to WT.

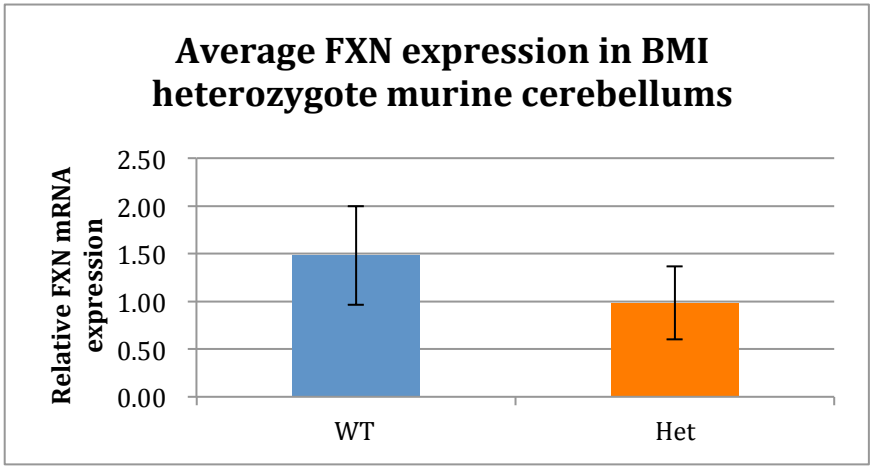

Figure 1.9: Average FXN expression in BMI WT and Het mice cerebellums. Mouse 47 not included in analysis. Expression relative to b-actin, normalized to WT. Error bars: STDEV.

Frataxin expression did not show a significant difference between the cerebellums of BMI(+/-) mice compared to WT (figure 1.8 & 1.9). Expression was recorded as greatly increased in mouse 47, this was potentially the result of RNA degradation or loading error (with an increase in β-actin CT value. It was not included in the average analysis (figure 1.9).

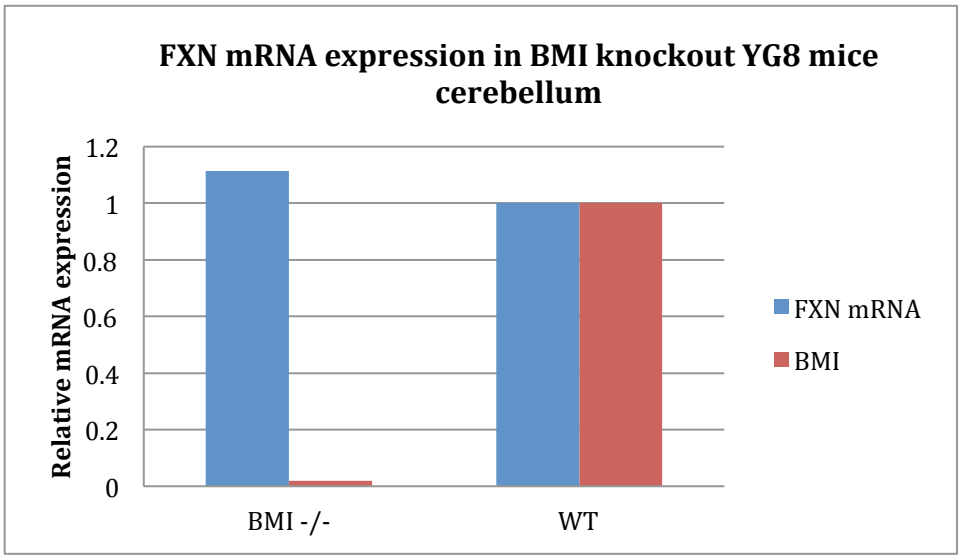

Fig 1.10. FXN mRNA expression in WT and BMI-/-. No change in FXN expression was found with BMI1 knockout. Expression relative to β-actin, normalized to WT.

Only one BMI(-/-) mouse was able to be successfully bred with an appropriate control mouse (identical genetic background aside from BMI homozygote knockout). Only a 1.1-fold increase in FXN expression was noted in the cerebellum.

The variation in endogenous expression of BMI1 between mice of WT and knockout genotypes provides a challenging background on which to base a conclusion on its effect on frataxin expression. Despite having only one complete knockout mouse and one isogenic control it appears that BMI1 does not have a regulatory role in pathological frataxin silencing in YG8R mice.

In vitro assessment of BMI was attempted in human dermal fibroblasts, however expression in this cell type was undetectable at baseline.

Chapter 2

Transient knockdown of SUV39H1 or SUV39H2 did not have a significant effect on frataxin expression in human dermal fibroblasts.

Summary

Human dermal fibroblasts (HDFs) from unaffected individuals (GM38530, GM07492 and GM04530) and FRDA patients (GM04078, GM03816, GM03665) were used to assess the effect on frataxin expression upon transient knockdown of SUV39H1 and/or SUV39H2. Despite considerable knockdown, a significant upregulation of FXN expression was not noted.

Introduction

The existence of excess H3K9me3 along the frataxin locus has been shown in vitro and in vivo.[52] Histone lysine methyltransferases (HKMT) are enzymes which catalyse the addition of methyl groups to the N-terminal tails of histone proteins. SUV39H1 and its isoform SUV39H2, which until recently were considered redundant with one another, are the primary HKMTs at pericentromeric heterochromatin.[66] G9a and SETDB1 are other SET domain proteins important in the formation of H3K9me3. Single gene knockout of either SUV39H enzymes are not known to result in a developmental phenotype.[40] The possible importance of SUV39H1 and SUV39H2 in frataxin gene silencing was highlighted by their single or dual knockout in hCD2 mice exhibiting PEV. This resulted in almost complete relief of GAA mediated silencing (Santiago Uribe-Lewis, unpublished result. Manuscript in preparation).

Results

HDFs were used due to their ease of siRNA transfection and the variation in repeat length and gender. Phenotypic data for each line is highlighted in the table below.

Human dermal fibroblast phenotypic data (* - siblings) (Coriell Institute for Medical Research)

Name	FRDA	Expansion	Sex
03665	Y	445/740	F
03816	Y	330/380	F*
04078	Y	541/420	M*
04503	N	9-27	F
07492	N	9-27	M
38530	N	9-27	M

Relative frataxin mRNA expression at baseline was confirmed in both FRDA and control lines (figure 2.0) prior to experimentation. Up to 50% reduction in FXN expression in FRDA lines (GM03665, GM03816, GM04078) when compared to lowest expressing control line (GM04503).

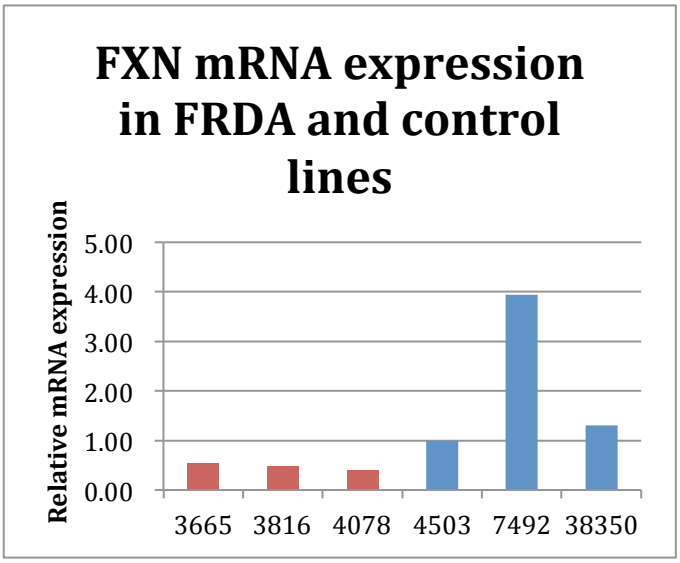

Fig 2.0: FXN mRNA expression at baseline relative to GM04503, which exhibited the lowest expression amongst control lines. n=1 Red bars: FRDA line. Blue bars: Control lines.

The effect on frataxin expression was measured after 72hrs following siRNA knockdown of SUV39H1 or SUV39H2 in HDFs from unaffected controls and FRDA patient lines (figure 2.1).

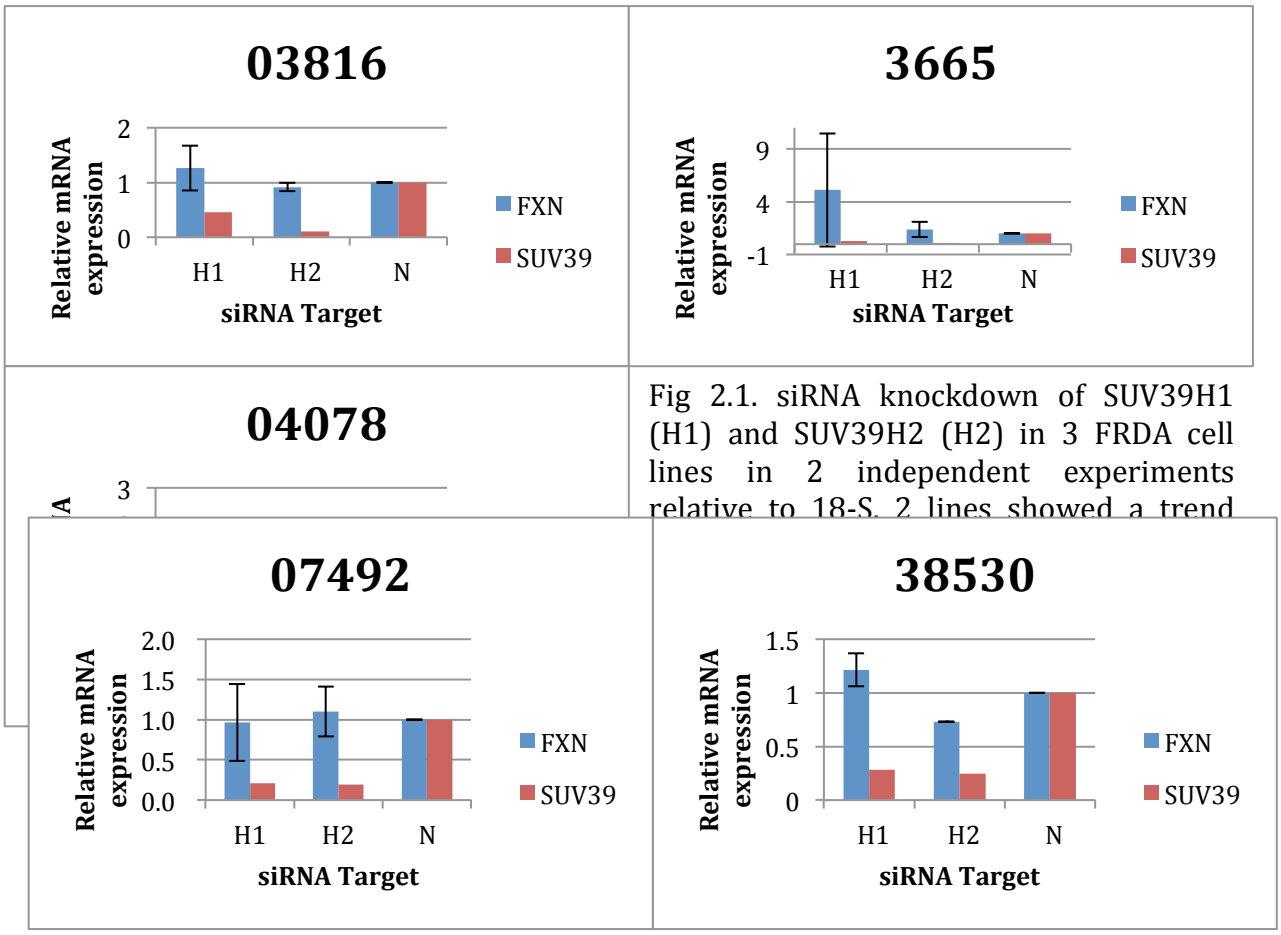

Fig 2.1. siRNA knockdown of SUV39H1 (H1) and SUV39H2 (H2) in 3 FRDA cell lines in 2 independent experiments relative to 18-S. 2 lines showed a trend

Fig 2.2. FXN expression in control lines following SUV39H1 or SUV39H2 siRNA knockdown. Upregulation was noted with H1 knockdown IN GM38530. Error bars= SEM.

siRNA knockdown of SUV39H1 or SUV39H2 in the 3 FRDA lines resulted in a trend towards upregulation in GM03816 only. The 4 fold upregulation noted with SUV39H1 knockdown in GM03665 may have been, in part, the result of aberrant reduction in expression of 18-S which was only observed in this cell line, although the occurrence in just one line makes this unlikely. RNA degradation with respect to the housekeeping PCR reaction may also explain this discrepancy but would have to have occurred in all the replicates making this unlikely. In the control lines a trend towards upregulation was seen with H1 knockdown in GM38530.

To assess the effect on frataxin relative to another housekeeping gene a further experiment was undertaken assessing the effect relative to GAPDH (fig 2.3 and 2.4). Frataxin preRNA or mRNA were not clearly upregulated in this experiment, aside from in GM04078 (1.1 fold). Within the control lines, GM07492 exhibited an upregulation of preRNA on H2 and H2 knockdown but a downregulation in frataxin.

Although, there was only one biological replicate in this experiment, taken together with the results presented in Fig 2.1 it seems unlikely that knockdown of SUV39H1 or SUV39H 2 leads to upregulation of FXN.

The effect on WT frataxin expression with knockdown of these potential modifiers may highlight a more complex role in regulation above that seen only in disease states.

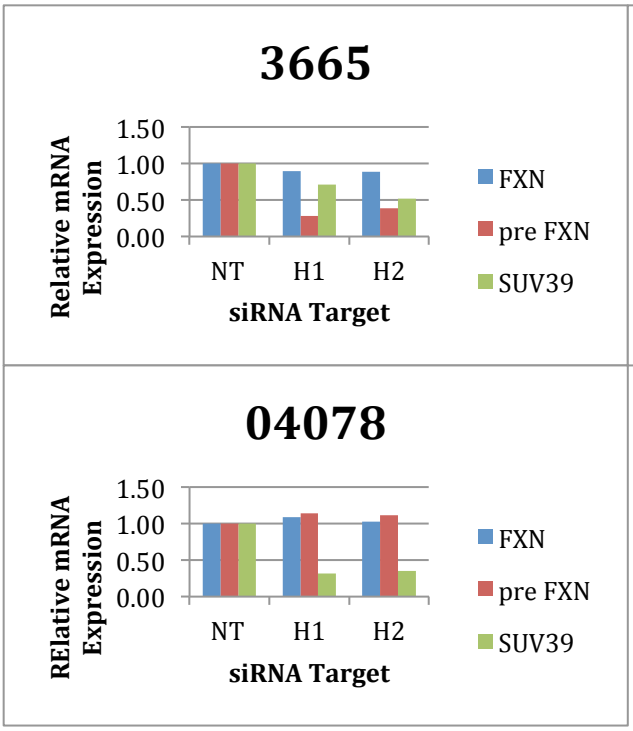

Fig 2.3 siRNA knockdown of SUV39H1 or SUV39H2 in 3 FRDA fibroblast lines in 1 preliminary experiment. A mild upregulation of FXN mRNA and primary transcript expression was noted only in 04078 when normalised to GAPDH.

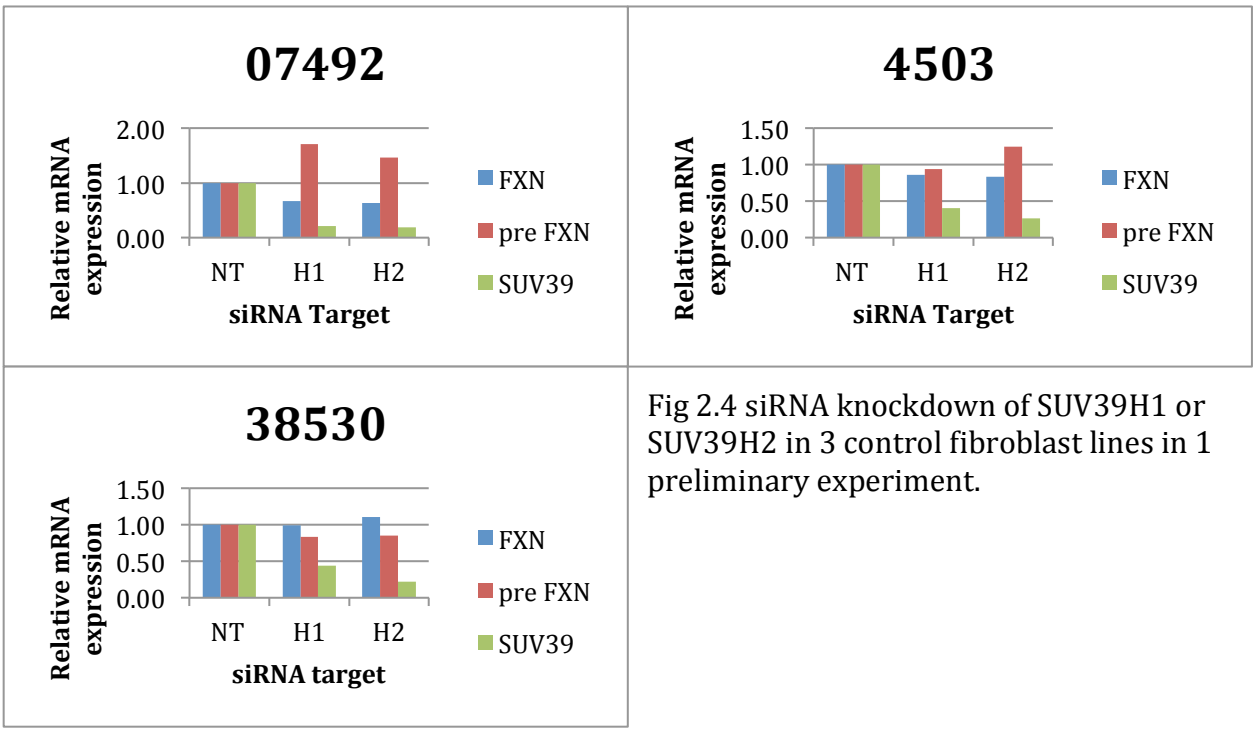

Fig 2.4 siRNA knockdown of SUV39H1 or SUV39H2 in 3 control fibroblast lines in 1 preliminary experiment.

The lack of a robust and consistent effect on frataxin expression with knockdown of either SUV39H1 or SUV39H2 may in part be the result of the redundancy between the function of both enzymes as well as the other HKMTs known to catalyse this modification (figure 2.1 & 2.2). Furthermore, the unusual co-existence of H3K9me3 and H3K27me3 at the frataxin locus may maintain silencing, when only lysine-9 modifiers are perturbed.[27] A means to abrogate both marks would allow investigation of this hypothesis.

To assess the effect of known SUV39H inter-isoform redundancy, a transient dual knockdown strategy was tested (figure 2.5 & 2.6).

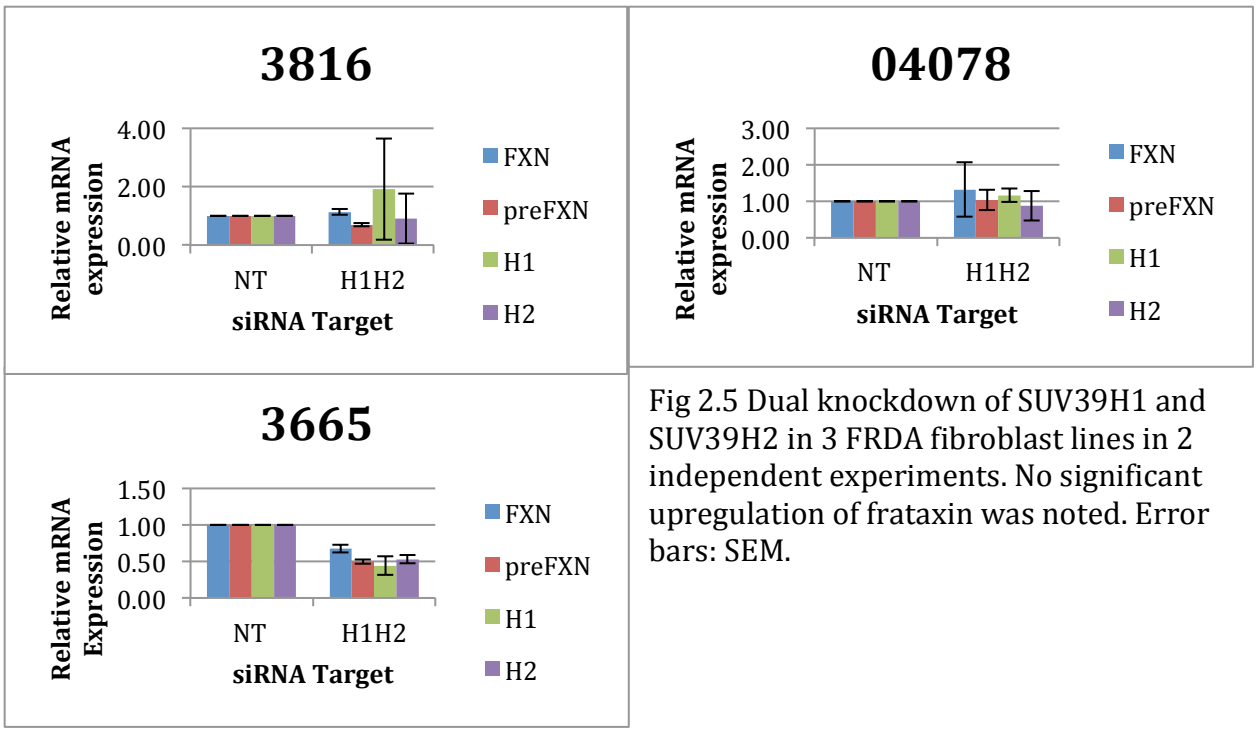

Fig 2.5 Dual knockdown of SUV39H1 and SUV39H2 in 3 FRDA fibroblast lines in 2 independent experiments. No significant upregulation of frataxin was noted. Error bars: SEM.

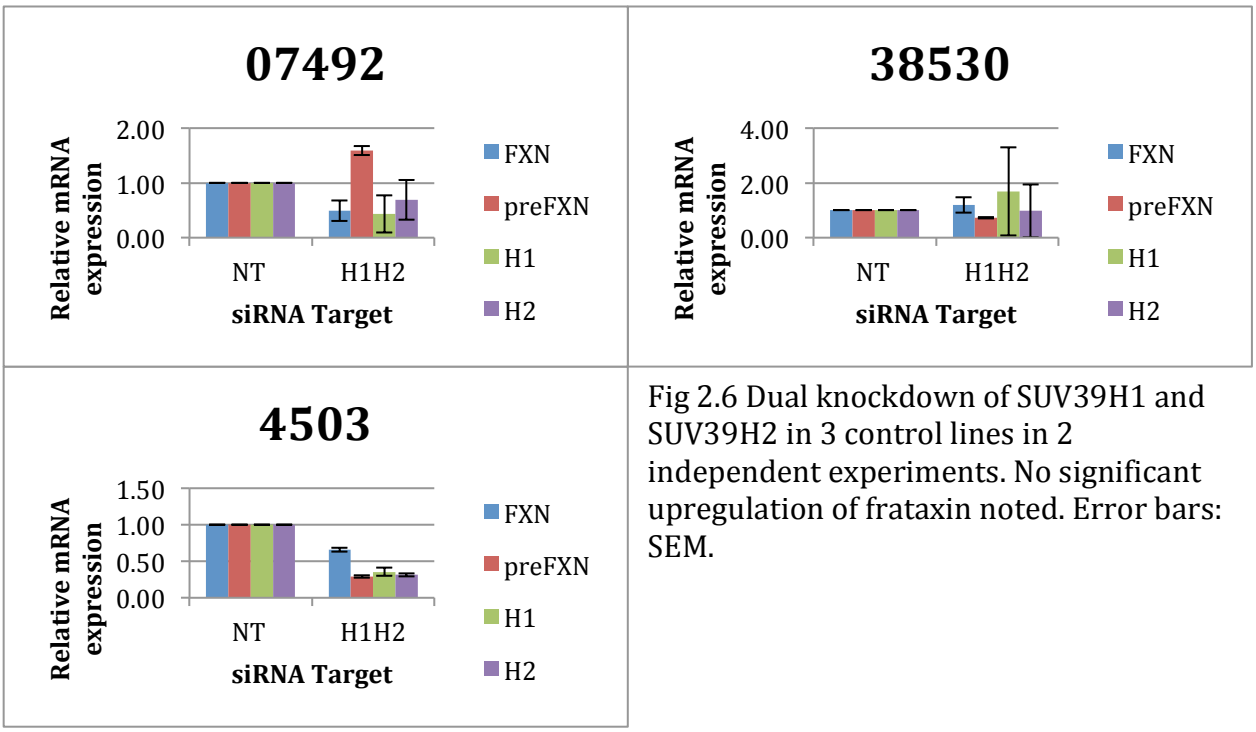

Fig 2.6 Dual knockdown of SUV39H1 and SUV39H2 in 3 control lines in 2 independent experiments. No significant upregulation of frataxin noted. Error bars: SEM.

Dual knockdown of SUV39H1 and SUV39H2 (fig 2.5 & 2.6) led to varying efficiency of knockdown between cell lines. This may highlight an interdependence between the expression of the isoforms. In the FRDA line downregulation of frataxin preRNA was seen in GM03816 and GM03665. GM03665 also saw a reduction in mRNA. Combined knockdown did not result in significant knockdown of either gene in GM04078, while individual siRNAs resulted in up to 89% knockdown. No effect was noted on frataxin expression in this line. In the control lines, as with the single siRNA approach GM07492 showed an increase in preRNA but a decrease in mRNA. A 27% reduction in preRNA expression was noted in GM38530, with no change in mRNA expression. This is also in agreement with the earlier single siRNA experiments. Unlike the single siRNA experiment, dual knockdown in GM04503 results in reduction in preRNA and mRNA.

These unexpected results, may, amongst other possibiities, implicate SUV39H in the physiological regulation of frataxin in a cell-line specific manner or be the result of indirect genome-wide effects. Here more targeted approaches might be useful (see final chapter on epigenomic editing).

Chapter 3

Stable knockdown of heterochromatin modifier SUV39H1 variably upregulates FXN expression in several FRDA cell lines.

Summary

Stable knockdown of SUV39H1 with shRNAs resulted in 1.5 fold upregulation of frataxin expression in 2 lines, which however did not reach statistical significance ($p>0.05$, students t-test). Knockdown in one control line had no effect on reduced frataxin expression.

Introduction

Lentiviral mediated knockdown of chromatin modifiers, allows for assessment on frataxin expression following several rounds of cell division following drug selection. SUV39H1 is an archetypal modifier of PEV and the dominant histone lysine methyltransferase at pericentromeric chromatin, catalysing the formation of H3K9me3. Knockout of SUV39H1 was able to almost completely relieve GAA repeat induced PEV in the hCD2 system.

Results

Three shRNA constructs targeting SUV39H1 were transduced into HDF lines and underwent puromycin selection. RNA was collected and analysed by qRT-PCR for efficiency of knockdown and the level of frataxin expression.

Frataxin mRNA was upregualted in 2 HDF lines, however this did not correlate with the level of knockdown. No effect was noted in the FRDA line GM03816 and the control line. (fig 3.0 & 3.1).

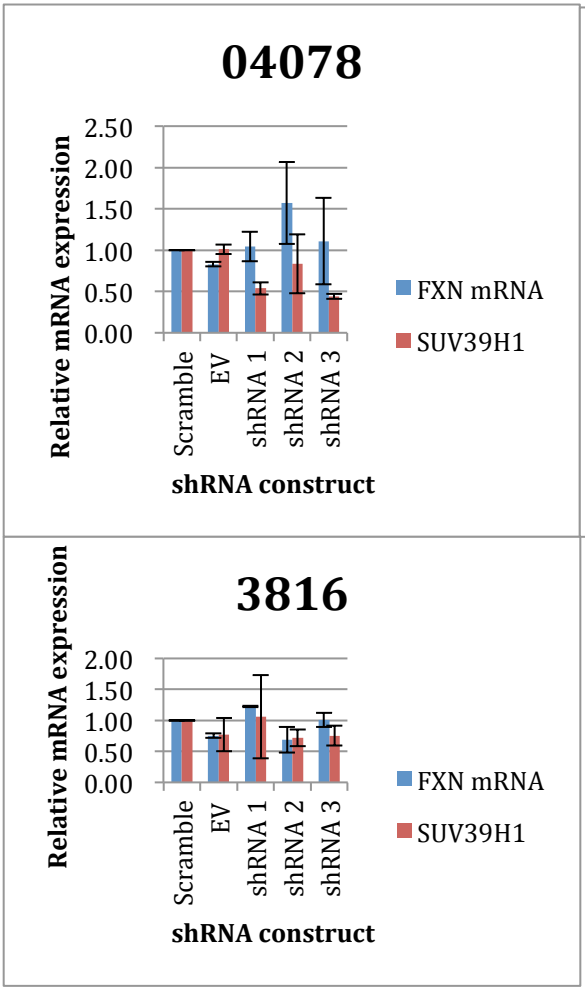

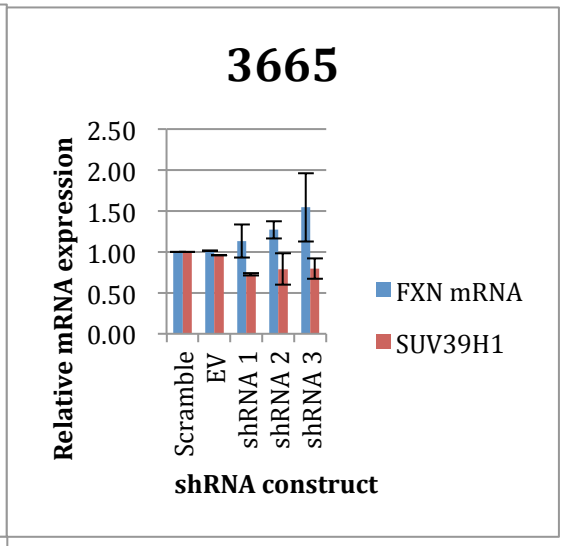

Fig 3.0 shRNA knockdown and FXN expression of SUV39H1 in 3 FRDA cell lines in 2 independent experiments. Trend towards FXN upregulation in 2 FRDA lines when normalised to 18S and scrambled shRNA. Y-axis: fold change relative to scramble. X-axis: different shRNA transductions in order of effect on SUV39H. Error bars= SEM.

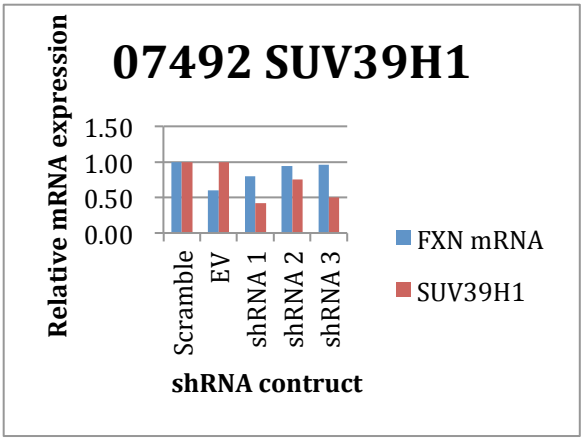

Fig 3.1 shRNA knockdown of SUV39H1 and FXN expression in 2 control cell lines. Preliminary result showing upregulation in one control line when normalised to scramble shRNA. Y-axis: fold change relative to scramble. X-axis: different shRNA transductions in order of effect on SUV39H.

Chapter 4

Stable knockdown of SUV39H2 upregulates FXN expression in a cell line dependent fashion

Summary

Stable knockdown of SUV39H2 indicated a trend towards upregulation of frataxin in 2 FRDA cell lines although there was no clear correlation with efficiency of knockdown. SUV39H2 was noted to be a lowly expressed gene in human dermal fibroblasts, which may in part explain the variability in error. SUV39H2 is a relatively low abundant modifier compared with SUV39H1, with expression being unrecordable by qRT-PCR in GM07492, however FXN upregulation was noted in some cell lines.

Introduction

Lentiviral mediated knockdown of chromatin modifiers, allows for assessment on frataxin expression following several rounds of cell division following drug selection. SUV39H2, an isoform of SUV39H1, is an archetypal modifier of position effect variegation and the dominant histone lysine methyltransferase (H3K9me3) at pericentromeric chromatin. Despite the dominance of SUV39H1 in alleviating GAA repeat mediated hCD2 silencing, knockout of SUV39H2 has previously been shown to further derepress the hCD2 transgene (Uribe-Lewis PhD).

Results

Four shRNA constructs targeting SUV39H2 were transduced into human dermal fibroblast lines and underwent puromycin selection. RNA was collected and analysed by qRT-PCR for efficiency of knockdown and the level of frataxin expression.

The effect of SUV39H2 knockdown was variable on frataxin expression (figure 4.0 & 4.1). The variation in efficiency of knockdown may be the result of varying endogenous expression of the gene or the shRNA, and polymorphisms within the target gene between cells. Varying levels of expression of SUV39H2 relative to GAPDH was confirmed by qPCR, highlighting that SUV39H2 is not expressed in some lines used (figure 4.2).

Two shRNAs upregulated frataxin expression in GM04078 and GM03816 although the GM04078 was found to express the lowest endogenous SUV39H2 relative to GM04503 (a control line). In control lines, SUV39H2 was found to be minimally expressed in GM07492. Despite this, upregulation was also noted in frataxin expression. This may imply an alternative means of upregulation caused by the use of lentivirus, as the empty vector (EV) also upregulated frataxin to the same extent. To help clarify this in future work alternative scramble shRNAs and EV contructs would be of value.

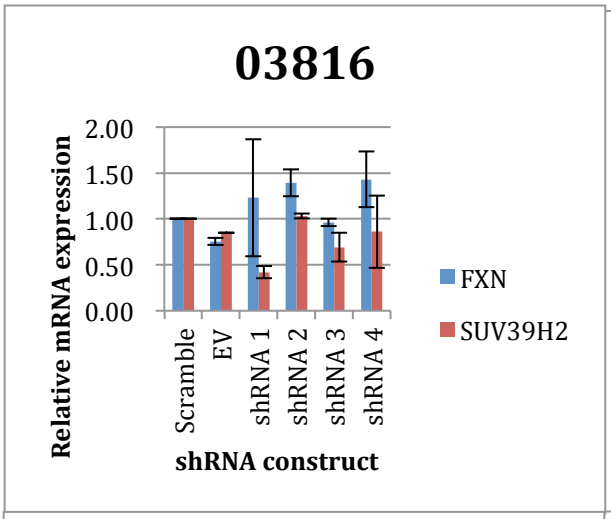

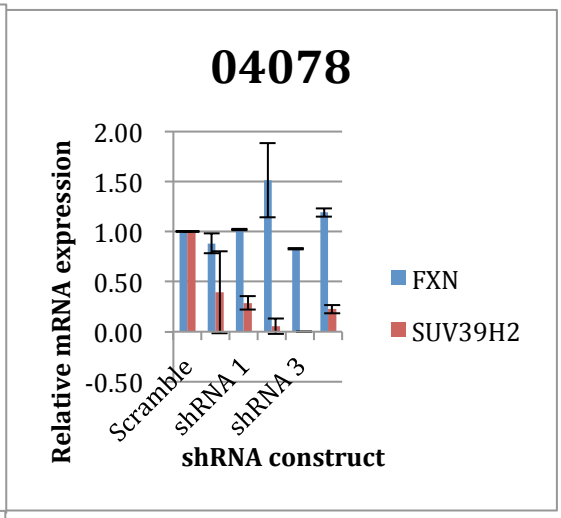

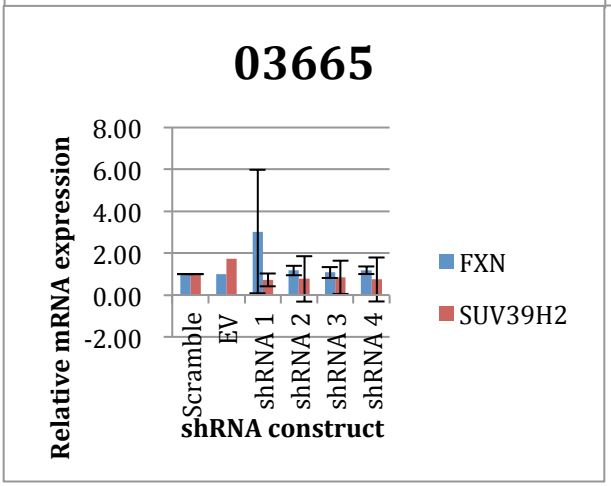

Fig 4.0 shRNA knockdown of SUV39H2 and FXN expression in 3 FRDA cell lines. FRDA lines show variable upregulation with knockdown of SUV39H2 when normalised to scramble shRNA. Y-axis: fold change relative to scramble. X-axis: different shRNA transductions in order of effect on SUV39h. Error bars= SEM

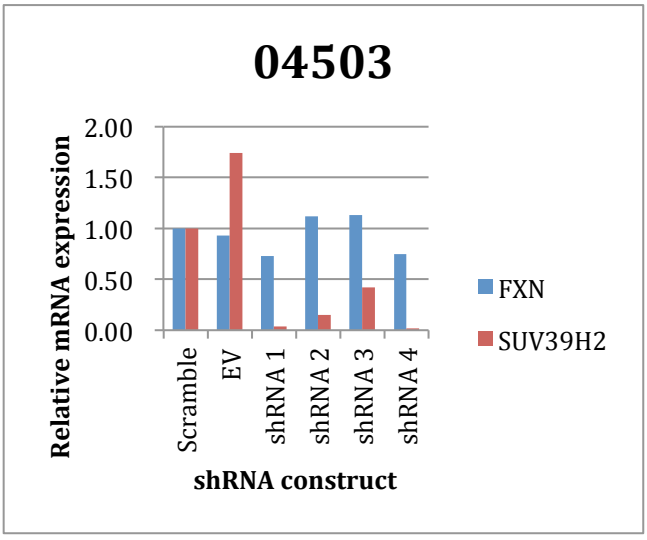

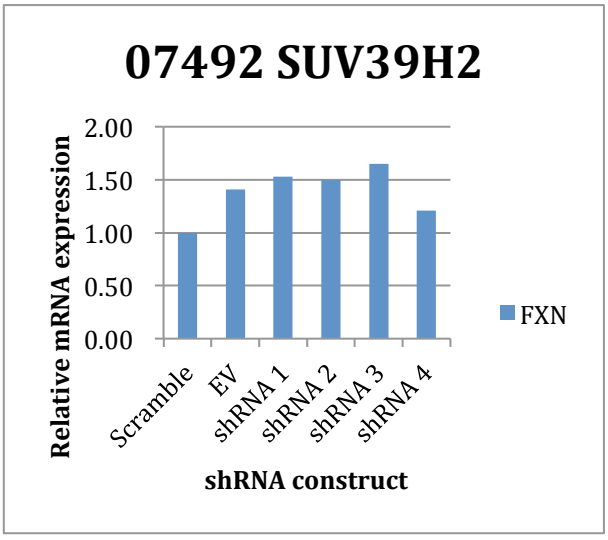

Fig 4.1 shRNA knockdown of SUV39H2 and FXN expression in 2 control cell lines. Preliminary result showing control lines exhibit marginal upregulation of FXN upon SUV39H2 knockdown when normalised to scramble shRNA with respect to transfection with empty vector (EV). SUV39H2 expression in 07492 is minimal even before knockdown and could not be quantified by qPCR. Y-axis: fold change relative to scramble. X-axis: different shRNA transductions in order of effect on SUV39H.

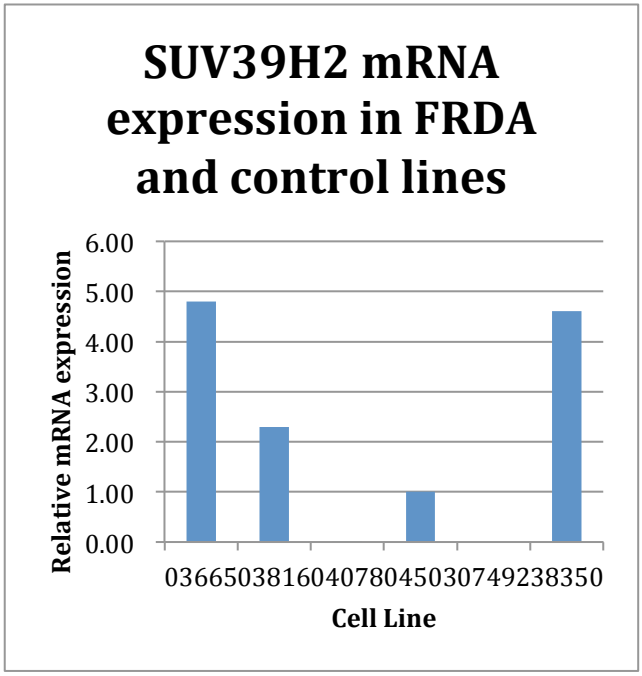

Fig 4.2 SUV39H2 expression in human dermal fibroblast lines. The FRDA lines GM04078 and control line GM07492 do not express SUV39H2. mRNA expression normalised to GAPDH. n=1

Chapter 5

Stable knockdown of SIRT1 has little effect on FXN expression in FRDA lines.

Summary
Due to variability in the level of knockdown between biological replicates, the effect of SIRT1 knockdown on frataxin expression is inconclusive.

Introduction

Lentiviral mediated knockdown of chromatin modifiers, allows for assessment of frataxin expression following several rounds of cell division following drug selection. Silent information regulator 1 (SIRT1) is an NAD+ (class III) dependent histone deacetylase (HDAC). SIRT1 is located in the nucleus and implicated in the formation of heterochromatin, particularly the deacetylation of H3K9. It is a potential candidate for the target of nicotinamide, in its ability to upregulate frataxin expression. SIRT1 was also shown to stabilise SUV39H1, its loss resulting in a reduction in the half-life of SUV39H1.[65]

Results

Six shRNA constructs targeting SIRT1 were transduced into human dermal fibroblast lines and underwent puromycin selection. RNA was collected and analysed by qRT-PCR for efficiency of knockdown and the level of frataxin expression.

There is significant variation between biological replicates in the FRDA lines upon SIRT1 knockdown. This is particularly the case when measuring the level of residual SIRT1. Although there is suggestion of upregulated frataxin expression in GM03665 and GM03816, repeated experimentation using shRNAs that were most efficient might be of value in order to draw a firmer conclusion on the role of SIRT1 in frataxin silencing. Curiously, in the control line, 07492, derived from a normal individual, SIRT 1 knockdown was most efficient (<0.2), however, it correlated with a minor reduction in frataxin levels. This effect might be contributed by the transduction procedure as the empty vector transfection also led to a reduction in frataxin expression. Most shRNAs downregulated frataxin expression in the control line assessed.

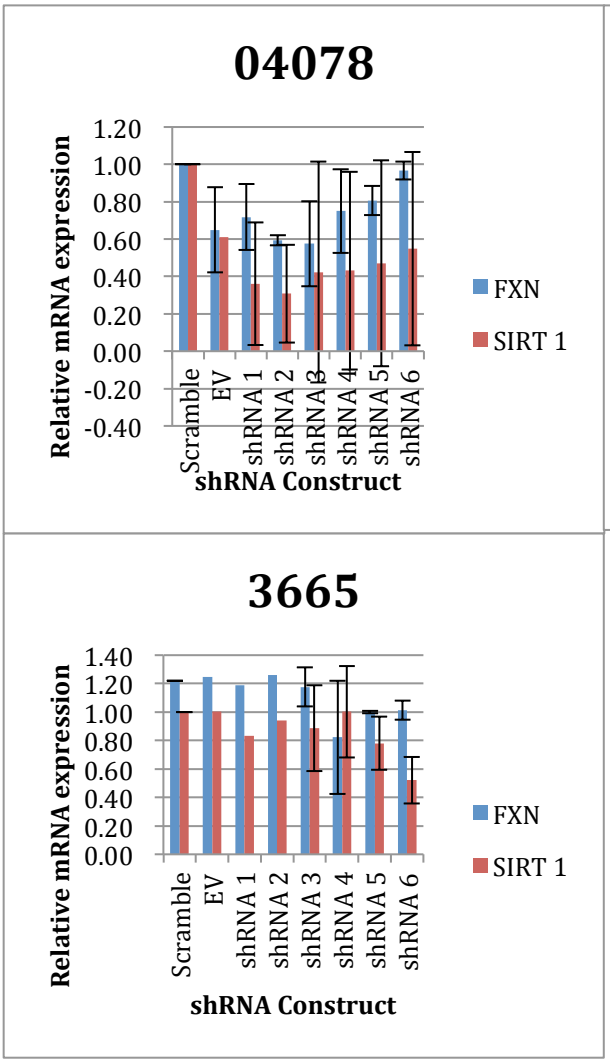

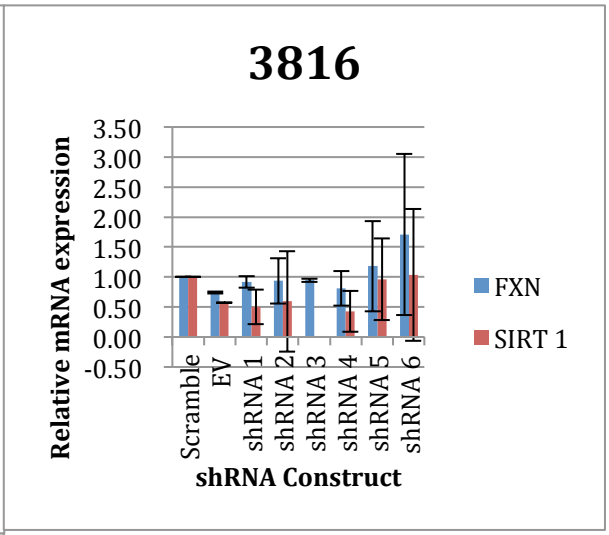

Fig 5.0 shRNA knockdown of SIRT1 and FXN expression in 3 FRDA cell lines. No significant change in frataxin expression was seen in 3 FRDA lines upon knockdown of SIRT1 when normalised to scramble shRNA. Y-axis: fold change relative to scramble. Error bars= SEM

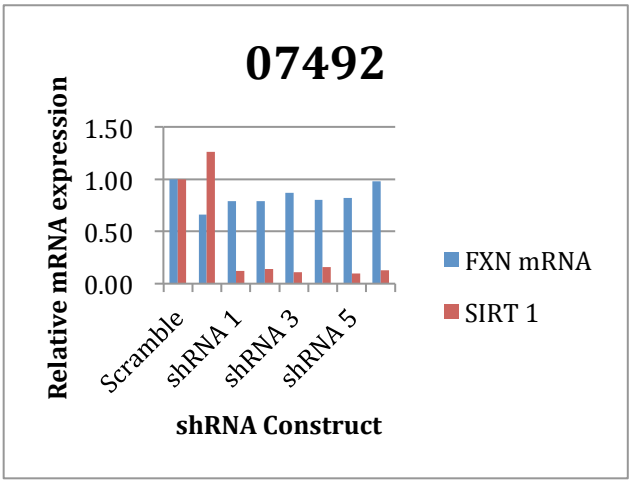

Fig 5.1 shRNA knockdown of SIRT1 and FXN expression in a control cell line. No effect on frataxin expression noted. Y-axis: fold change relative to scramble. X-axis: different shRNA transductions in order of effect on SIRT1. Error bars= SEM

It is apparent from these shRNA experiments that the efficiency of knockdown is variable and cell line dependent. Potential reasons for this difference may be due to differences in expression of each shRNA due to position effects secondary to the site of integration of the vector and variation in other gene expression modifiers between cells (figure 2.0 & 4.2). The effect on control lines is in agreement with the increase in FXN expression previously noted in control lines with nicotinamide, although to a lesser extent.[27] As noted in the shRNA experiments, there does not appear to be a clear correlation between the level of knockdown of these modifiers and FXN expression. The possible explanations for this lack of correlation between the level of knockdown of target proteins and expression of FXN may be due to either the protein being not relevant to frataxin regulation, redundancy within the silencing mechanism, varying repeat length or other genetic differences between each line.

As the physiological function of frataxin is not clearly defined, but is implicated in protection from reactive oxidative stress (ROS), inadvertent cell stress induced by the procedures may be confounding these experiments.[39] Puromycin containing vectors have been shown to induce ROS in human cells.[40] Although such effects might be controlled for by the normalisation to scrambled shRNA as well as siRNA knockdown for SUV39H1 and SUV39H2 which was undertaken.

Having undertaken the above experiments and noting the variation in knockdown efficiency between different shRNAs I subsequently opted to screen future shRNAs, selecting only those showing greatest efficiency of knockdown for more definitive experiments.

Furthermore, the lack of effect noted with knockdown methodologies may be intrinsic to the technique itself, requiring conditional tissue-specific knockout or complete knockout, to more effectively delineate an effect on frataxin expression.

Chapter 6

The Human Silencing Hub complex (HUSH) and frataxin regulation.

Summary

Stable knockdown of several components of the Human Silencing Hub complex (HUSH) showed little effect on frataxin expression. However, in particular knockdown of the lysine methyltransferase SETDB1 led to upregulation of frataxin expression in both FRDA lines, however this effect did not reach statistical significance. This finding was verified with transient siRNA knockdown of SETDB1.

Introduction

Although the modifiers of PEV I have examined in relation to frataxin gene silencing were able to attenuate hCD2 expression in a murine transgenic model[43], their inability to have a clear effect in human cells may relate to species or cell-type specific effects. As such, a recent study identified the HUSH (Human Silencing Hub) complex as being implicated in PEV in a human cell line.[44] Its discovery was by use of a genetic screen. It was initially noted that integration of a GFP construct produced two populations of cells upon flow cell sorting. One population was 'bright' in expression, while the other 'dim' (silenced). The dim population were then used in a viral mutagenesis screen and those in which this silencing was alleviated were analysed to assess which genes were knocked out to reverse the silencing. Subsequent proteomic approaches identified the HUSH complex and SETDB1 as key regulators of PEV in this system. The HUSH complex comprises three nuclear proteins: transgene activation Suppressor (TASOR/FAM208A), M-phase phosphoprotein 8 (MPP8), and periphilin (PPHLN1). The complex was found to be recruited to genomic regions rich in H3K9me3 and subsequently recruited the histone lysine methyltransferase SETDB1, both through MPP8, to further propagate this modification.

Results

An shRNA approach was taken and all hairpins targeting the HUSH complex proteins were screened (figure 6.0). The most efficient were taken forward to assess knockdown on frataxin gene expression in 2 FRDA lines and one control cell line (figure 6.1-6.3).

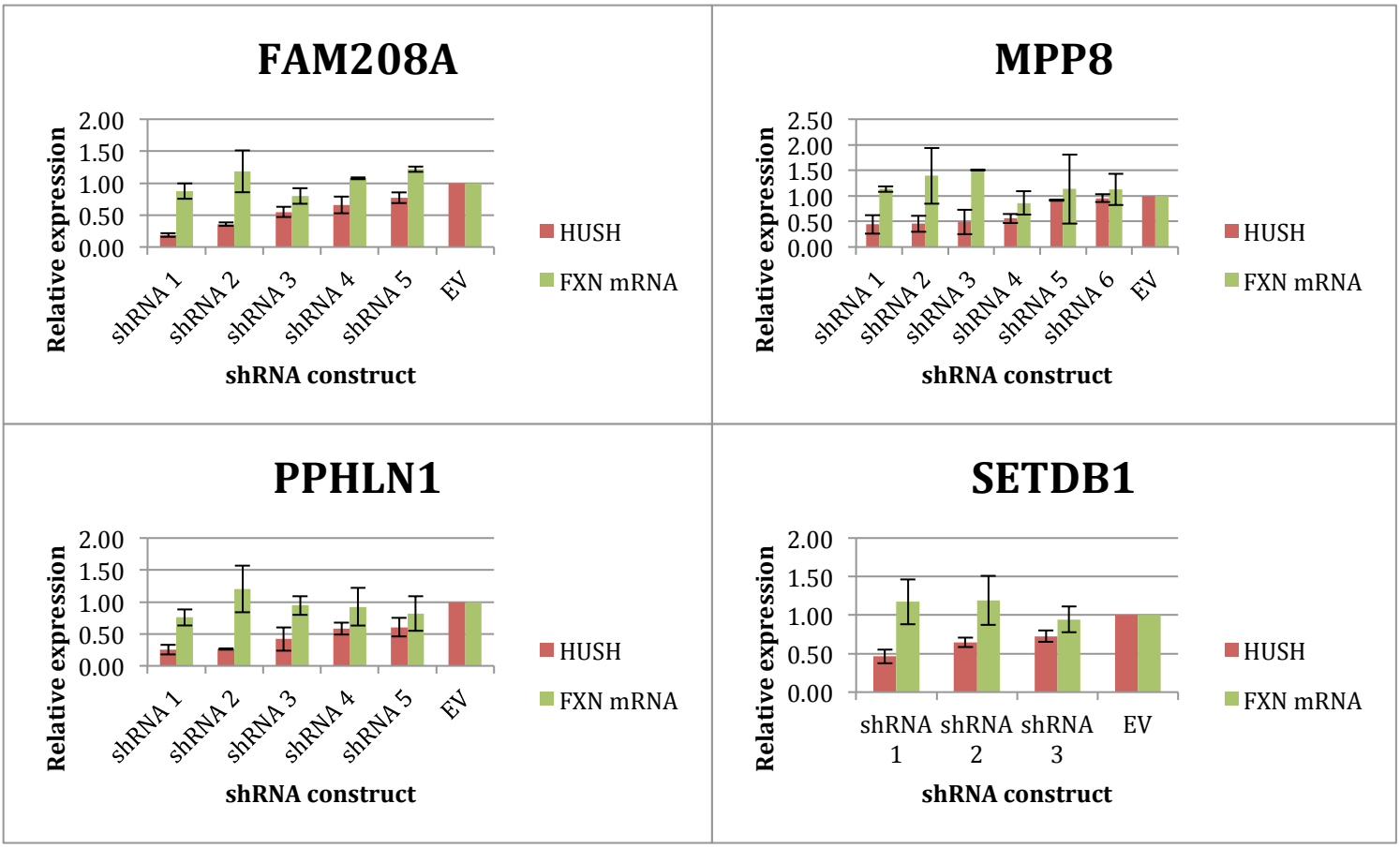

Fig 6.0 Screening of shRNAs for components of human silencing hub complex (HUSH) components and SETDB1 in FRDA fibroblast line GM04078 normalised to empty vector shRNA. shRNA 1 (ordered by level of knockdown efficiency) taken forward for further testing. Error bars: SEM between technical replicates.

Initial screening revealed a potential upregulatory effect on frataxin expression following knockdown with shRNAs against MPP8 (shRNA 1, 2 and 3) and SETDB1 (shRNA 1 and 2) (figure 6.0). This is intriguing as MPP8 is able to read H3K9me3 as well as recruit SETDB1 for propagation of the mark.

In the 2 FRDA lines (GM04078 and GM03816) assessed with shRNAs against HUSH complex components only SETDB1 knockdown resulted in a trend towards upregulation in frataxin (figure 6.1 and 6.2). Further biological replicates may be required to highlight true significance. The ability to re-repress expression would also

be valuable through reintroduction of the enzyme. MPP8 knockdown, however, showed no effect on frataxin expression in all lines. PPHLN1 knockdown appears to upregulate frataxin in GM04078, yet there was significant variation between replicates. No effect was noted in GM03816. Interestingly, no upregulation of frataxin expression was noted in the control line tested (GM07492) suggesting that the effects seen may be GAA-repeat expansion dependent (figure 6.3).

Given the suggestion of a common effect on frataxin expression by SETDB1 knockdown. A transient knockdown was undertaken for independent verification of the result (figure 6.4), here frataxin expression increased in both disease lines and not in the control line.

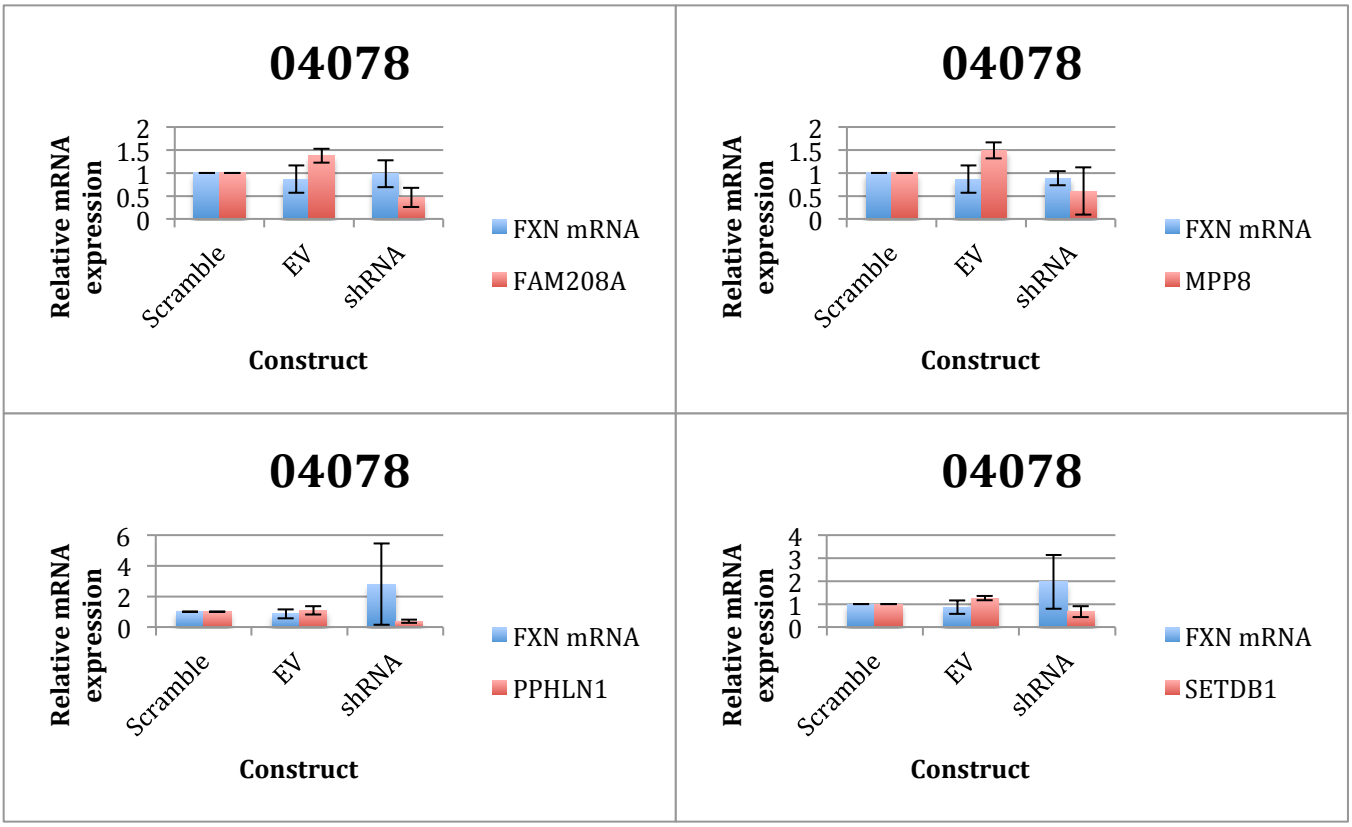

Fig 6.1 shRNA knockdown of human silencing hub complex componenets (HUSH) and SETDB1 in FRDA fibroblast line 04078 normalised to scramble shRNA. A trend towards upregulation in frataxin expression was noted following SETDB1 knockdown. Error bars: SEM of 2 independent experiments.

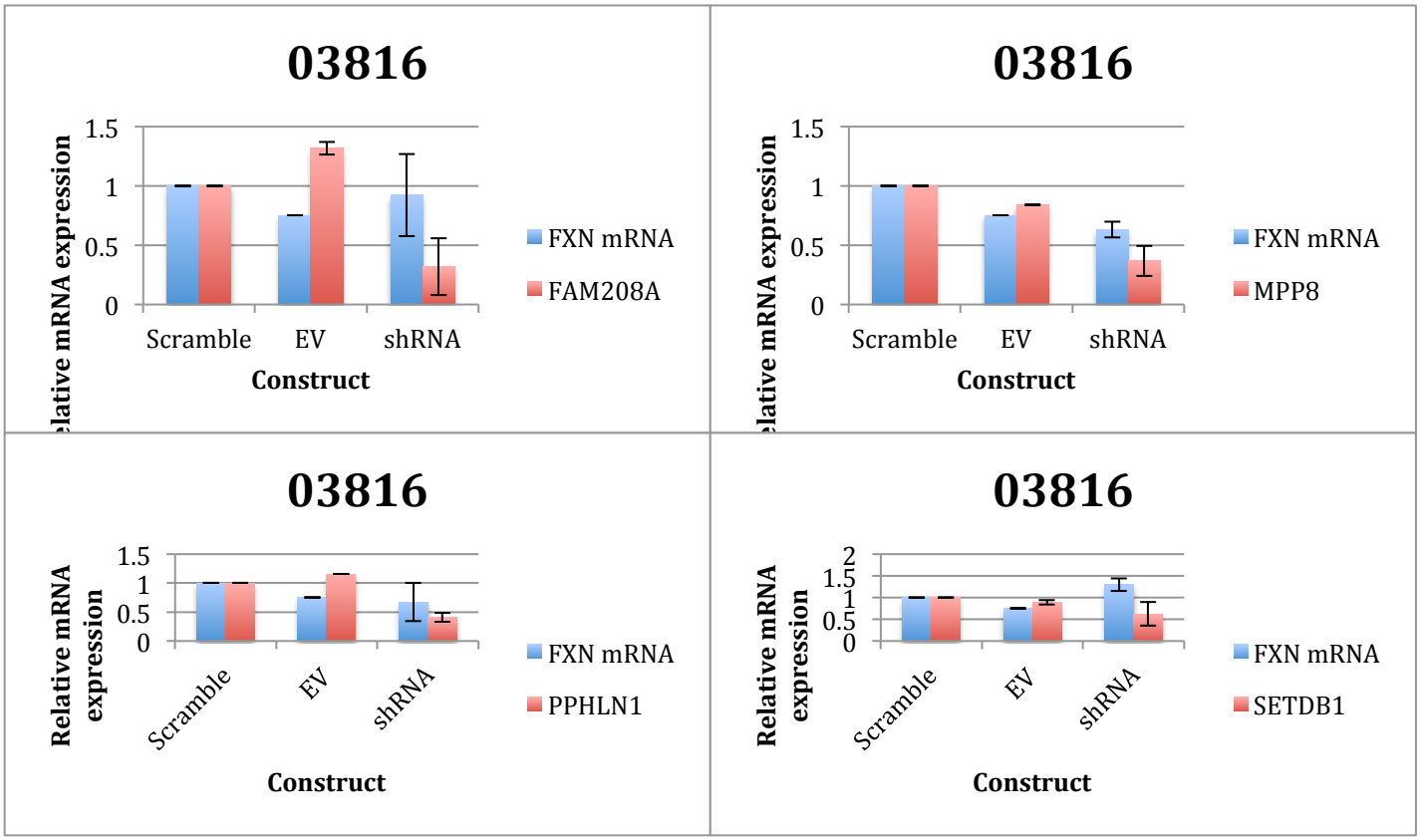

Fig 6.2 shRNA knockdown of human silencing hub complex components (HUSH) and SETDB1 in FRDA fibroblast line GM03816 normalised to scramble shRNA. Trend towards upregulation noted with SETDB1. Error bars: SEM of 2 independent experiments.

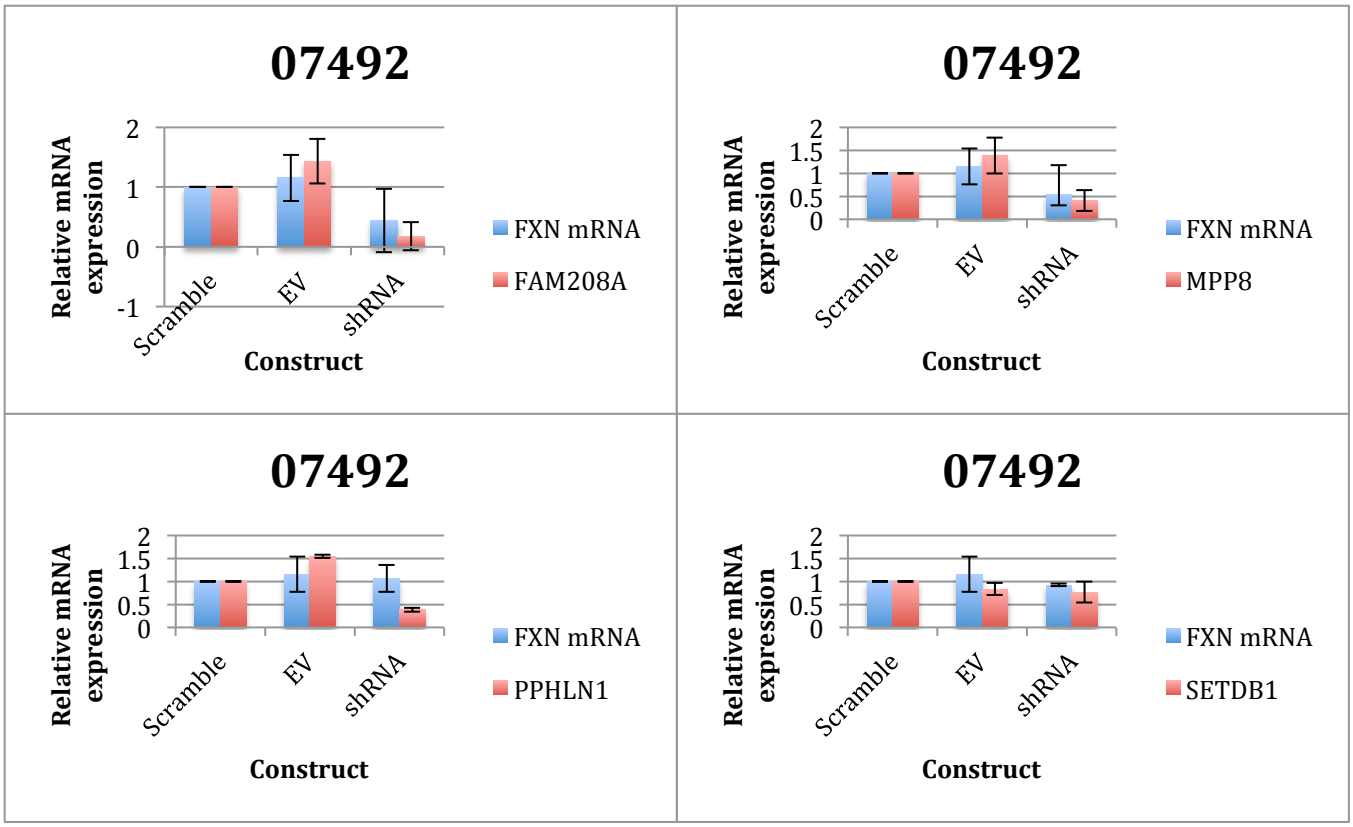

Fig 6.3 shRNA knockdown of human silencing hub complex components (HUSH) and SETDB1 in control fibroblast line GM07492 normalised to scramble shRNA. No effect on frataxin

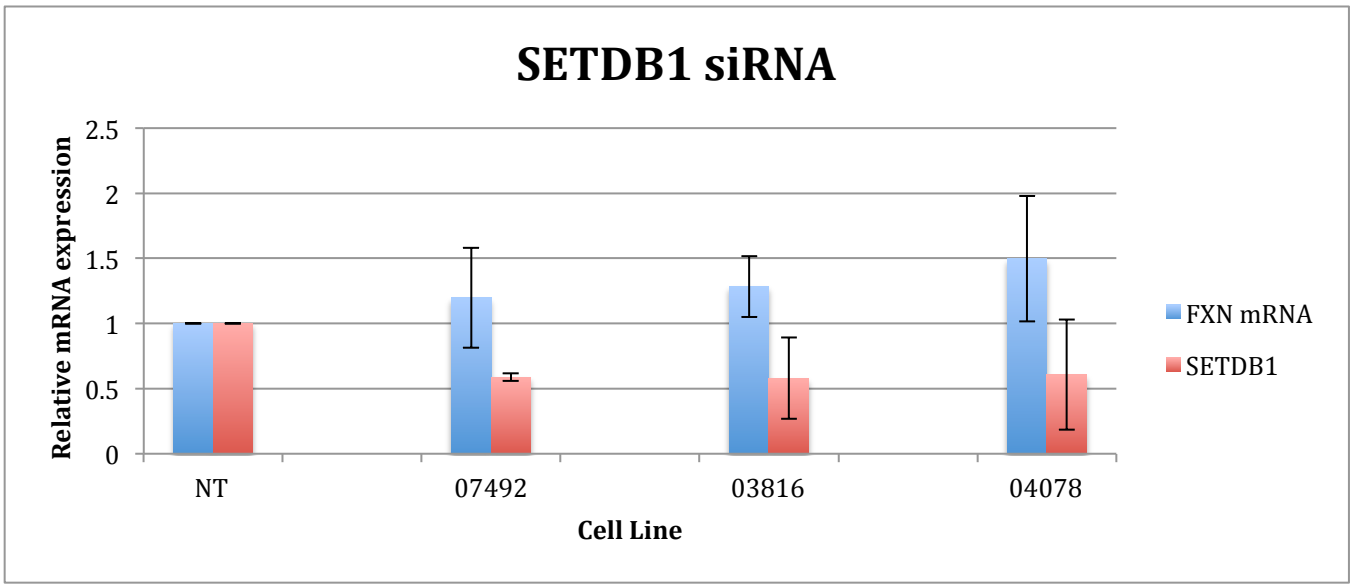

Fig 6.4: siRNA knockdown of SETDB1 in 2 FRDA lines (GM03816 and GM04078) and 1 control line (GM07492). Upregulation of frataxin expression in FRDA lines normalised to scramble shRNA. Error bars: SEM of 2 independent experiments.

siRNA knockdown of SETDB1 to assess the acute effect on frataxin expression supports the findings of the shRNA experiments for a potential regulatory role in pathological frataxin silencing (figure 6.4).

Chapter 7

Transcriptional activation of the FXN gene using dCas9-p300 by targeting the locus using CRISPR

Summary

Frataxin expression was upregulated by 1.5 fold by targeted Cas9 proteins fused to the histone acetyltransferase p300. Targeted promoter sequences vary in their ability to alter gene expression, with some lowering overall expression. This may be related to interruption of transcription factor binding or enhancer interaction.

Introduction

Frataxin (FXN) gene silencing is the result of an abnormal trinucleotide expansion within intron 1 of the FXN gene.[1] This has been shown to result in an abnormal epigenomic environment within the locus, with the presence of the silencing chromatin modifications H3K9me3 and H3K27me3.[27] Although several components have been implicated in the establishment of this environment, from aberrant histone and DNA methylation, heterochromatin and R-loop formation and antisense transcription, the direct causality of each of these factors and its relevance to FXN gene silencing remains elusive, as well as the relative importance of each factor with respect to different intra-locus elements (e.g. promoter, upstream of GAA and downstream of GAA). With the advent of RNA guided endonuclease technology (CRISPR), there is now the possibility to interrogate these factors in a locus-specific fashion. To do this, nuclease dead Cas9 fused to epigenome modifiers and transcriptional activators.[34] Such an approach will not only provide insight into the mechanism of aberrant FXN silencing but might also lead to a novel and radical therapeutic approach for FRDA and potentially other epigenetically regulated disorders.

With CRISPR technology regions of the genome can be targeted in 20 nucleotide sections. This specificity means that several questions regarding the relative importance of histone modifications and other epigenetic regulatory mechanisms at the promoter, the upstream region of the GAA expansion and the downstream region can be directly addressed.

Results

Hypothesis: Targeting dCas9 activators to the frataxin locus will upregulate gene expression.

Modified HEK293T lines which contain an integrated frataxin BAC were used due to ease of transfection (Figure 7.0).[45] gRNAs pools (13 gRNAs targeted to the promoter, 5 upstream of the GAA repeat region and 5 downstream) were transfected with dCas9 activators and mRNA expression was measured 48 hrs after transfection. Primers spanning the exon 5a luciferase boundary region were used to differentiate

endogenous frataxin expression from that of the BAC (figure 7.0). Expression was measured in both a disease model line (Figure 7.1: FXN-GAA-Luc) and unaffected line (Figure 7.2: FXN-Luc) (Gift from Michael Lufino, Oxford, UK).[45] Verification of integration was undertaken through PCR and Sanger sequencing. Maintenance of hygromycin selection ensures transgene expression is maintained.

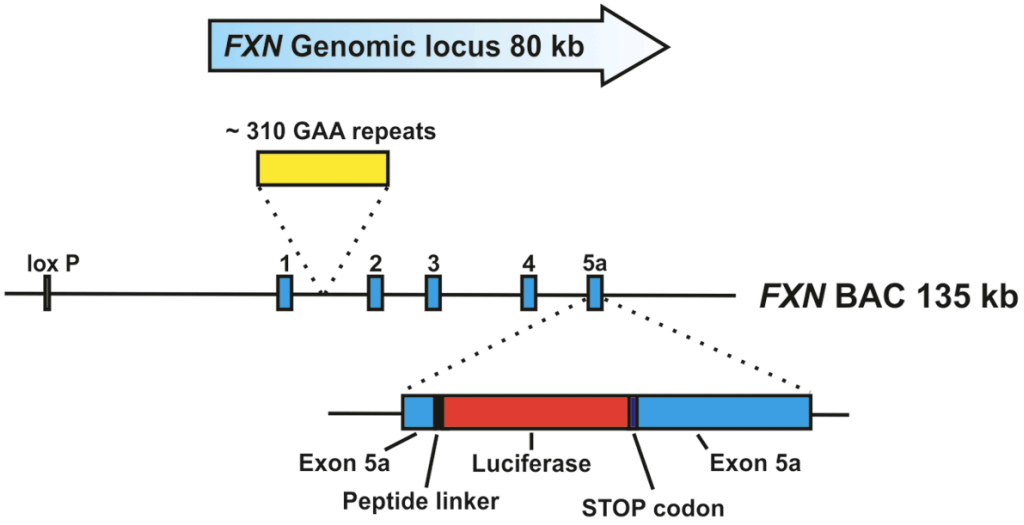

Figure 7.0 Modified frataxin BAC. Luciferase is inserted within exon 5a. The entire BAC was integrated in to chromosome 1p and clones with a single integration were selected. Image adapted from Lufino et al HMG 2013.[45]

Results shown are from 3 biological replicates. Targeting dCas9-VPR to the promoter and upstream regions of the frataxin BAC with pools of gRNAs did not result in any upregulation of expression. There is a suggestion of upregulated expression when targeting the downstream region, although significance was not reached. Using dCas9-p300 a trend towards upregulation is noted when targeting the upstream region of the GAA repeat, up to 1.4 fold upregulation on FXN expression was noted with use of pooled guides in the disease model line (figure 7.1).

The same pooled gRNA transfections were undertaken in an isogenic line without the GAA expanded transgene. Here the dCas9-VPR downregulated expression at all targeted loci. dCas9-p300 again showed a trend towards upregulation when targeted to the upstream region in an unexpanded line. As targeting of dCas9 within gene bodies is known to act as inhibitor of transcription (CRISPRi) the overall effect seen may be the combined effect of that between both an increase in transcription afforded by the activator/p300 and CRISPRi.[65] Additionally the use of pooled guides may mask the upregulatory effect of specific regions as noted when using single guides targeting the promoter (figure 7.3).

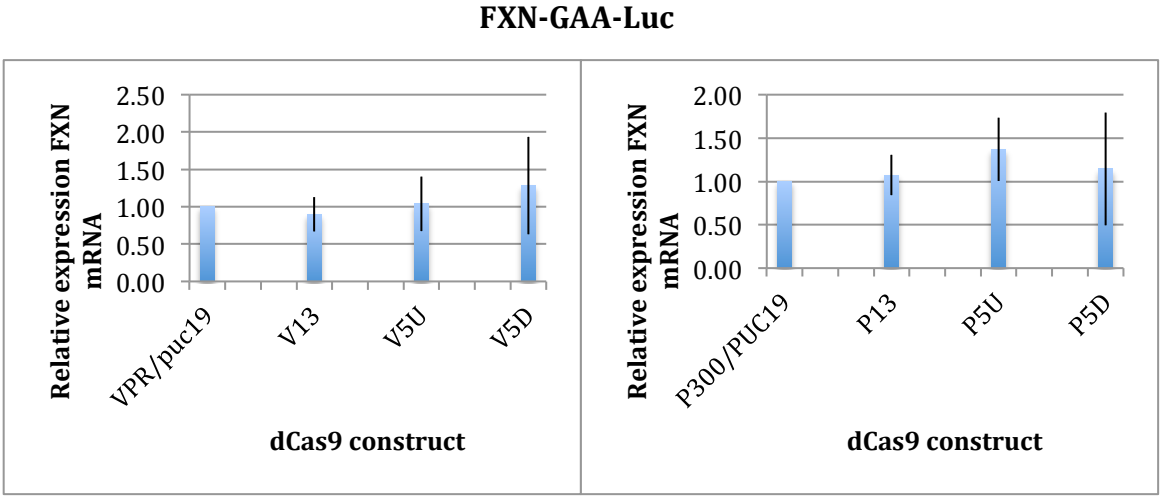

Fig 7.1 Relative expression of FXN mRNA normalised to GAPDH in FXN-GAA-Luc line. Left: dCas9-VPR and puc19 (VPR/puc19), dCas9-VPR and 13 gRNA pool to FXN promoter (V13), dCas9-VPR and 5 gRNA pool to upstream GAA and dCas9-VPR and 5 gRNA pool to downstream GAA. Right: As left with dCas9-p300.

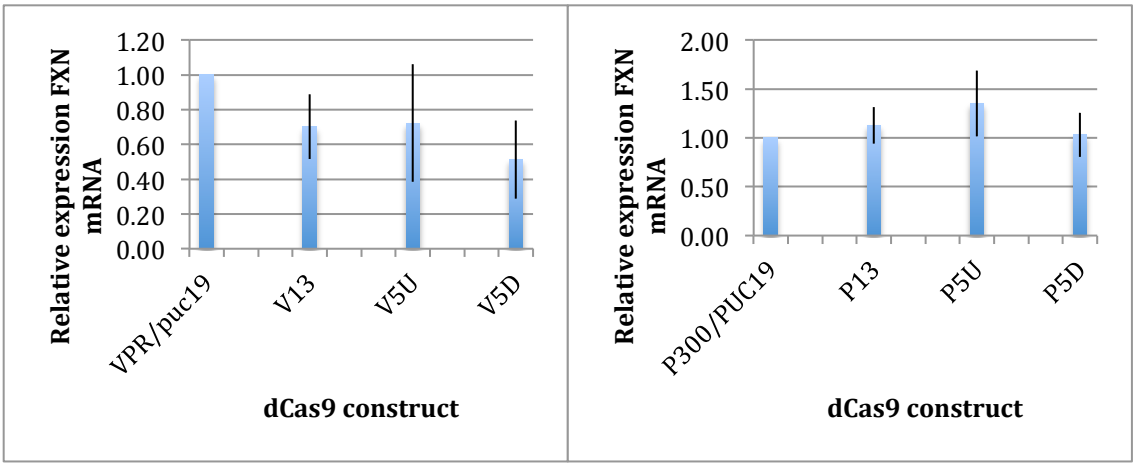

Fig 7.2 Relative expression of FXN mRNA normalised to GAPDH in FXN-Luc line. Left: dCas9-VPR and puc19 (VPR/puc19), dCas9-VPR and 13 gRNA pool to FXN promoter (V13), dCas9-VPR and 5 gRNA pool to upstream GAA and dCas9-VPR and 5 gRNA pool to downstream GAA. Top right: As left with dCas9-p300.

However individual gRNA transfections were able to highlight that specific gRNAs upregulated expression, while others did not alter it, or even inhibited it (figure 7.3).[45]

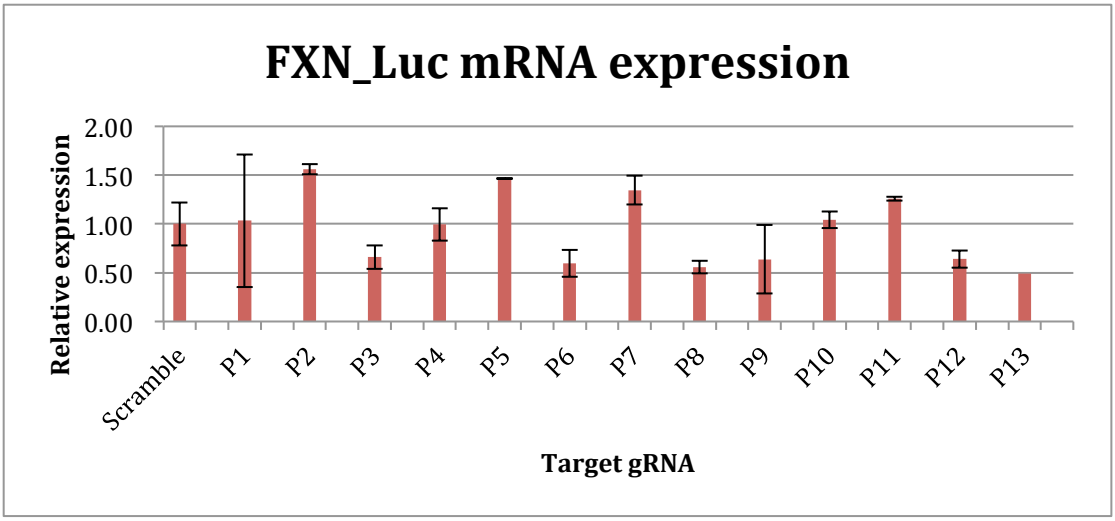

Fig 7.3: Individual gRNAs targeting dCas9-p300 to FXN promoter. Up to 1.5 fold upregulation was noted at target sites P2, P5 and P7. n=2, error bars: SEM.

This data suggests that targeting the acetyltransferase p300 to the silent FXN locus is able to increase gene expression. Targeting other modifiers of chromatin to the locus are worthwhile avenues of investigation to delineate a potential hierarchy or network of factors important in FXN gene silencing. This approach may also be applied in other cell types specifically affected in FRDA, particularly cardiomyocytes and neurones, in which developmental programs will differ and may highlight varying causes of gene silencing.

Chapter 8

Targeted histone mutant peptides upregulate frataxin expression

Summary

dCas9 fused to N-terminal tails of histone 3.3 wild type and mutant peptides can upregualte frataxin expression when targeted to specific regions within the frataxin locus. Significant upregulation was noted when H3.3 was targeted downstream of the GAA and H3K9M was targeted to the promoter (two tailed t-test, $p<0.05$). Significant downregulation was noted upon targeting H3K27M to the promoter and downstream of the of the GAA repeat (two tailed t-test, $p<0.05$).

Introduction

The histone modifications H3K9me3 and H3K27me3 are found to be associated with the pathologically silenced frataxin gene in FRDA. It is unknown whether their presence is necessary or sufficient to induce frataxin gene silencing.

It has recently been discovered that several cancers result from somatic mutations in histone 3.3 genes (H3F3A and H3F3B), whereby lysine-to-methionine substitutions occur at position 9 or 27 of their N-terminal tails.[66,67,68] These substitutions function as dominant negatives, resulting in genome-wide reduction of H3K9me3 and H3K27me3, respectively. Subsequent work has shown these histone mutants allosterically inhibit H3K9 and H3K27 methltransferases (e.g. SUV39H1, G9A and SUZ12). Small molecule inhibitors of these methyltrasferases exist, however as the enzymatic systems are distinct, a dual inhibitor has not been described. However, lysine-to-methionine substitution at position 27 of the N-terminal tail was able to cause global reduction of H3K27me3 in Drosophila as well as, to a lesser extent, H3K9me3. This provides evidence for a possible single modifying method that can potentially address both histone modifications associated with frataxin gene silencing.

Results

Transient overexpression of histone 3.3 (H3.3) in FXN-GAA-Luc cells resulted in significant upregulation of frataxin expression with WT H3 and H3K9K27M. A trend towards upregulation was also noted with H3K27M (figure 8.0).

Stable lentiviral integration with subsequent selection and assessment at 1 week resulted in decreased expression of frataxin in all lines (figure 8.1). The downregulation noted on prolonged expression may be due to induction of secondary pathways and toxicity.

As transient overexpression of H3.3, H3K27M and H3K9K27M resulted in upregulation of frataxin but did not do so in stable expression, this highlights the potential need for locus-specific assessment as well as temporal control of expression. Both transient expression and stable expression will likely result in genome-wide changes.

As such WT and mutant N-terminal tail peptides were fused to the C-terminus of dCas9 and targeted to the frataxin locus (figure 8.3). Upregulation of expression was noted with constructs containing WT H3.3 targeted to the promoter (H3.3 PRO13), the downstream region of GAA (H3.3 5D, $p<0.05$), H3K9M targeted to the promoter (K9 PRO13, $p<0.05$) and H3K27 to the upstream GAA region (K27 5U). Downregulation was seen with H3.3 targeted to the upstream GAA region (H3.3 5U), H3K27M to the promoter (K27 PRO13, $p<0.05$) and downstream of the GAA (K27 5D, $p<0.05$).

It is interesting that both in transient and locus-specific experiments WT H3.3 was able to upregulate frataxin expression. A potential mechanism for this could relate to sequestration of factors from silenced chromatin (including frataxin) resulting in upregulation. Alternatively, H3.3 is known to be associated with active genes and facilitate the loading of RNA Pol II at gene promoters, which may explain the upregulation in frataxin.[69]

The changes in frataxin expression noted upon targeting may be the result of local inhibition of methylation. This could be assessed by chromatin immunoprecipitation (ChIP).

From this data a possible hierarchy of factors may be established such as the importance of K9 methylation at the promoter relative to K27, as upregulation was not noted with the latter.

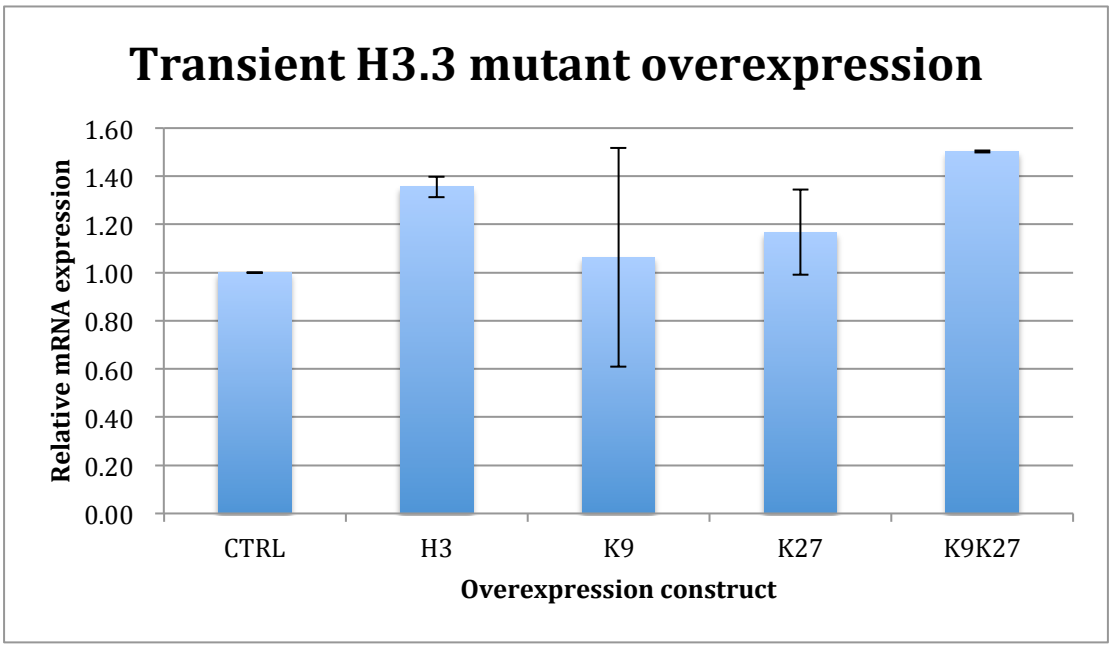

Fig 8.0 Transient overexpression of empty vector (CTRL), histone H3.3 (H3), H3K9M (K9), H3K27M (K27) and H3K9K27M (K9K27) in FXN-GAA_Luc cells. FXN_Luc mRNA expression was measured relative to GAPDH at 48hrs. H3.3 and H3K9K27M overexpression at 48hrs resulted in significant upregulation of frataxin ($p<0.05$). Error bars: SEM from 2 biological replicates.

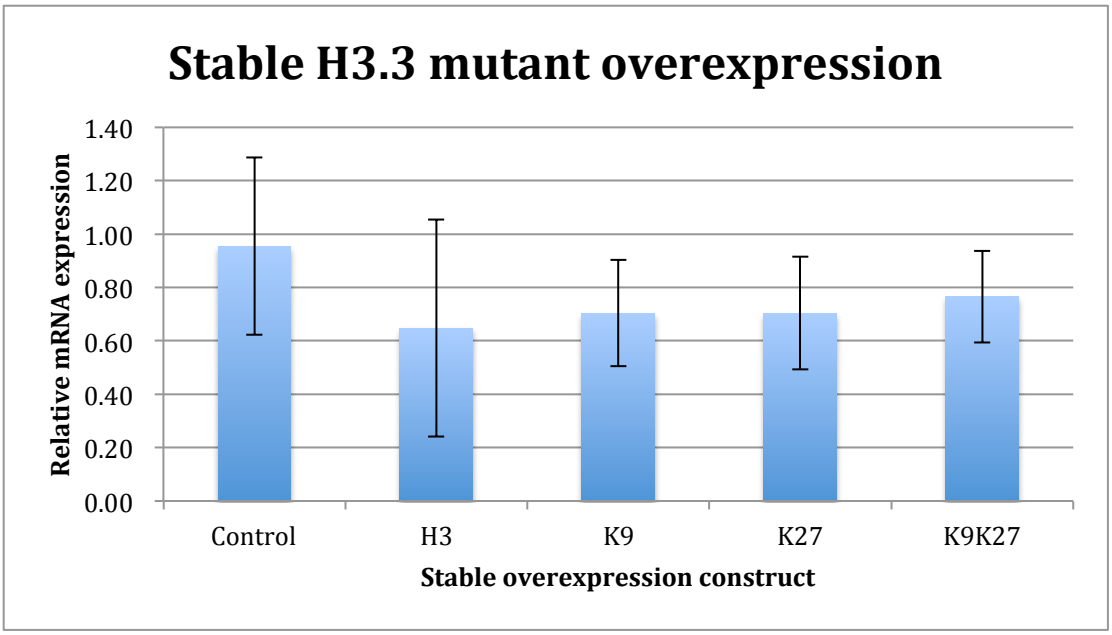

Fig 8.1 FXN-Luc mRNA expression measured after selection and stable expression at 1 week. Downregulation of frataxin noted from all lines (K9, $p<0.05$). Error bars: SEM from 4 biological replicates.

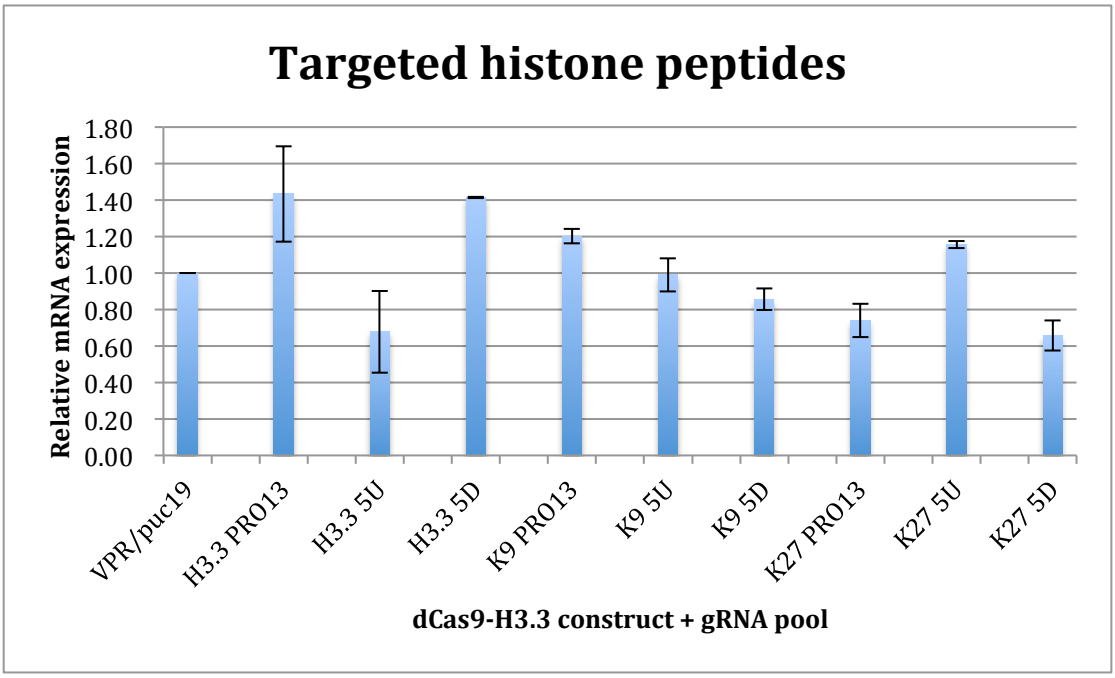

Fig 8.2 FXN-Luc expression measured after 48hrs following transfection with dCas9-H3.3 fusions using pooled gRNAs (PRO13 – 13 promoter gRNAs, 5U 5 GAA upstream gRNAs, 5D – 5 GAA downstream gRNAs). Wild type H3.3 (H3.3). K9 (H3K9M), K27 (H3K27M). Error bars: SEM from 2 independent experiments.

Discussion

The ability to produce mRNA from the pathologically silenced frataxin allele in FRDA provides both an interesting model of gene silencing as well as the hope that a therapeutic agent can be found.[2] I have investigated various epigenetic gene silencing mechanisms that are thought to be important in FXN silencing, in particular heterochromatin mediated silencing.

Since the description of frataxin gene silencing in FRDA, a number of epigenetic mechanisms have been implicated including DNA methylation, antisense transcription, R-loop formation as well as histone methylation.[17] Recently insights into 3D chromatin structure have also indicated alterations at the FXN locus, which may also introduce gene regulation by way of altered contact with regulatory elements such as enhancers.[27]

Despite the various avenues investigated in this thesis, an inconclusive result was seen in many of the pathways addressed. Given the complexity and the interrelation of gene regulatory mechanisms, it is likely that significant alteration in frataxin expression will result from methods addressing several and potentially all mechanisms of silencing. Establishing a hierarchy of these regulatory mechanisms, may point to a seed event in heterochromatin mediated gene silencing stemming from DNA repeats.

The earliest insight into an epigenetic silencing mechanism in frataxin gene silencing was shown through a murine model of PEV, where expression of a human CD2 transgene with a GAA expansion at its 3' end was altered by dosage off archetypal modifiers of position effect variegation (PEV) (e.g. HP1 and SUV39H1).[43]

The work I have conducted, in addition to my gained understanding of the field over the course of my doctorate has led me to consider that further evidence is required to support the claim that Friedreich's Ataxia is a prototypic PEV mediated disease, as speculated by Savielev et al.[43] A PEV mediated disease, is one in which pathological gene expression states are the result of proximity to regions of heterochromatin. This transcriptional state or program would then be 'locked in' through cell division, but amenable to attenuation or reversal through alteration of components implicated in heterochromatin formation and/or maintenance. Further evidence to support the claim that *fxn* is subjected to PEV would include single-cell methodologies to assess heterogeneity in frataxin expression within a population of human cells and their sensitivity to modifiers of variegation. Recently single cell immunofluorescence studies have showed that the diseased allele locates near the nuclear periphery (where heterochromatin is frequently located) and upon treatment with nicotinamide and other compounds that increase frataxin expression moved toward the centre of the nucleus.[64] The findings of Saveliev et al. are specific to the regulation of transgene expression in association with trinucleotide repeats in mammalian systems. It should be noted that in this system CTG repeats also induced position independent variegation,[43] which is interesting as these repeats are associated with the disease myotonic dystrophy type 1 (DM1), which is known to be result from toxic gain-of-

function of the transcribed repeats through sequestration of RNA binding proteins.[46] However the CTG repeats, which are within the 3' UTR of the DMPK gene resulting in loss of a nearby hypersensitive site are also within the promoter of the Six5 gene, downregulation of which is thought to result in adult onset cataracts, the commonest ocular phenotype in DM1.[47] The HUSH complex (FAM208A, MPP8, PPHLN1) was recently shown to modify transgene related PEV in human cells.[44] The lack of effect seen upon knockout of this complex also supports that an alternate hypothesis to PEV mediated silencing is implicated in frataxin gene silencing. Interestingly however the lysine methyltransferase SETDB1, which is known to associate with the HUSH complex, upregulated frataxin expression upon knockdown. SETDB1 is able to both dimethylate H3K9 and subsequently trimethylate it in association with the human homolog of mAM, a murine ATFa-associated factor.[48] ATF7IP was recently shown to phenocopy SETDB1 knockout. ATF7IP knockout permits SETDB1 nuclear transport and protection from proteosomal degration.[49] This is particularly interesting as, unlike SUV39H1 the archetypal H3K9 trimethylase, a hallmark of pericentromeric heterochromatin and modifier of PEV, SETDB1 links both gene silencing (H3K9me2) and heterochromatin formation (H3K9me3). It has been shown however that several H3K9 methyltransferases (Suv39h1, G9a, GLP and SETDB1) also exist as a multimeric complex.[50] Knockdown of this entire complex may be interesting to assess its effect on frataxin expression. At present no direct inhibitor of SETDB1 exists. As SET domains are common to many proteins, inhibitors of this domain are likely to result in significant 'off-target' effects. Molecules that can interfere with the association of ATF7IP and SETDB1 may form a new class of compounds that can more directly attenuate SETDB1 function on the pathologically silenced frataxin locus.[49]

One rationale for the screening approach of modifiers of variegation (SUV39H1 and SUV39H2 – H3K9 trimethylases, BMI1 – a component of the polycomb repressor complex which methylates H3K27) used in this thesis was to determine the potential targets of nicotinamide, which has been shown in cellular and murine models, as well as human subjects to relieve frataxin gene silencing.[27] In addition another potential target of nicotinamide assessed was SIRT1, which is an NAD+ dependent deacetylase.[51] Treatment with nicotinamide deprives the enzyme of NAD+ and prevents deacetylation. Chromatin immunoprecipitation following nicotinamide treatment showed a reduction of both H3K9me3 and H3K27me3 at the frataxin locus along with an increase in mRNA expression.[52] This result suggests that relief of both heterochromatin marks is necessary to promote frataxin expression. As the mammalian genome is distinctly organised into chromatin domains and sub-domains, agents that perturb epigenetic marks genome wide will likely result in off-target gene expression.[53]

Transcriptional activation by DNA binding proteins fused to transcriptional activators has been shown with both TALEN and CRISPR technologies.[54] Yet these methodologies do not address the gene suppression imparted by the variety of epigenetic modifications associated with the frataxin locus. I have attempted to do this with the use of dCas9-P300, which can acetylate H3K27 residues and H3K122 residues, as well as non-histone proteins.[55] This chromatin modification is found

along the silenced *fxn* allele.[17] The modest effect seen with these experiments on frataxin upregulation is likely the result of the need in this system to address multiple epigenetic regulatory mechanisms in tandem (H3K9 methylation, DNA methylation and R-loop formation). With the evolving ability to multiplex CRISPR technologies, and the variety of CRISPR associated proteins being discovered (e.g. Cpf1) it can be imagined that combinatorial experiments may be conducted at one locus, through targeting several factors that may relieve each layer of frataxin silencing.[56]

How to identify key regulators of frataxin expression and repression

The work I have conducted during my doctorate can be described as a targeted or biased screen. This forms the basis of much scientific research, which is hypothesis driven, building on previous work in the field. However it could be argued, that where the underlying mechanisms of gene regulation are poorly understood, adopting an unbiased approach might be more likely to result in discovery of the most pertinent pathways. With the development of a number of genome-wide approaches and the ability to subsequently carry these forward in a locus specific manner, the combination of these methods is likely to provide the greatest and most robust insight into frataxin gene regulation.

A potential experiment

Isogenic lines in both sexes are created from FRDA or carrier lines, with and without GAA expansion. This controls the genetic background between disease and control lines. One such model line has been created by zinc-finger mediated excision of the GAA repeats, with resulting correction of mRNA and protein expression, resolution of chromatin signature to that of a non-disease allele and this was maintained through reprogramming and differentiation to neurones.[4] A correction of the mitochondrial bioenergetic phenotype was also shown. Where untransformed lines are used, and to overcome the slow growth phenotype seen with many fxn lines they can be reversibly immortalised, such as through integration and expression of hTERT, BMI1 and tTag under a Cre-lox system.[57,58] Appropriate characterisation to ensure these do not alter frataxin expression would be needed before experimentation.

A reporter could be integrated into the endogenous frataxin locus. Either an RNA or protein reporter should be integrated into the 3' end of the endogenous locus. Such an RNA reporter would be a MS2 binding loop, which would allow in-vivo imaging of frataxin RNA expression. In-frame knock-in of green fluorescent protein (GFP) would permit real-time protein expression analysis as well as fluorescent cell sorting. HEK293T cellular based models using MS2 based RNA imaging and endogenous frataxin expression (although in an unexpended allele) have been previously created for screening.[59] Use of the endogenous frataxin locus will permit more physiological assessment without confounding from polyploidy and altered genetic environment seen with 293T lines.

Following creation and validation of these tools, whole exome (for potential therapeutic targets) or genome (for regulatory elements) CRISPR knockout screens on

the disease lines (at least one from each sex) with subsequent cell sorting for increased fluorescent protein expression and enrichment analysis may identify endogenous regulators of frataxin expression. This screening would require a significant level of optimisation, as the dynamic range of frataxin expression is limited and should be able to detect from 1.5 fold upregulation as a positive hit. These hits may then be verified by knockdown or knockout. Undertaking this experiment in the isogenic repeat-excised (control) lines may provide important information regarding physiological frataxin regulation.

The lack of effect noted with the archetypal modifiers of position effect variegation assessed in this thesis may be explained in a number of ways. The first of these is through the existence of several other chromatin modifiers introducing biological redundancy to the system. To address this an attempt to sequentially as well as in concert knockout the known lysine methyltransferases would be of value to assess the relative importance in silencing. With the recent discovery of dominant negative mutations in histone *H3F3A* and *H3F3B* genes that result in genome-wide reduction in H3K9me3 or H3K27me3, expression of either or both these mutant proteins may provide insight into the relative importance of each heterochromatic mark to frataxin silencing.[60] Within the hCD2 system it appears that despite the sequence of repeats tested (GAA, CTG, Igf2) this was able to result in PEV silencing, which was sensitive to several modifiers (SUV39h1 and HP1).[43] Conducting this experiment in a human system, with the relative (though not trivial) ease of genome engineering, within endogenous genes may provide more physiologically relevant insights into repeat induced silencing and potentially PEV.

The seed event, that triggers gene silencing downstream of the GAA expansion still remains illusive. As excision of these repeats has been shown to reverse the cellular phenotype, introduction of repeats into intron 1, may help to identify this event.[4] One could imagine an experiment using an inducible promoter system to assess in a time-course the effect of transcription through a frataxin locus with and without GAA repeats. Such an experiment could assess for the presence and change in epigenetic regulatory mechanisms at the locus.

Repeat induced silencing has also been shown to be sensitive to imprinting, with greater silencing noted through maternal inheritance of the repetitive allele.[61] The possible relevance of this to fxn silencing could be investigated through introduction of single nucleotide polymorphisms into the FXN BAC such that maternally and paternally inherited transgenes and their methylation state could be differentiated in offspring.[62]

In summary, epigenetic silencing of the frataxin locus is maintained by several layers of complex regulation that appear to work in concert, with significant biological redundancy. The ability to reactivate the gene (e.g. with Nicotinamide) and upregulate endogenous expression is a promising therapeutic avenue. Seed events establishing heterochromatin mediated silencing at the frataxin locus are yet to be elucidated as well as the potential for epigenetic memory within silencing and reactivation.

Future work

With respect to the data presented in this thesis I am continuing to work on several areas with a view to publication:

1. Further clarifying the relevance of SETDB1 as a modifier of frataxin expression. I am doing this through further knockdown experiments, chromatin immunoprecipitation of H3K9me3 along the FXN locus and western blot.
2. Delineating which gRNAs along the frataxin locus result in upregulation of frataxin and aligning these to assess for transcription factor binding sites. I will also be undertaking chromatin immunoprecipitation of H3K9me3 and H3K27me3.
3. Chromatin immunoprecipitation of H3K9me3 and H3K27me3 in cells transfected with targeted histone mutant peptides.

References

1. Campuzano, V. et al. "Friedreich's Ataxia: Autosomal Recessive Disease Caused By An Intronic GAA Triplet Repeat Expansion". Science 271.5254 (1996): 1423-1427.
2. Punga, Tanel, and Marc Bühler. "Long Intronic GAA Repeats Causing Friedreich Ataxia Impede Transcription Elongation". *EMBO Molecular Medicine* 2.4 (2010): 120-129.
3. Lazaropoulos, Michael et al. "Frataxin Levels In Peripheral Tissue In Friedreich Ataxia". *Annals of Clinical and Translational Neurology* 2.8 (2015): 831-842.
4. Li, Yanjie et al. "Excision Of Expanded GAA Repeats Alleviates The Molecular Phenotype Of Friedreich's Ataxia". *Molecular Therapy* 23.6 (2015): 1055-1065.
5. Greene, Eriko et al. "Ancient Repeated DNA Elements And The Regulation Of The Human Frataxin Promoter". *Genomics* 85.2 (2005): 221-230.
6. Kumari, D., R. E. Biacsi, and K. Usdin. "Repeat Expansion Affects Both Transcription Initiation And Elongation In Friedreich Ataxia Cells". *Journal of Biological Chemistry* 286.6 (2010): 4209-4215.
7. Burke, T W, and J T Kadonaga. "Drosophila TFIID Binds To A Conserved Downstream Basal Promoter Element That Is Present In Many TATA-Box-Deficient Promoters.". *Genes & Development* 10.6 (1996): 711-724.
8. Li, Kuanyu et al. "Expression Of Human Frataxin Is Regulated By Transcription Factors SRF And TFAP2". *PLoS ONE* 5.8 (2010): e12286.
9. Puspasari, Novita et al. "Long Range Regulation Of Human FXN Gene Expression". *PLoS ONE* 6.7 (2011): e22001.
10. Bit-Avragim, Nana et al. "The GAA Repeat Expansion In Intron 1 Of The Frataxin Gene Is Related To The Severity Of Cardiac Manifestation In Patients With Friedreich's Ataxia". *Journal of Molecular Medicine* 78.11 (2000): 626-632.

11. Evans-Galea, Marguerite V. et al. "FXN Methylation Predicts Expression And Clinical Outcome In Friedreich Ataxia". *Annals of Neurology* 71.4 (2012): 487-497.
12. De Biase, Irene et al. "Somatic Instability Of The Expanded GAA Triplet-Repeat Sequence In Friedreich Ataxia Progresses Throughout Life". *Genomics* 90.1 (2007): 1-5.
13. Al-Mahdawi, S. et al. "The Friedreich Ataxia GAA Repeat Expansion Mutation Induces Comparable Epigenetic Changes In Human And Transgenic Mouse Brain And Heart Tissues". *Human Molecular Genetics* 17.5 (2007): 735-746.
14. Cinesi, Cinzia et al. "Contracting CAG/CTG Repeats Using The CRISPR-Cas9 Nickase". *Nature Communications* 7 (2016): 13272.
15. Montermini, L. "The Friedreich Ataxia GAA Triplet Repeat: Premutation And Normal Alleles". *Human Molecular Genetics* 6.8 (1997): 1261-1266.
16. Arcot, Santosh S et al. "Identification And Analysis Of A 'Young' Polymorphic Alu Element". *Biochimica et Biophysica Acta (BBA) - Gene Structure and Expression* 1263.1 (1995): 99-102.
17. Yandim, Cihangir, Theona Natisvili, and Richard Festenstein. "Gene Regulation And Epigenetics In Friedreich's Ataxia". *Journal of Neurochemistry* 126 (2013): 21-42.
18. Sakamoto, N. et al. "Sticky DNA, A Self-Associated Complex Formed At Long GAA{Middle Dot}TTC Repeats In Intron 1 Of The Frataxin Gene, Inhibits Transcription". *Journal of Biological Chemistry* 276.29 (2001): 27171-27177.
19. Groh, Matthias et al. "R-Loops Associated With Triplet Repeat Expansions Promote Gene Silencing In Friedreich Ataxia And Fragile X Syndrome". *PLoS Genetics* 10.5 (2014): e1004318.
20. Kapuscinski, Jan. "DAPI: A DNA-Specific Fluorescent Probe". *Biotechnic & Histochemistry* 70.5 (1995): 220-233.
21. Jenuwein, T. "Translating The Histone Code". *Science* 293.5532 (2001): 1074-1080.
22. Vieux-Rochas, Maxence et al. "Clustering Of Mammalianhoxgenes With Other H3k27me3 Targets Within An Active Nuclear Domain". *Proceedings of the National Academy of Sciences* 112.15 (2015): 4672-4677.
23. Moore, Lisa D, Thuc Le, and Guoping Fan. "DNA Methylation And Its Basic Function". *Neuropsychopharmacology* 38.1 (2012): 23-38.
24. Greene, E. et al. "Repeat-Induced Epigenetic Changes In Intron 1 Of The Frataxin Gene And Its Consequences In Friedreich Ataxia". *Nucleic Acids Research* 35.10 (2007): 3383-3390.
25. De Biase, Irene et al. "Epigenetic Silencing In Friedreich Ataxia Is Associated With Depletion Of CTCF (CCCTC-Binding Factor) And Antisense Transcription". *PLoS ONE* 4.11 (2009): e7914.
26. Chan, P. K. et al. "Heterochromatinization Induced By GAA-Repeat Hyperexpansion In Friedreich's Ataxia Can Be Reduced Upon HDAC Inhibition By Vitamin B3". *Human Molecular Genetics* 22.13 (2013): 2662-2675.

27. Liang, Puping et al. "CRISPR/Cas9-Mediated Gene Editing In Human Tripronuclear Zygotes". *Protein & Cell* 6.5 (2015): 363-372.
28. Jinek, M. et al. "A Programmable Dual-RNA-Guided DNA Endonuclease In Adaptive Bacterial Immunity". *Science* 337.6096 (2012): 816-821.
29. Cho, S. W. et al. "Analysis Of Off-Target Effects Of CRISPR/Cas-Derived RNA-Guided Endonucleases And Nickases". *Genome Research* 24.1 (2013): 132-141.
30. Kleinstiver, Benjamin P. et al. "Engineered CRISPR-Cas9 Nucleases With Altered PAM Specificities". *Nature* 523.7561 (2015): 481-485.
31. Hirano, Seiichi et al. "Structural Basis For The Altered PAM Specificities Of Engineered CRISPR-Cas9". *Molecular Cell* 61.6 (2016): 886-894.
32. Stricker, Stefan H., Anna Köferle, and Stephan Beck. "From Profiles To Function In Epigenomics". *Nature Reviews Genetics* 18.1 (2016): 51-66.
33. Liu, S. John et al. "Crispri-Based Genome-Scale Identification Of Functional Long Noncoding RNA Loci In Human Cells". *Science* 355.6320 (2016): eaah7111.
34. van Lohuizen, Maarten et al. "The oncogene and Polycomb-group gene bmi-1 regulates cell proliferation and senescence through the ink4a locus." *Nature* 397.6715 (1999): 164-168. 15 May 2017.
35. van der Lugt, N M et al. "Posterior Transformation, Neurological Abnormalities, And Severe Hematopoietic Defects In Mice With A Targeted Deletion Of The Bmi-1 Proto-Oncogene.". *Genes & Development* 8.7 (1994): 757-769.
36. Gray, Felicia et al. "BMI1 Regulates PRC1 Architecture And Activity Through Homo- And Hetero-Oligomerization". *Nature Communications* 7 (2016): 13343.
37. Gu, Minxia et al. "Heterozygous Knockout Of The Bmi-1 Gene Causes An Early Onset Of Phenotypes Associated With Brain Aging". *AGE* 36.1 (2013): 129-139.
38. Peters, Antoine H.F.M. et al. "Loss Of The Suv39h Histone Methyltransferases Impairs Mammalian Heterochromatin And Genome Stability". *Cell* 107.3 (2001): 323-337.
39. Runko, Alexander P., Anthony J. Griswold, and Kyung-Tai Min. "Overexpression Of Frataxin In The Mitochondria Increases Resistance To Oxidative Stress And Extends Lifespan Indrosophila". *FEBS Letters* 582.5 (2008): 715-719.
40. Moran, Diarmuid M, Hong Shen, and Carl G Maki. "Puromycin-Based Vectors Promote A ROS-Dependent Recruitment Of PML To Nuclear Inclusions Enriched With HSP70 And Proteasomes". *BMC Cell Biology* 10.1 (2009): 32.
41. Saveliev, Alexander et al. "DNA Triplet Repeats Mediate Heterochromatin-Protein-1-Sensitive Variegated Gene Silencing". *Nature* 422.6934 (2003): 909-913.
42. Tchasovnikarova, I. A. et al. "Epigenetic Silencing By The HUSH Complex Mediates Position-Effect Variegation In Human Cells". *Science* 348.6242 (2015): 1481-1485.

43. Lufino, M. M. P. et al. "A GAA Repeat Expansion Reporter Model Of Friedreich's Ataxia Recapitulates The Genomic Context And Allows Rapid Screening Of Therapeutic Compounds". *Human Molecular Genetics* 22.25 (2013): 5173-5187.
44. Nageshwaran, Sathiji, and Richard Festenstein. "Epigenetics And Triplet-Repeat Neurological Diseases". *Frontiers in Neurology* 6 (2015): n. pag.
45. Winchester, C. "Characterization Of The Expression Of DMPK And SIX5 In The Human Eye And Implications For Pathogenesis In Myotonic Dystrophy". *Human Molecular Genetics* 8.3 (1999): 481-492.
46. Wang, Hengbin et al. "Mam Facilitates Conversion By ESET Of Dimethyl To Trimethyl Lysine 9 Of Histone H3 To Cause Transcriptional Repression". *Molecular Cell* 12.2 (2003): 475-487.
47. Timms, Richard T. et al. "ATF7IP-Mediated Stabilization Of The Histone Methyltransferase SETDB1 Is Essential For Heterochromatin Formation By The HUSH Complex". *Cell Reports* 17.3 (2016): 653-659.
48. Fritsch, Lauriane et al. "A Subset Of The Histone H3 Lysine 9 Methyltransferases Suv39h1, G9a, GLP, And SETDB1 Participate In A Multimeric Complex". *Molecular Cell* 37.1 (2010): 46-56.
49. Canto, C., and J. Auwerx. "Targeting Sirtuin 1 To Improve Metabolism: All You Need Is NAD+?". *Pharmacological Reviews* 64.1 (2011): 166-187.
50. Libri, Vincenzo et al. "Epigenetic And Neurological Effects And Safety Of High-Dose Nicotinamide In Patients With Friedreich's Ataxia: An Exploratory, Open-Label, Dose-Escalation Study". *The Lancet* 384.9942 (2014): 504-513.
51. Zhou, Vicky W., Alon Goren, and Bradley E. Bernstein. "Charting Histone Modifications And The Functional Organization Of Mammalian Genomes". *Nature Reviews Genetics* 12.1 (2010): 7-18.
52. Chavez, Alejandro et al. "Highly Efficient Cas9-Mediated Transcriptional Programming". *Nature Methods* 12.4 (2015): 326-328.
53. Hilton, Isaac B et al. "Epigenome Editing By A CRISPR-Cas9-Based Acetyltransferase Activates Genes From Promoters And Enhancers". *Nature Biotechnology* 33.5 (2015): 510-517.
54. Vora, Suhani et al. "Next Stop For The CRISPR Revolution: RNA-Guided Epigenetic Regulators". *The FEBS Journal* 283.17 (2016): 3181-3193.
55. Salmon, Patrick et al. "Reversible Immortalization Of Human Primary Cells By Lentivector-Mediated Transfer Of Specific Genes". *Molecular Therapy* 2.4 (2000): 404-414.
56. Cotticelli, M. Grazia et al. "Phenotypic Screening For Friedreich Ataxia Using Random Shrna Selection". *Journal of Biomolecular Screening* 20.9 (2015): 1084-1090.
57. Villaseñor, Rodrigo et al. "Genome-Engineering Tools To Establish Accurate Reporter Cell Lines That Enable Identification Of Therapeutic Strategies To Treat Friedreich'S Ataxia". *Journal of Biomolecular Screening* 20.6 (2015): 760-767.

58. Lewis, P. W. et al. "Inhibition Of PRC2 Activity By A Gain-Of-Function H3 Mutation Found In Pediatric Glioblastoma". *Science* 340.6134 (2013): 857-861.
59. Williams, A. et al. "Position Effect Variegation And Imprinting Of Transgenes In Lymphocytes". *Nucleic Acids Research* 36.7 (2008): 2320-2329.
60. Wong, Hui-Lee et al. "Rapid And Quantitative Method Of Allele-Specific DNA Methylation Analysis". *BioTechniques* 41.6 (2006): 734-739.
61. Barski, Artem et al. "High-Resolution Profiling Of Histone Methylations In The Human Genome". *Cell* 129.4 (2007): 823-837.
62. Silva, A. M. et al. "Expanded GAA Repeats Impair FXN Gene Expression And Reposition The FXN Locus To The Nuclear Lamina In Single Cells". *Human Molecular Genetics* 24.12 (2015): 3457-3471.
63. Vaquero, Alejandro et al. "SIRT1 Regulates The Histone Methyl-Transferase SUV39H1 During Heterochromatin Formation". *Nature* 450.7168 (2007): 440-444.
64. Maison, Christèle et al. "The Methyltransferase Suv39h1 Links The SUMO Pathway To Hp1α Marking At Pericentric Heterochromatin". *Nature Communications* 7 (2016): 12224.
65. Larson, Matthew H et al. "CRISPR Interference (Crispri) For Sequence-Specific Control Of Gene Expression". *Nature Protocols* 8.11 (2013): 2180-2196.
66. Herz, H.-M. et al. "Histone H3 Lysine-To-Methionine Mutants As A Paradigm To Study Chromatin Signaling". *Science* 345.6200 (2014): 1065-1070.
67. Lewis, P. W. et al. "Inhibition Of PRC2 Activity By A Gain-Of-Function H3 Mutation Found In Pediatric Glioblastoma". *Science* 340.6134 (2013): 857-861.
68. Chan, K.-M. et al. "The Histone H3.3K27M Mutation In Pediatric Glioma Reprograms H3K27 Methylation And Gene Expression". Genes & Development 27.9 (2013): 985-990.
69. Jin, C., and G. Felsenfeld. "Nucleosome Stability Mediated By Histone Variants H3.3 And H2A.Z". Genes & Development 21.12 (2007): 1519-1529.
70. Bürk, K. (2017). Friedreich Ataxia: current status and future prospects. *Cerebellum & Ataxias*, 4(1).
71. Parkinson, M., Boesch, S., Nachbauer, W., Mariotti, C. and Giunti, P. (2013). Clinical features of Friedreich's ataxia: classical and atypical phenotypes. *Journal of Neurochemistry*, 126, pp.103-117.
72. Bürk, K., Schulz, S. and Schulz, J. (2013). Monitoring progression in Friedreich ataxia (FRDA): the use of clinical scales. *Journal of Neurochemistry*, 126, pp.118-124.
73. Perdomini, M., Belbellaa, B., Monassier, L., Reutenauer, L., Messaddeq, N., Cartier, N., Crystal, R., Aubourg, P. and Puccio, H. (2014). Prevention and reversal of severe mitochondrial cardiomyopathy by gene therapy in a mouse model of Friedreich's ataxia. *Nature Medicine*, 20(5), pp.542-547.

74. Vyas, P., Tomamichel, W., Pride, P., Babbey, C., Wang, Q., Mercier, J., Martin, E. and Payne, R. (2011). A TAT–Frataxin fusion protein increases lifespan and cardiac function in a conditional Friedreich's ataxia mouse model. *Human Molecular Genetics*, 21(6), pp.1230-1247.
75. Pastore, A. and Puccio, H. (2013). Frataxin: a protein in search for a function. *Journal of Neurochemistry*, 126, pp.43-52.
76. Zanella, I., Derosas, M., Corrado, M., Cocco, E., Cavadini, P., Biasiotto, G., Poli, M., Verardi, R. and Arosio, P. (2008). The effects of frataxin silencing in HeLa cells are rescued by the expression of human mitochondrial ferritin. *Biochimica et Biophysica Acta (BBA) - Molecular Basis of Disease*, 1782(2), pp.90-98.
77. Runko, A., Griswold, A. and Min, K. (2008). Overexpression of frataxin in the mitochondria increases resistance to oxidative stress and extends lifespan inDrosophila. *FEBS Letters*, 582(5), pp.715-719.
78. Bhaya, D., Davison, M. and Barrangou, R. (2011). CRISPR-Cas Systems in Bacteria and Archaea: Versatile Small RNAs for Adaptive Defense and Regulation. *Annual Review of Genetics*, 45(1), pp.273-297.
79. Jinek, M., Chylinski, K., Fonfara, I., Hauer, M., Doudna, J. and Charpentier, E. (2012). A Programmable Dual-RNA-Guided DNA Endonuclease in Adaptive Bacterial Immunity. *Science*, 337(6096), pp.816-821.
80. Shalem, O., Sanjana, N. and Zhang, F. (2015). High-throughput functional genomics using CRISPR–Cas9. *Nature Reviews Genetics*, 16(5), pp.299-311.
81. Al-Mahdawi, S., Pinto, R., Varshney, D., Lawrence, L., Lowrie, M., Hughes, S., Webster, Z., Blake, J., Cooper, J., King, R. and Pook, M. (2006). GAA repeat expansion mutation mouse models of Friedreich ataxia exhibit oxidative stress leading to progressive neuronal and cardiac pathology. *Genomics*, 88(5), pp.580-590.
82. Du, J., Campau, E., Soragni, E., Ku, S., Puckett, J., Dervan, P. and Gottesfeld, J. (2017). Role of Mismatch Repair Enzymes in GAA·TTC Triplet-repeat Expansion in Friedreich Ataxia Induced Pluripotent Stem Cells.
83. van Lohuizen, M., Jacobs, J., Kieboom, K., Marino, S. and DePinho, R. (1999). *Nature*, 397(6715), pp.164-168.

Appendix

7th Annual International IEEE EMBS Conference on Neural Engineering
Montpellier, France, 22 - 24 April, 2015

f2MOVE: fMRI-compatible haptic object manipulation system for closed-loop motor control studies

Anastasia Sylaidi[1,4], Pedro Lourenco[1,4], Sathiji Nageshwaran[3,4,5], Chin-Hsuan Lin[1], Marisol Rodriguez[1], Richard Festenstein [3,4,5] & A. Aldo Faisal[1,2,4], *Member IEEE*

***Abstract*— Functional neuroimaging plays a key role in addressing open questions in systems and motor neuroscience directly applicable to brain machine interfaces. Building on our low-cost motion capture technology (fMOVE), we developed f2MOVE, an fMRI-compatible system for 6DOF goal-directed hand and wrist movements of human subjects enabling closed-loop sensorimotor haptic experiments with simultaneous neuroimaging. f2MOVE uses a high-zoom lens high frame rate camera and a motion tracking algorithm that tracks in real-time the position of special markers attached to a hand-held object in a novel customized haptic interface. The system operates with high update rate (120 Hz) and sufficiently low time delays (< 20 ms) to enable visual feedback while complex, goal-oriented movements are recorded. We present here both the accuracy of our motion tracking against a reference signal and the efficacy of the system to evoke motor control specific brain activations in healthy subjects. Our technology and approach thus support the real-time, closed-loop study of the neural foundations of complex haptic motor tasks using neuroimaging.**

I. Introduction

Neuroscience has systematically studied sensorimotor functions for more than 100 years. Common methodological approaches have involved the use of psychophysical experiments and computational theories of inference and policy formation [1],[2],[3],[4],[5],[6]. The latter provide insight into the patterns of adaptive responses in tasks that introduce target, workspace or force-field perturbations [7],[8] and examine multisensory integration [9], body and world representation [10] or performance optimization in the face of sensory and motor noise [11].

However, despite this substantial progress in the investigation of motor behavior, less advancement has been achieved in associating motor psychophysics and computational models of sensorimotor control to their underlying neural foundation. A growing number of studies have attempted to address this challenge with the use of fMRI technology, which they primarily employed during lab-constrained simple hand reaching movements or non-specific open-loop manipulations (e.g. finger tapping). The main reason for this restriction lies in the technical constraints of fMRI, which is often incompatible to advanced motion tracking systems, that could monitor more complex motor behavior.

Here we designed and developed, f2MOVE, a novel 6DOF fMRI-compatible motion tracking system to support realistic object manipulation (haptic) tasks during a neuroimaging session. The development was motivated by a rapidly growing body of studies that focuses on life-like tasks, which enable movements in naturalistic settings without the usual confines of strict lab protocols. This work supports a better understanding of human natural movement statistics [12],[13], provides insight into the structure of motor primitives and thus carries, through movement predictability, direct implications for neuroprosthetic approaches and brain-machine interfaces [14].

f2MOVE was built upon our low-cost motion capture technology, fMOVE [15], which we expanded to adjust to the fMRI environment (Clinical Imaging Facility, Hammersmith Hospital, London). We complemented our system with a methodological platform, which can support closed-loop task contexts to encourage learning based on online sensory feedback of performance. f2MOVE′s motion

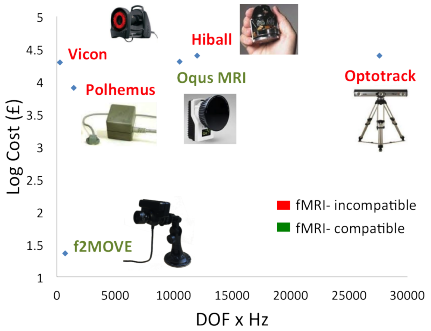

Fig. 1. Frugal innovation for motion tracking: Cost versus efficiency of established motion tracking systems (not fMRI compatible) against which f2MOVE (fMRI compatible) is compared. f2MOVE corresponds to the lowest cost level (camera expenses) and possesses satisfactory motion tracking performance within the range of state-of-the-art motion trackers (e.g. Polhemus, Vicon).

Brain & Behaviour Lab - [1]Dept. of Bioengineering & [2]Dept. of Computing, Imperial College London, South Kensington Campus, SW7 2AZ, London, UK, [3] Gene control mechanisms & disease group, Division of Brain Sciences, Faculty of Medicine, Imperial College London, [4]Imperial Clinical Research Facility , Imperial Centre for Translational and Experimental Medicine, W12 0NN London, UK, [5]MRC Clinical Sciences Centre, Hammersmith Hospital Campus, W12 0NN, London, UK - a.faisal at imperial.ac.uk

*This work was supported by a Colin Caro Bioengineering Fellowship, a scholarship from the Foundation for Education and European Culture (AS), a Wellcome Trust-GSK Fellowship to SN (No. WT103456MES), Fellowship of the Taiwanese Ministry of Education (1001163-2-UK-003) to CHL and a NIHR/BRC Rare Diseases grant (RF & AAF). The authors also wish to thank Albert L. Busza and Julie A. Fitzpatrick for their valuable support in undertaking fMRI sessions at the C.I.F. of Hammersmith Hospital, London.

978-1-4673-6389-1/15/$31.00 ©2015 IEEE

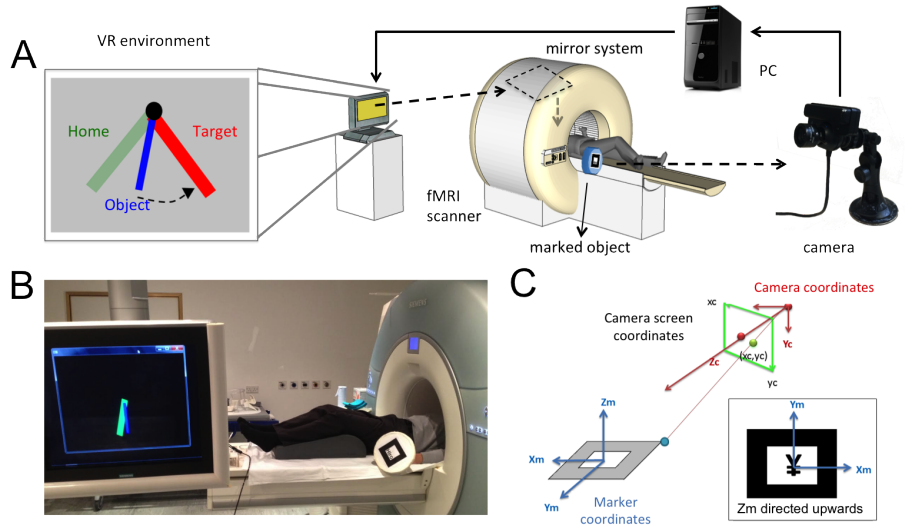

Fig. 2. Experimental setup: (A) displays the system's components which interact during an actual experimental session (B) to support closed-loop haptic object manipulation experiments. The object position is tracked by our customized marker-based motion tracker, which provides a PC-run software module with continuous information about the subject 's movements. The software platform displays a virtual online feedback of the monitored behavior and performance, which is in turn presented to the subject via a computer screen and a mirror system adjusted to the scanner. (C) The marked object position is estimated based on transformations between a marker-based (X_m, Y_m, Z_m) and a camera-based (X_c, Y_c, Z_c) coordinate system.

tracking performance lies in the same range as established fMRI-incompatible motion tracking methods (e.g. in Fig. 1 Vicon with 1DOF motion tracking at 250 Hz, Polhemus Liberty with 6DOF at 240 Hz). Furthermore, it presents a significant cost-efficiency benefit compared to other motion-tracking technologies with advanced features (e.g. Hiball with 6DOF motion tracking at 2000 Hz, Optotrack with 6DOF at 4600 Hz, Oqus MRI with 6DOF at 1750 Hz).

II. Methods

A. Hardware

Our system allows a closed-loop interaction of human subjects lying inside a 3T fMRI scanner and a PC-handled experimental paradigm (Fig. 2 A,B). Subjects use their dominant hand to hold and manipulate a compact object so as to move it correctly between some instructed home and target orientation. The exact task conditions are displayed to them via a mirror system built inside the scanner, which reflects the virtual progression of the task on a computer screen. Motor performance is tracked by a high-zoom lens, low cost camera (Playstation 3 Eye) positioned on one of the scanner room walls, at a $3.5m$ outside of the scanner, facing the foot-end view of the cylinder. The camera operates at a 120Hz frame-rate for a 320 x 240 pixel resolution with low time delays ($<20ms$) and can track 6DOF movement of the object, based on a customized 2D marker adjusted on the latter. We mounted it on a customized platform that allows a 6DOF rotation and precice alignment of the camera orientation with the scanner opening. The motion tracking system feeds all acquired images into a PC-based software, module, which monitors motor behavior and determines the transition between consecutive experimental phases. This module communicates with the subject via the scanner-based mirror system, on which it provides visual access to the task goals, and real-time feedback of motor performance.

B. Continuous closed-loop object manipulation

The camera continuously records images, which support the estimation of the object position and the visualization of its virtual analogue based on a software library for designing Augmented Reality applications (ARToolkit). In particular, f2MOVE estimates the object position, based on two coordinate systems which are related via an affine transformation (Fig. 2 C): a camera based (3D) and a marker based (3D). The marker based X_m and Y_m axes are aligned with the horizontal and vertical marker sides respectively, while Z_m points away vertically from the 2D plane defined by X_m and Y_m. The marker center is located at $(X_m, Y_m, Z_m) = (0, 0, 0)$. The module is designed based on a custom made motorlib C code library and opengl and operates by defining consecutive experimental stages as finite states which allow transition, depending on the monitored motion information.

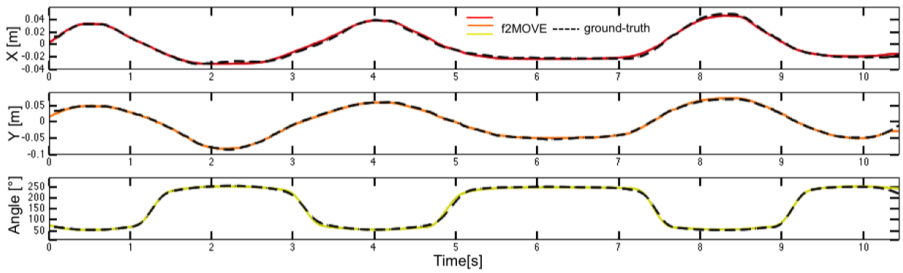

Fig. 3. Testing the tracking accuracy: We compared the f2MOVE signal against the signal monitored by Optitrack Flex-13, which was used as reference. Both signals were acquired simultaneously in a lab setting simulating the experimental conditions of an object manipulation paradigm designed for clinical studies inside the fMRI environment. The f2MOVE signal demonstrates a satisfactory matching to the reference motion tracking performance (z-signal not included since movement in this axis is minimal).

We developed a novel haptic interface that includes a light fMRI-compatible object. The design consists of a plastic handle, used as the reception for mounting multifaceted objects of variable shape and dynamics. For the needs of our first clinical sessions we designed and used an object with thin cylindrical body that hosted a single marker tractable by our motion tracking system (Fig. 2 B). Depending on the needs of the experimental study and the complexity of the examined movement, the number of markers on the tracked object can be increased to ensure that occasionally obscured markers, are substituted by more visible ones. This offers flexibility to the experimental design and allows us to investigate motor behavior during haptic interaction with complex objects.

C. Tracking accuracy

We tested the tracking accuracy of f2MOVE against a standardized motion tracking system (Optitrack Flex-13). In particular, our reference is a state-of-the-art infrared marker-tracking system that offers millimiter resolution of 3D spatial displacements and operates with accuracy at 100 Hz. In order to compare the signal acquired by the two systems, we aligned the f2MOVE camera with one of the three used Optitrack cameras. We placed 4 Optitrack markers at the corners of the f2MOVE 2D marker, so as to create a rigid body with the same center to f2MOVE′s marker center. We acquired motion information from a healthy female subject, based on an experimental paradigm designed for the Clinical Imaging Facility at Hammersmith Hospital, London. In this paradigm the subject continuously moves the marked object between an instructed home and target orientation.

After data acquisition, the f2MOVE signal was downsampled to match the reference signal. The two signals were subsequently aligned temporally by matching the first trial initiation after a resting period. A mean affine transformation was estimated for resting period data, to match the f2MOVE signal to the reference signal, via rotation and translation. The transformed signals we compared based on *RMSE* and R^2 to determine f2MOVE tracking accuracy.

III. Results

We tested the operating features and tracking accuracy of our system, f2MOVE, in lab conditions and inside the fMRI environment to establish its utility for closed-loop object manipulation tasks. f2MOVE operates successfully at 120 Hz frame-rate with low time-delays and tracks 6DOF movement of the marked object.

f2MOVE′s precise tracking accuracy was estimated against an established infrared marker-tracking system (Optitrack Flex-13) in a lab setting simulating the current experimental setting of our system at the Clinical Imaging Facility at Hammersmith Hospital, London. We measured motion information for a task instructing the manipulation of the experimental object inside a specified orientation range. We aligned the two acquired signals in the temporal and spatial domain to achieve matching, after which we estimated their RMSE difference. Fig. 3 reveals good consistency of movement measurements between f2MOVE and our reference system, both in the 2 dimensions used for our experimental paradigm (the execution was instructed on a 2D xy plane and movement in the z dimension was minimal) and in the angle rotation domain of the xy plane. The matching between signals was estimated at $R^2 = 0.98$ and $RMSE = 2$ mm, $R^2 = 0.99$ and $RMSE = 2.6$ mm, $R^2 = 0.99$ and $RMSE = 1.02$ mm, $R^2 = 0.99$ and $RMSE = 4.2^\circ$ for the x,y,z translation and rotation of the xy plane around the z-axis respectively.

Our tested system was transferred and adjusted to the fMRI setting at the Clinical Imaging Facility at Hammersmith Hospital, London. It was used to support scanning sessions on healthy subjects during an object manipulation paradigm. Fig. 4.A illustrates 3D rendered views of activation patterns for task-versus-rest conditions in our paradigm. These views reflect the enhanced role of specific brain areas (e.g. cerebellum, SMA) in error-driven closed-loop object

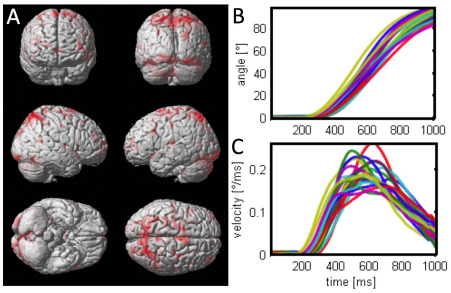

Fig. 4. Linking neuroimaging and motor psychophysics: f2MOVE enabled fMRI sessions on a healthy subject during a closed-loop object manipulation task, equivalent to the one tested in our simulated lab conditions (moving object between home and target orientation). (A) Our methodological platform allowed the acquisition of cortical activation patterns in task-versus-rest conditions. An examination of these patterns reveals the role of the cerebellum and SMA in error-driven motor learning. Network-level analysis can support a further understanding of the neural implementation of motor behavior in complex naturalistic manipulations. (B) The object orientation and (C) angular velocity over time (trial start at 0 ms). across trials can be examined in parallel with the cortical activation patterns, so as to determine behavioral performance measures that can be subsequently employed as regressors against the fMRI signal.

manipulations. Furthermore, the simultaneously acquired behavioral data (Fig. 4.B,C) can be regressed against activation patterns to examine neural correlates of behaviorally determined motor control mechanisms. Such approaches can shed further light into the foundation of sensorimotor functions in naturalistic motor tasks, such as the one examined by our system.

IV. Conclusion

We designed and developed an fMRI-compatible haptic object manipulation system (f2MOVE) for closed-loop 6 DOF motor control studies. We built upon our previously developed 3 DOF marker-based motion tracking system to adjust our technology to the fMRI environment and to expand it so as to accommodate motor experiments with goal-directed hand and wrist movements as well as the interaction with objects of variable dynamics.

f2MOVE poses technical benefits for high frequency data acquisition inside the fMRI environment, which is commonly incompatible to most currently established motion tracking systems. Moreover, building on our previous experience on low-cost wearable kinematic body-sensor networks [16], we aimed at developing an easily affordable neurotechnological tool. Its cost is limited to the customized camera price, in contrast to the expences involved in fMRI-compatible motion tracking approaches which rely on a robotic manipulandum for motion detection and/or perturbation [17],[18]. f2MOVE, thus offers an accessible technological and methodological platform to re-approach the objectives of motor neuroscience in examining the neural foundation of sensorimotor control and learning. It also supports the design of clinically-valuable behavioral and neuroimaging markers to monitor motor coordination in healthy or pathological cases (e.g. neurodegenerative diseases).

References

[1] D. M. Wolpert, J. Diedrichsen, and J. R. Flanagan, "Principles of sensorimotor learning," *Nat. Rev. Neurosci.*, vol. 12, no. 12, pp. 739–751, 2011.

[2] E. Todorov, "Optimality principles in sensorimotor control," *Nat. Neurosci.*, vol. 7, no. 9, pp. 907–915, 2004.

[3] S. H. Scott, "Optimal feedback control and the neural basis of volitional motor control," *Nat. Rev. Neurosci.*, vol. 5, no. 7, pp. 532–546, 2004.

[4] K. J. Friston, J. Daunizeau, and S. J. Kiebel, "Reinforcement learning or active inference?" *PloS one*, vol. 4, no. 7, p. e6421, 2009.

[5] K. Friston, "The free-energy principle: a unified brain theory?" *Nat. Rev. Neurosci.*, vol. 11, no. 2, pp. 127–138, 2010.

[6] K. P. Körding and D. M. Wolpert, "Bayesian decision theory in sensorimotor control," *Trends Cogn. Sc.*, vol. 10, no. 7, pp. 319–326, 2006.

[7] R. Shadmehr and F. A. Mussa-Ivaldi, "Adaptive representation of dynamics during learning of a motor task," *J. Neurosci.*, vol. 14, no. 5, pp. 3208–3224, 1994.

[8] R. Shadmehr and Z. M. Moussavi, "Spatial generalization from learning dynamics of reaching movements," *J. Neurosci.*, vol. 20, no. 20, pp. 7807–7815, 2000.

[9] S. Vaziri, J. Diedrichsen, and R. Shadmehr, "Why does the brain predict sensory consequences of oculomotor commands? optimal integration of the predicted and the actual sensory feedback," *J. Neurosci.*, vol. 26, no. 16, pp. 4188–4197, 2006.

[10] A. Sylaidi and A. A. Faisal, "What is the hierarchical representation of tasks involving objects with complex internal dynamics?" *Front. Comput. Neurosc.*, vol. Bernstein Conference, 2012.

[11] A. A. Faisal, L. P. Selen, and D. M. Wolpert, "Noise in the nervous system," *Nat. Rev. Neurosci.*, vol. 9, no. 4, pp. 292–303, 2008.

[12] J. N. Ingram, K. P. Körding, I. S. Howard, and D. M. Wolpert, "The statistics of natural hand movements," *Exp. Brain Res.*, vol. 188, no. 2, pp. 223–236, 2008.

[13] I. S. Howard, J. N. Ingram, K. P. Körding, and D. M. Wolpert, "Statistics of natural movements are reflected in motor errors," *J. Neurophysiol.*, vol. 102, no. 3, pp. 1902–1910, 2009.

[14] A. A. Thomik, D. Haber, and A. A. Faisal, "Real-time movement prediction for improved control of neuroprosthetic devices," in *Neural Engineering (NER), 2013 6th International IEEE/EMBS Conference on*. IEEE, 2013, pp. 625–628.

[15] M. Rodriguez, A. Sylaidi, and A. A. Faisal, "Developing a novel fmri-compatible motion tracking system for haptic motor control experiments," in *Neurotechnix, 2014*, 2014.

[16] C. Gavriel and A. A. Faisal, "Wireless kinematic body sensor network for low-cost neurotechnology applications in-the-wild," in *Neural Engineering (NER), 2013 6th International IEEE/EMBS Conference on*. IEEE, 2013, pp. 1279–1282.

[17] J. Diedrichsen, Y. Hashambhoy, T. Rane, and R. Shadmehr, "Neural correlates of reach errors," *J. Neurosci.*, vol. 25, no. 43, pp. 9919–9931, 2005.

[18] S. Menon, M. Yu, K. Kay, and O. Khatib, "Haptic fmri: Accurately estimating neural responses in motor, pre-motor, and somatosensory cortex during complex motor tasks," in *Engineering in Medicine and Biology Society (EMBC), 2014 36th Annual International Conference of the IEEE*. IEEE, 2014, pp. 2040–2045.

Kinematic body sensor networks and behaviourmetrics for objective efficacy measurements in neurodegenerative disease drug trials

Constantinos Gavriel[1,4], Andreas A. C. Thomik[2,4], Pedro Rente Lourenço[2,4], Sathiji Nageshwaran[3,4], Stavros Athanasopoulos[3,4,5], Anastasia Sylaidi[2,4], Richard Festenstein[3,4,5], A. Aldo Faisal[1,2,4,5], Members IEEE

***Abstract*—We have deployed body sensor network (BSN) technology in clinical trials and developed behavioural analytics to quantify and monitor longitudinally the progression of Friedreich's Ataxia (FRDA) outside the lab. Patients and their carers administered themselves our ETHO1 wireless BSN and we captured motion time-series from patient sleep. We extracted behavioural biomarkers that objectively capture the progression of the disease throughout time and compares well with the SARA clinical scale gold-standard. Such clinical scales require patients to go through a series of lengthy tasks where clinicians observe patients' performance and aggregate a score that represents the stage of the disease. Unfortunately, such scales have been shown to be inconsistent across and within clinicians, as they are observation based subjective measures: Scales are highly dependent on the assessor's experience and they also have low sensitivity and resolution that fails to capture the slow disease progression in short periods of time, requiring longer clinical testing time frames. Using the neurobehavioural data we collected in our clinical trials, we extracted three behavioural biomarkers (MIM, SIM & KIM) based on patient movement intensity, activity and stillness while in bed. Our behavioural biomarkers correlation with the SARA clinical scale allows us to capture the disease progression in FRDA patients and establishes a proof of concept for BSN technology that we are applying towards more rapid efficacy measurements of drugs.**

I. Introduction

Neurodegenerative disorders affect millions of people around the world, causing progressive degeneration and eventual death of neurons, which can cause problems with movement control (e.g. ataxia) or mental functioning (e.g. dementia). Currently, there is no disease modifying treatment for many forms of neurodegeneration, especially rare diseases. For a few, drugs have been developed to improve patients' quality of life or even slow the progression of the disease [1], [2]. Due to the nature of these diseases, providing care and continuous monitoring to patients can be increasingly more complicated and expensive as it requires lengthy hospitalisation periods [3]. Therefore, it is important to be able to quantitatively assess the stage of the disease, both for adjustment of drug dosages and also providing direct feedback on the effects of different drugs.

Brain & Behaviour Lab - [1]Dept. of Computing & [2]Dept. of Bioengineering, Imperial College London, London, UK; [3]Gene control mechanisms & disease group, Division of Brain Sciences, Faculty of Medicine, Imperial College London, [4]Imperial Clinical Research Facility, W12 0NN London, UK, [5]MRC Clinical Sciences Centre, W12 0NN, London, UK - Contact for correspondence: a.faisal@imperial.ac.uk

*This work was supported by the EPSRC, the Luxembourg Research Fund (1229297), the Wellcome Trust-GSK Fellowship (No. WT103456MES) and our NIHR/BRC Rare Diseases grant.

978-1-4673-7201-5/15/$31.00 ©2015 IEEE

This study focuses on Friedreich's ataxia (FRDA), an inherited neurodegenerative disease with slow progression that affects the central nervous system causing severe mobility issues subtle changes in patient's behaviour that worsen over time. FRDA starts developing itself during childhood and the main symptoms include poor balance (disequilibrium), gradual loss of strength and sensation in the limbs, muscle stiffness (spasticity), curvature of the spine (kyphoscoliosis), impaired speech, hypertrophic cardiomyopathy and it has also been associated with diabetes, difficulty with bladder control (incontinence), impaired vision and hearing loss [4], [5]. FRDA affects 1 in 40,000 [6], [7] people mainly from European, Middle Eastern and North African backgrounds and, at present, there is no known effective treatment, However, after longitudinal monitoring of the progression of the disease, many of the symptoms can be treated to enable patients maintain optimal functioning as long as possible [8]–[10]. Crucially, we have shown that a disease modifying treatment for FRDA is within our reach [10] and, thus, our publicly funded trials are now underway – we believe body sensor networks and behaviour analytics will be crucial in capturing changes more objectively and in shorter time span, than conventional clinical measures. Thereby enabling us to reduce the duration of clinical trials and thus drug development costs for this rare disease.

Currently, the only way of evaluating the progression of FRDA disease in patients is through a series of score-based tests [11]. Clinicians observe patients performing the tasks and extract scores, which can qualitatively define the stage of the disease. The most commonly used clinical scales are the Scale for the Assessment and Rating of Ataxia (SARA), the Composite Cerebellar Functional Severity Score (CCFS), the Inventory of Non-Ataxia Signs (INAS), the Spinocerebellar ataxia Functional Index (SCAFI) and the Friedreich's Ataxia Rating Scale (FARS) [11]–[15]. All these scales can assess patient's motor control and coordination skills through a series of evaluation tests, such as the 8m walk, the 9-hole peg test, the finger-nose test, the finger tapping test, the heel-shin-slide test etc. Evaluating the overall clinical stage of the FRDA disease requires combining the evaluated scores with patient's physiological information (e.g. stance, walking gait, sitting posture, use of supports etc.), some neurological parameters (e.g. muscle atrophy, spontaneous speech, etc.) and also the patient's ability of performing Activities of Daily Living (ADL) by themselves.

The main issue with these clinical scales is the low sensitivity level that makes it extremely difficult to pick up the slow disease progression in short periods of time. This has a major

impact on drug research as it implies that much longer studies are required to measure any outcome at all [11]. Furthermore, the FRDA scales typically produce inconsistent results, mainly because their underlying components are based on subjective estimates made by the clinical staff [16], [17]. Although, this variability can be minimised with training sessions [18], patient's effort, fatigue issues and psychological state can also affect the outcome of the tests [19]. Consequently, there is a clear need for new methods that can capture high-resolution behavioural markers from the patients and objectively assess the clinical state and progression of the ataxia.

In a recent study, we have introduced the use of non-intrusive wireless body sensor network (BSN) technology for monitoring the sleep behavioural patterns of FRDA patients in clinical trials [20]. Using the collected motion data we extracted the Stillness Intervals Marker (SIM), the mean (μ) and standard deviation (σ) of the log-normal fit on the distribution of stillness durations in bed [21]. We have then shown that the SIM exhibits trends consistent with the clinical assessments of the FRDA disease, however, more features were required for more precise evaluation of the patient's state.

In this paper, we present two new sets of biomarkers extracted from the patients' motion data that can also highlight the progression of the FRDA disease in patients, namely the Movement Intervals Markers (MIM) and the Kinematic Intensity Marker (KIM). Our set of behavioural biomarkers establish a proof of concept showing that BSN technology can be directly used in clinical trial for monitoring the progression of neurodegenerative disorders in an objective manner while providing a much higher level of precision. This high level of accuracy can be extremely important for achieving rapid efficacy measurements in clinical diagnostics which will allow more precise evaluation of patients' clinical stage, more accurate adjustments on drug dosages or even potentially enable detection of the diseases at a very early stage.

II. Methods

A. Study Design, Patients and Experimental Setup

Nine participants (6 female, aged 24-56) participated in our study. They had all been diagnosed with Friedreich's ataxia based on clinical criteria [10] and they had provided written informed consent before any study-related procedures were initiated. Our clinical trial was approved by the UK Medicines and Healthcare Products Regulatory Agency (MHRA; EudraCT 2011-002744-27), the Riverside Research Ethics Committee (11/LO/0998), and the Imperial College London Joint Research & Compliance Office.

The participants were asked to sleep alone in a hospital room for one night while wearing 4 of our ETHO1 wireless BSN nodes [22], [23] on their wrists and ankles as shown in 1. ETHO1 is a set of body sensor network (BSN) nodes with an integrated 9 degrees of freedom (DOF) motion tracking technology (accelerometer, gyroscope, magnetometer) that enables real-time wireless transmission of data at 50 Hz to a nearby base-station for up to 10 hours. Using the ETHO1 technology we monitored subject's movement activity throughout the whole night (mean sleep duration: 7.1 hours). The same experiment was repeated three more times (after 3 weeks, 3 months and 9 months) and this enabled collection of

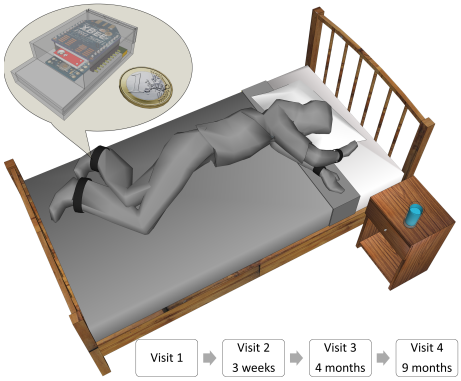

Fig. 1. The Experimental Setup: 9 FRDA patients were asked to sleep alone during the night in a controlled hospital room while wearing our ETHO1 wireless kinematics tracking BSN technology [22] on their wrists and ankles. The experiment was repeated after 3 weeks, 3 months and 9 months to capture the underlying changes in the motor control system on a longitudinal scale.

behavioural data that can be used in monitoring the progression of the ataxic disease on a longitudinal scale. At each visit, the subjects were also instructed by clinicians and followed the tasks required for the estimation of the SARA score. SARA scale is typically used in the assessment and rating of the ataxia and it will serve as a benchmark against our extracted behavioural biomarkers.

The ETHO1 nodes were carefully placed on by trained clinical personnel using the elastic Velcro straps when subjects were about to enter the bed and were taken off as soon as they woke up in the morning. The sensor nodes were consistently placed over or under the subject's clothes according to their personal preference. The ETHO1 nodes were labelled RW and LW for the right and left wrist and RA and LA for the right and left ankle respectively and clinicians ensured that sensors were tight enough to restrict free movement while at the same time comfortable enough for the subject to wear all night. Preferably all 4 nodes should be strapped onto the participants, however, a minimum of 2 was required: on the dominant hand and foot (right handed people should use the right hand; the dominant foot is typically the foot that would kick a ball). Since the ETHO1 nodes stream data using wireless technology, to ensure data quality, the patient's bed was placed within 10 metres from the base-station. Patients were also not allowed to come close to electro motors (in beds, wheelchairs), magnets or use mobile phones during the experiment session since the ETHO1 sensors are sensitive to magnetic fields. Although these devices would not damage the sensor components, they could degrade the quality of the data collected.

For extracting our biomarkers, it was extremely important that the patient was sleeping alone in the bed and the times when nodes were switched on, taken off or have fallen off were recorded onto the trial worksheets. Additionally, if the subject needed to go to the bathroom, it was, for both hygienic and privacy reasons, necessary to completely remove the ETHO1 nodes beforehand following the procedure detailed above. The

978-1-4673-7201-5/15/$31.00 ©2015 IEEE

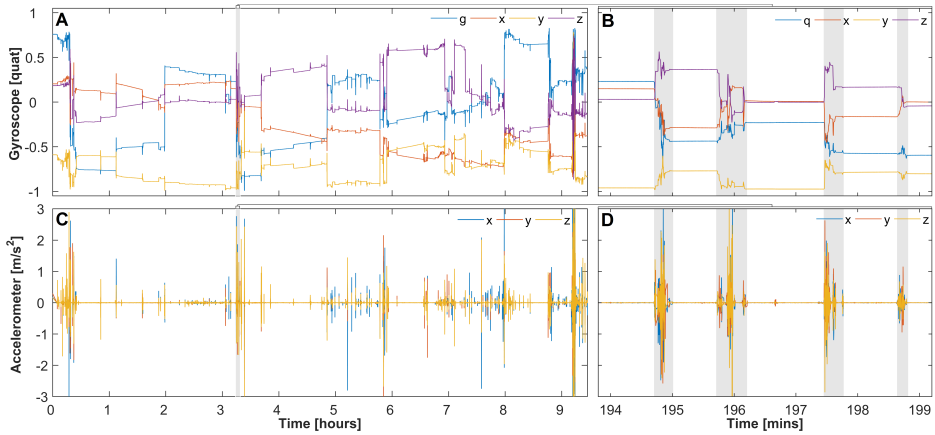

Fig. 2. A typical time series of behavioural data collected using our ETHO1 sensor placed on the right ankle of a single subject over a night. Plot **A** shows the wrist rotation data in quaternion format based on the fused accelerometer, gyroscope and magnetometer sensor data and plot **C** shows the gravity-compensated acceleration. Plots **B** & **D** present the output of our motion detection algorithm applied on a 5-mins window from the **A** & **C** plots respectively. The grey shaded regions represent the areas in which movement was detected.

times that the subjects left the bed were recorded and any data captured within these periods were excluded from the analysis.

B. Movement Segmentation

The raw kinematic data from all subjects, visits and sensors were imported into Matlab 2014b [Mathworks Inc., Natick, MA] for analysis. 2 shows the typical behavioural signal collected from the right ankle of a subject on a single visit. 2.A represents the relative ankle rotation in quaternion format based on the fusion of our ETHO1 9 degrees of freedom (DoF) data and 2.C is the limb's gravity-compensated acceleration. Both signals were filtered using the method described in our previous study [20].

One of the main effects of FRDA disease on patients is the impaired motor control and coordination. Therefore we segmented the behavioural signals collected during the experiments into movement and non-movement regions. This enables comparison of the movement patterns throughout time and features can be extracted that can reveal information regarding the stage of progression of the FRDA disease [24]. To achieve this segmentation on the collected acceleration and rotation signals, we implemented an algorithm based on empirical thresholds that detects and extracts the movement regions. These thresholds are estimated by computing a histogram (100 bins) evenly spaced over the data range and choosing the value for which data had a probability less than 5%. The movement regions were then selected by finding the areas that exceed the threshold value. The algorithm was applied on each signal dimension independently and the results where combined afterwards using a logical disjunction operator. Finally a series of morphological erosion (windows: 20ms, 50ms, 100ms) and dilation filters (windows: 20ms, 100ms, 300ms) were applied on the output of the algorithm to eliminate the spikes from sensor noise and smooth out any gaps between long movement periods. 2.B&D represent the typical output of our segmentation algorithm applied to a 5mins window of rotation and acceleration data respectively. The grey shaded regions represent the areas where movement was detected. We then calculated the duration of the detected movement and stillness regions, as inter-event timings has been previously proven to carry useful behavioural information even in very noisy datasets [25].

C. Behavioural Biomarker

For this study, we focused on the movement durations and we tried to capture in a principled manner the changes across the subject's visits. Therefore we fitted various parametric probability distributions on the movement durations of each subject and we selected the distribution that best fits the data (the one that minimises the Akaike Information Criterion). From our analysis we have consistently found that the distribution of moment data is best described by a log-normal probability distribution. This result is shown in 3.A where we plot with blue bars the probability density function (PDF) and with red line cumulative density function (CDF) of the movement durations from a single subject's visit on a logarithmic x-axis. We also plot the cumulative density function (CDF) of the log–normal distribution (black line). We then fitted a log-normal distribution on the distribution of motion durations from each subject's visit and we extracted the Movement Interval Markers (MIM): the mean (μ) and standard deviation (σ) of the fit.

III. Results

A. Movement Interval Markers (MIM)

In 5.A-B we present the trends in the μ and σ of our MIM biomarker as extracted from the patients' sleep behavioural data across different visits. The red lines are the regression line fits on these biomarkers, highlighting an increasing length (5.A) and a decreasing variability (5.B) in the movement

978-1-4673-7201-5/15/$31.00 ©2015 IEEE

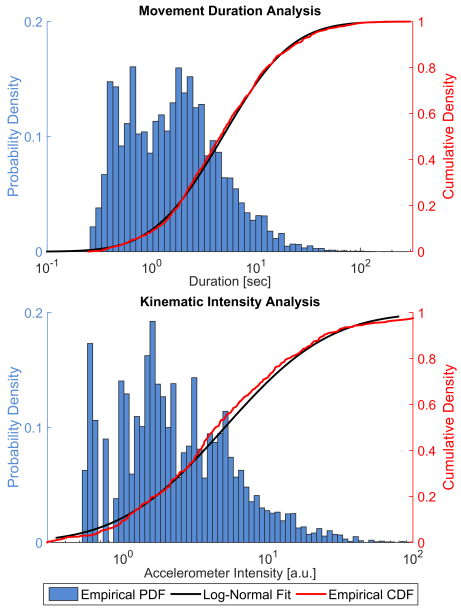

Fig. 3. The probability density function (PDF) of the movement durations (**A**) and kinematic intensities (**B**) for a single subject based on the data extracted from our segmentation algorithm. Note that the x-axis on both plots is on $\log_{10}$ scale. The red lines represent the cumulative density function (CDF) of the fitted data and the black lines represent the CDF of a log–normal distribution. Observing the data across all subjects we noticed that the distributions of both movement durations and averaged kinematic intensity during sleep are more likely to follow a log-normal distribution.

durations, meaning that the subjects' movement durations are becoming longer and more standardised across time. This trend is similar to the one recently observed in our SIM parameters (5.C-D) where the regression lines reveal a decrease in both the length and the variability of the stillness durations, meaning that the subjects' movement incidents are happening more often are becoming longer and more standardised across time [20]. The trends in both MIM and SIM biomarkers are consistent with the decrease in the patient's mobility over time.

B. Kinematic Intensity Marker (KIM)

An additional feature we extracted from the patient behavioural data is the movement intensity. FRDA disease causes gradual loss of strength and muscle stiffness, therefore monitoring the intensity of the movements during sleep can potentially reveal information about the stage and the progression of the disease. To achieve this, we used the raw acceleration data from the movement segments of a single patient's visit to calculate the average motion jerk within each region. Then we looked at the distribution of these motion jerks across the entire subject visit and tried to fit various parametric probability distributions as with our MIM biomarker. The results are shown in 3.B where we plot the PDF (blue bars) and CDF (red line) of the movement intensities from a single subject's visit on a logarithmic x-axis. We also plot the cumulative density function (CDF) of the log–normal distribution (black line). Observing the fit on all subjects' data, we found that movement intensities are more likely to follow a log-normal distribution. The mean (μ) and standard deviation (σ) of the log-normal fit on serves as our extracted the Kinematic Intensity Marker (KIM) which provides us with an indication on the patient's smoothness or sharpness during movements. The evolution of KIM parameters throughout time is shown in 5.E where we plot the average jerk (μ) for each subject with respect to the time since the first visit. The red regression line fit on the data reflects a clear decrease in the movement intensity which is consistent with the effects of the FRDA disease on the patient's motor abilities.

C. SIM, MIM & KIM biomarkers vs SARA

To determine the relevance of our extracted MIM, SIM and KIM behavioural biomarkers with respect to the stage of the disease progression, we first observed the trends in the SARA scores over the different visits. In 4 we present the evolution of the SARA scores for each individual subject as collected by the trained clinical personnel on each visit. Each coloured line represents a different subject, however, note that one subject dropped out after Visit 2 and one of our subjects did not participate in the last stage of the experiments yet. Based on the trends in the graph, all subjects exhibit an increase of their SARA score relative to the first visit over the duration of our experiments, something that is consistent with the progressive nature of the FRDA disease. You can clearly notice that a heterogeneous patient population has been used in the experiments, with different stages and progression speed of the disease something that explains the huge variability observed in the graph.

For evaluating the effectiveness of our extracted biomark-

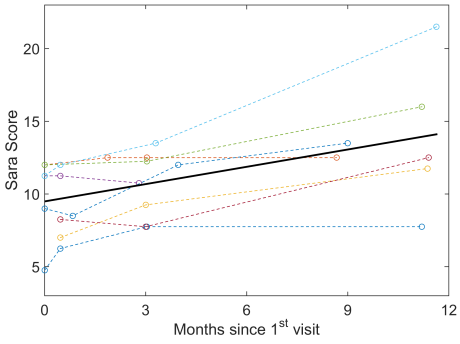

Fig. 4. The evolution in the patients' SARA scores across different visits. Each coloured line represents a single visit from a single subject and x axis is the difference in months since patient's first visit. The graph shows a systematic increase in subjects' SARA score across time (black line). From the graph you can observe that a heterogeneous patient population has been used with different stages and progression speeds of the disease. Note that one subject dropped out the study after Visit 2 and one of our subjects did not participate in the last stage of the experiments yet.

978-1-4673-7201-5/15/$31.00 ©2015 IEEE

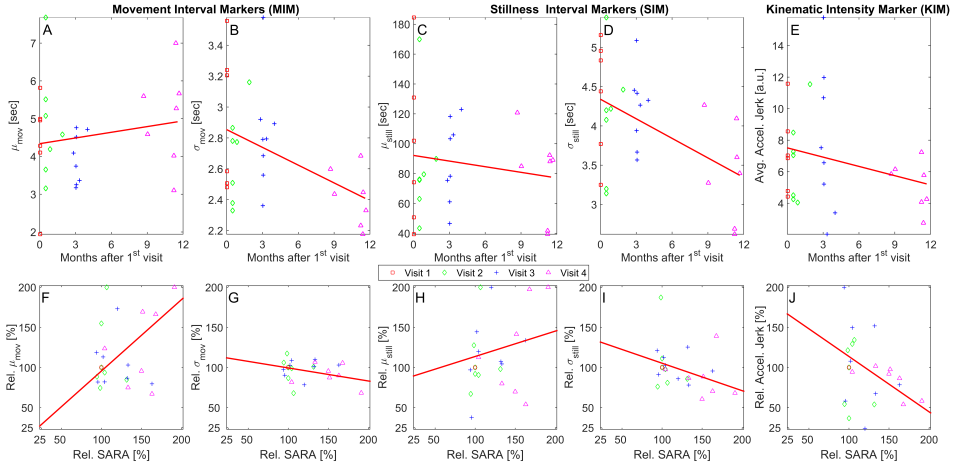

Fig. 5. The trends in our Movement Interval Markers (MIM), Stillness Interval Markers (SIM) and Kinematic Intensity Marker (KIM) across different visits as extracted from the patients' sleep behavioural data. Plots **A** & **B** show the evolution of our MIM biomarkers, namely the μ (**A**) and σ (**B**) parameters from the fitted log-normal distribution on the movement durations. Each data-point represents the parameter evaluated using the data for a single visit and it is plotted against the number of days since subject's first visit. The red line is a regression line fitted on the biomarkers, highlighting an increasing length and a decreasing variability in the movement durations, meaning that the subjects' movement durations are becoming longer and more standardised across time. **C** & **D** show the same analysis applied to our SIM biomarkers specifically, the μ (**C**) and σ (**D**) parameters from the log-normal distribution fitted on the stillness durations. The red regression lines highlight a decreasing trend in both the length and the variability of the stillness durations. Plot **E** represents the trends in our KIM parameter across different visits. KIM represents the average accelerometer jerk using the signal from the detected movement regions. The regression line shows a decrease in the subject's movement intensity across time. The trends in our MIM, SIM and KIM biomarkers are consistent with the decrease in the patient's mobility over time. Plots **F - J** represent the relative change of our MIM, SIM and KIM biomarkers plotted against the relative change in SARA scores. The red lines represent the total least square regression fit on the biomarker parameters and the SARA scores after data have been grouped and averaged per visit. The plots **F** & **J** show a strong correlation between the relative changes in the μ parameter of the movement durations distribution and the average intensity with respect to the relative changes in SARA score.

ers, we compared the relative changes in our MIM, SIM and KIM parameters with respect to the relative changes in the SARA scores over the different patient visits. The results are shown in 5.F-J where the red line represents the total least square regression fit between the biomarker parameters and the SARA scores after data have been grouped and averaged per visit. The plots F & H show a correlation between the relative change of μ in movement and stillness durations with respect to the relative change in SARA scores (r = 0.36). This is a confirmation that our behavioural biomarkers capture information relevant to the progression of the FRDA disease, however, none of the parameters can be independently used to report significant information regarding the state of the disease.

Therefore, we implemented a non-linear least-squares regression approach that applies a linear combination of our biomarker features to provide a mapping between the changes in MIM, SIM and KIM parameters and the change in SARA scores over the different visits. This regression algorithm was then applied on the parameters of each biomarker independently as well as all combinations and by applying a leave one out cross validation, we evaluated the coefficient of determination (R^2) between the estimated and actual relative change in SARA score. The results are shown in 6.A where a low prediction performance is achieved when each biomarker is used independently but the efficiency increases when all MIM, SIM and KIM features are combined together, achieving a maximum R^2 of 0.64. In 6.B we plot the predicted versus the actual change in SARA score as reported by the least square regression algorithm when all biomarkers are combined together. These results establish the effectiveness of our biomarkers in monitoring the progression of the disease throughout time.

IV. Discussion

In this paper, we have taken wireless kinematic body sensor network (BSN) technology and analytics outside the controlled laboratory context and we deployed it in "in-the-wild" during clinical trials to achieve objective quantification of the progress of Friedreich's Ataxia (FRDA) disease in patients. Using our low-cost ETHO1 body sensor networks [22], we monitored the behaviour of 9 FRDA patients during their sleep on a longitudinal scale and using the collected motion time-series, we derived novel biomarkers that objectively highlight the stage of FDRA disease. We, note that sensors were put on by patients and/or their carers following our standardised operating procedure, thus making this a true patient-centred investigation. We extracted three novel biomarkers: 1. Movement Interval Marker (MIM), 2. Stillness Interval Marker (SIM) and 3. Kinematic Intensity Marker (KIM). These markers characterise the probability distributions of movement and stillness durations and the average intensity of the movements on each visit. We have also performed comparisons against one of the gold-standard clinical scales, the SARA score, proving

978-1-4673-7201-5/15/$31.00 ©2015 IEEE

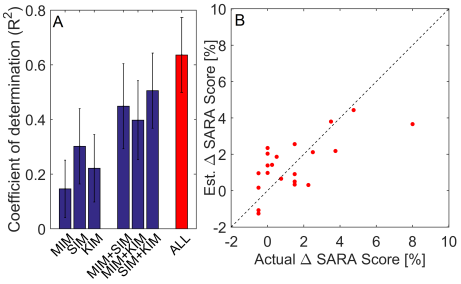

Fig. 6. **A:** Comparison of the performances achieved during cross validation by applying the least squares regression algorithm on a single biomarker versus a combination of our biomarkers. The error bars represent the standard deviation and the best performance is achieved by using a sum of power laws on all biomarker parameters (R^2 = 0.64). **B:** The actual change in SARA score plotted against the prediction from the least square regression algorithm combining all MIM, SIM and KIM biomarkers.

that our biomarkers can efficiently capture the trends in the progression of the disease, without need for expert clinicians and interruption of the patients' daily routine in the home.

Our method serves as additional step towards more personalised healthcare and diagnostic tools through continuous patient monitoring. This is something that the currently used clinical methods are unable to perform due to the high levels of variability, the low sensitivity in the slow disease progression, the high dependency on the assessor's ability and mainly due to the infrequent data collection. These clinical tests are sparsely performed (on monthly, quarterly or biannually basis) and this makes them prone to daily fluctuations of subject's behaviour, physiological and psychological state. To this extent, BSN technology can be deployed for continuous and remote monitoring patients, something that will provide clinicians with a more comprehensive history of the subject's biomarkers. Our developed biomarkers establish a proof of concept that the continuous monitoring can be applied to neurodegenerative disorders for achieving more objective and higher resolution data, which can be extremely important for achieving rapid efficacy measurements in clinical diagnostics which will allow more accurate adjustment of drug dosages. Additionally, collecting data from a large set of patients provide better understanding on the underlying changes of the motor control system caused by the disease which can potentially enable detection of the diseases at very early stages, even before symptoms can be visually observed. The method we present in this paper is another example of our frugal engineering approach to neurotechnology which combines low-cost hardware [26], [27] along with intelligent algorithms [28]–[30] and smart calibration procedures [31] to understand the variability of human behaviour in natural daily life activities.

References

[1] P. Dunkel *et al.*, "Clinical utility of neuroprotective agents in neurodegenerative diseases: current status of drug development for alzheimer's, parkinson's and huntington's diseases, and amyotrophic lateral sclerosis," *Expert opinion on investigational drugs*, 21, pp. 1267–1308, 2012.

[2] F. Mangialasche *et al.*, "Alzheimer's disease: clinical trials and drug development," *Lancet Neurology*, 9 (7), pp. 702–716, 2010.

[3] J Olesen *et al.*, "The economic cost of brain disorders in europe," *Eur. J.Neurol.*, 19 (1), pp. 155–162, 2012.

[4] P. Gibilisco and A. P. Vogel, "Friedreich ataxia," *BMJ*, 347, 2013.

[5] A. Dürr *et al.*, "Clinical and genetic abnormalities in patients with Friedreich's ataxia," *New Eng. J Med*, 335 (16), pp. 1169–1175, 1996.

[6] A. H. Koeppen, "Friedreich's ataxia: pathology, pathogenesis, and molecular genetics," *J. Neurol Sc.*, 303 (1), pp. 1–12, 2011.

[7] A. H. Koeppen, "Nikolaus Friedreich and degenerative atrophy of the dorsal columns of the spinal cord," *J. Neurochem.*, 126, pp. 4–10, 2013.

[8] R. Lodi *et al.*, "Antioxidant treatment improves in vivo cardiac and skeletal muscle bioenergetics in patients with Friedreich's ataxia," *Annals of neurology*, 49 (5), pp. 590–596, 2001.

[9] D. R. Lynch and K. H. Fischbeck, "Nicotinamide in Friedreich's ataxia: useful or not?" *Lancet*, 384 (9942), pp. 474 –475, 2014.

[10] V. Libri *et al.*, "Epigenetic and neurological effects and safety of high-dose nicotinamide in patients with Friedreich's ataxia: an exploratory, open-label, dose-escalation study," *Lancet*, 2014.

[11] M. Fahey *et al.*, "How is disease progress in Friedreich's ataxia best measured? A study of four rating scales," *J.Neurol, Neurosur. & Psych.*, 78 (4), pp. 411–413, 2007.

[12] T Schmitz-Hübsch *et al.*, "Scale for the assessment and rating of ataxia development of a new clinical scale," *Neurology*, 66 (11), pp. 1717–1720, 2006.

[13] S. T. Du Montcel *et al.*, "Composite cerebellar functional severity score: validation of a quantitative score of cerebellar impairment," *Brain*, 131 (5), pp. 1352–1361, 2008.

[14] H Jacobi *et al.*, "Inventory of non-ataxia signs (INAS): validation of a new clinical assessment instrument," *Cerebellum*, 12 (3), pp. 418–428, 2013.

[15] T Schmitz-Hübsch *et al.*, "SCA Functional index: a useful compound performance measure for spinocerebellar ataxia," *Neurology*, 71 (7), pp. 486–492, 2008.

[16] M. J. Fillyaw *et al.*, "Quantitative measures of neurological function in chronic neuromuscular diseases and ataxia," *J Neurol Sc*, 92 (1), pp. 17–36, 1989.

[17] S. Subramony *et al.*, "Measuring Friedreich ataxia: interrater reliability of a neurologic rating scale," *Neurology*, 64, pp. 1261–1262, 2005.

[18] E. Storey *et al.*, "Inter-rater reliability of the Int. Cooperative Ataxia Rating Scale (ICARS)," *Movement disorders*, 19, pp. 190–192, 2004.

[19] N. A. Di Prospero *et al.*, "Neurological effects of high-dose idebenone in patients with Friedreich's ataxia: a randomised, placebo-controlled trial," *Lancet Neurology*, 6 (10), pp. 878–886, 2007.

[20] C. Gavriel *et al.*, "Towards neurobehavioral biomarkers for longitudinal monitoring of neurodegeneration with wearable body sensor networks," in *IEEE Neural Eng. Conf.*, 2015.

[21] J. Barbenel *et al.*, "Monitoring the mobility of patients in bed," *Med. Biol. Eng. Comput.*, 23 (5), pp. 466–468, 1985.

[22] C. Gavriel and A. A. Faisal, "Wireless kinematic body sensor network for low-cost neurotechnology applications in-the-wild," *IEEE Neural Eng. Conf.*, pp. 1279–1282, 2013.

[23] N. Sim *et al.*, "The head mouse - Head gaze estimation in-the-wild with low-cost inertial sensors for BMI use," *IEEE Neural Eng. Conf.*, pp. 735–738, 2013.

[24] E. Ramos *et al.*, "Quantification of upper extremity function using kinematic analysis," *Arch. Phys. Med. Rehabil.*, 78 (5), pp. 491–496, 1997.

[25] G. Tavares and A. Faisal, "Scaling-laws of human broadcast communication enable distinction between human, corporate and robot twitter users," *PloS one*, 8 (7), e65774, 2013.

[26] W. W. Abbott and A. A. Faisal, "Ultra-low-cost 3d gaze estimation: an intuitive high information throughput compliment to direct brain-machine interfaces.," *J Neural Eng*, 9 (4), p. 046 016, 2012.

[27] S. Fara *et al.*, "Robust, ultra low-cost mmg system with brain-machine-interface applications," *IEEE Neural Eng. Conf.*, pp. 723–726, 2013.

[28] A. A. Thomik *et al.*, "Real-time movement prediction for improved control of neuroprosthetic devices," *IEEE Nerual Eng. Conf.*, pp. 625–628, 2013.

[29] D. Haber *et al.*, "Unsupervised time series segmentation for high-dimensional body sensor network data streams," *IEEE Body Sensor Networks Conf.*, 2014.

[30] S. Fara *et al.*, "Prediction of arm end-point force using multi-channel mmg," *IEEE Body Sensor Networks Conf.*, 2014.

[31] A. P. Vicente and A. A. Faisal, "Calibration of kinematic body sensor networks: Kinect-based gauging of data gloves in the wild," *IEEE Body Sensor Networks Conf.*, pp. 1–6, 2013.

978-1-4673-7201-5/15/$31.00 ©2015 IEEE

7th Annual International IEEE EMBS Conference on Neural Engineering
Montpellier, France, 22 - 24 April, 2015

Towards neurobehavioral biomarkers for longitudinal monitoring of neurodegeneration with wearable body sensor networks

Constantinos Gavriel[1,4], Andreas A. C. Thomik[2,4], Pedro Rente Lourenço[2,4], Sathiji Nageshwaran[3,4], Stavros Athanasopoulos[3,4,5], Anastasia Sylaidi[2,4], Richard Festenstein[3,4,5], A. Aldo Faisal[1,2,4,5], *Members IEEE*

***Abstract*— This study focuses on the objective quantification of the disease progression in patients with Friedreich's Ataxia (FRDA) through the use of kinematic body sensor network technology. Currently, this quantification is performed through a series of task-oriented score-based metrics, which, although they provide an efficient way of quantifying the ataxic disease, they are dependent on the assessor's experience and they also present high levels of variability. We used our ETHO1 inertial motion capturing sensors for longitudinal monitoring of FRDA patients during sleep and we collected behavioural timeseries from which we extracted biomarkers that can objectively highlight the subtle changes of patients' motor control system. These biomarkers exhibit trends consistent with the clinical assessments of the disease.**

I. Introduction

Friedreich's ataxia (FRDA) is a progressive neurodegenerative disease which affects the nervous system and causes severe movement problems that worsen over time. It typically starts manifesting itself during childhood and is estimated to affect 1 in 40,000 [1], [2] people mainly from European, Middle Eastern, or North African background. The features of this condition include the gradual loss of strength and sensation in the legs and arms, muscle stiffness (spasticity), poor balance, impaired speech, hypertrophic cardiomyopathy and it is associated with diabetes, impaired vision and hearing loss [3], [4].

No effective treatment for FRDA currently exists. Additionally, the only way for medical staff to assess the progress of the disease through time is by having patients complete a series of score-based exercises [5]. Based on the weighted average of the scores taken for each sub-task, the progress of disease can be qualitatively defined. The most commonly used tests are the Scale for the Assessment and Rating of Ataxia (SARA) [6], the Composite Cerebellar Functional Severity Score (CCFS) [7], the Inventory of Non-Ataxia Signs (INAS) [8], the Spinocerebellar ataxia Functional Index (SCAFI) [9] and the Friedreich's Ataxia Rating Scale (FARS) [5]. All these tests assess subject's motor control and coordination skills through a series of tasks such as the 8 meter walk, the 9-hole peg test, the finger-nose test, finger tapping, the heel-shin-slide etc. Evaluating the clinical stage of the ataxia requires combination of task metrics, the patient's physiological information (e.g. stance, walking gait, sitting posture, use of supports etc.), neurological parameters (e.g. muscle atrophy, spontaneous speech, etc.), as well as the ability of performing Activities of Daily Living (ADL) by themselves.

Although those score-based metrics provide an efficient way of quantifying the ataxic disease, they still present some variability as some of their components are based on subjective estimates of the clinical abnormalities by the clinical staff [11], [12]. This variability can be minimised with extensive training sessions [13], however, there are still effort and fatigue issues which are affected by the patient's psychological state and can diverge the output of the tests [14]. Apart from the aforementioned variability in scoring, those methods also have low sensitivity, making it difficult to pick up the slow disease progression. This has a major impact on drug research as it implies that much larger study groups need to be used to measure any outcome at all [5]. Consequently, there is a clear need for new technologies that can achieve collection of high-resolution of behavioural markers from the patients which can then be

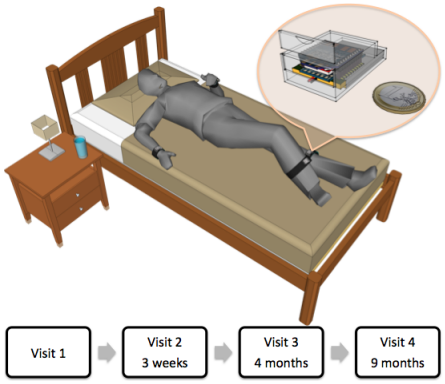

Fig. 1. The Experimental Setup: 9 FRDA patients were asked to sleep alone during the night in a controlled hospital room while wearing our ETHO1 wireless kinematics tracking BSN technology [10] on their wrists and ankles. The experiment was repeated several times to capture the underlying longitudinal changes in the motor control system.

Brain & Behaviour Lab - [1]Department of Computing & [2]Department of Bioengineering, Imperial College London, South Kensington Campus, SW7 2AZ, London, UK, [3]Gene control mechanisms & disease group, Division of Brain Sciences, Faculty of Medicine, Imperial College London, [4]Imperial Clinical Research Facility , Imperial Centre for Translational and Experimental Medicine, W12 0NN London, UK, [5]MRC Clinical Sciences Centre, Hammersmith Hospital Campus, W12 0NN, London, UK - a.faisal at imperial.ac.uk

*This work was supported by the EPSRC, the Wellcome Trust-GSK Fellowship (No. WT103456MES) and the NIHR/BRC Rare Diseases grant.

978-1-4673-6389-1/15/$31.00 ©2015 IEEE

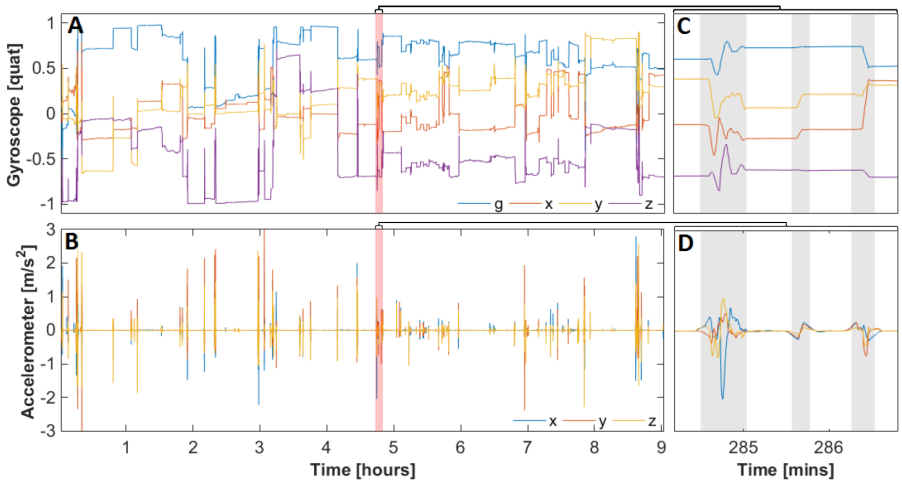

Fig. 2. A typical representation of the behavioural data collected using our ETHO1 sensor placed on the left wrist of a subject over a single night experiment. (**A**) The rotation data collected from the fused accelerometer, gyroscope and magnetometer sensor data in quaternion format. (**B**) The gravity compensated acceleration of the left wrist. (**C & D**) A zoomed in view of the output of our segmentation algorithm when applied on the fused gyroscope (**A**) and gravity compensated accelerometer data (**B**). The shaded areas represent the regions in which movement was detected.

used to objectively assess the clinical state and the progress of the ataxia.

To date, only a small subset of these clinical measures have been re–designed and validated to include objective assessment of patient performance: finger tapping ability [15], gait stability [16] and reaching movements [17]. However, most of these are too complicated for standard clinical use with FRDA patients [13].

This study focuses on the collection of sleep behavioural patterns of FRDA patients using non-intrusive highly-portable wireless technology. More specifically, by deploying our low-cost, non-invasive wearable body sensor networks (BSN) with the embedded high-resolution motion trackers, we collect the movement activities of the subjects on a longitudinal basis. The movement patterns enable us to extract biomarkers which can highlight the subtle changes of the motor control system with much higher accuracy and in an objective manner. A similar approach is used for monitoring the progression of restless legs syndrome (RLS) [18] where authors use wearable kinematic sensors for tracking the leg movement events per hour [19].

II. Methods

A. Study Design and Patients

Nine participants (6 female, aged 24-56) participated in our study. All had been diagnosed with Friedreich's ataxia based on clinical criteria and a genetically confirmed GAA-repeat expansion on both alleles of the FXN gene [20]. Our clinical trial was approved by the UK Medicines and Healthcare Products Regulatory Agency (MHRA; EudraCT 2011-002744-27), the Riverside Research Ethics Committee (11/LO/0998), and the Imperial College London Joint Research & Compliance Office. All participants provided written informed consent before any study-related procedures were initiated.

B. Experimental Setup

The participants were asked to sleep alone in a hospital room for one night while wearing 4 of our wireless (BSN) nodes called ETHO1 [10], [21] on their wrists and ankles as shown in Figure 1. The ETHO1 nodes were carefully placed on by trained clinical personnel using Velcro straps when subjects were about to enter the bed and were taken off as soon as they woke up in the morning. If during the night the subjects had to leave the bed for any reason, the time was recorded and the data were excluded from the analysis.

Our ETHO1 nodes, with the integrated 9 degrees of freedom (DOF) motion tracking technology (accelerometer, gyroscope, magnetometer) monitored subject's movement throughout the whole night (mean duration: 7.1 hours) at 50 Hz and the data were streamed in real time to a local base-station for storage. During each visit, the subjects were also instructed to follow the tasks required for the estimation of SARA score. SARA was estimated both before and after the sleep session. The same experiment was repeated 3 more times (after 3 weeks, 3 months and 9 months) and this enabled us to collect behavioural data from the FRDA patients that can be used for longitudinal monitoring of the progress of ataxia. The data from all subjects, visits and sensors were afterwards imported into Matlab 2014b [Mathworks Inc., Natick, MA] for further off-line analysis.

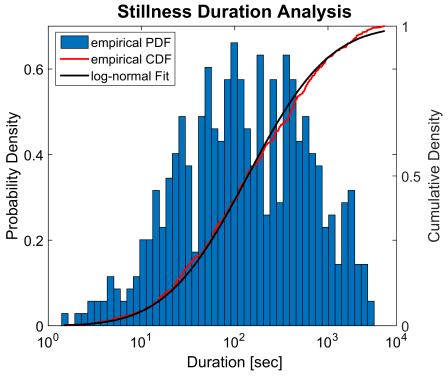

Fig. 3. The probability density function (PDF) of the stillness durations for a single subject based on the data extracted from our segmentation algorithm. Note that the x-axis is on $\log_{10}$ scale. The red line represents the cumulative density function (CDF) of the data and the black line represents the CDF of a log–normal distribution. Observing the data across all subjects we noticed that the distribution of stillness durations during sleep are more likely to follow a log-normal distribution.

C. Filtering Kinematic Data

Our ETHO1 BSN nodes output the gravity compensated acceleration and the relative rotation data in quaternion format. However, these kinematic signals include some high-level noise components mainly caused by the sensor noise, the magnetic interference picked up by the magnetometer data and instabilities in the network communication. To overcome this problem, we used a 4^{th} order low-pass Butterworth filter with a 4 Hz cut-off frequency to filter our data and then we smoothed the signals using two 1^{st} order Savitzky-Golay polynomial smoothing filters with 51 and 251 point windows. This provided us with smooth accelerometer and gyroscope data (Figure 2 **A & B**) which can be easily used for extracting and comparing features both across subjects as well as on a longitudinal basis.

III. Results

A. Movement Detection

Our first step was to separate the data in movement and non-movement, using a segmentation algorithm we developed that uses empirical thresholds for both the gravity compensated acceleration and the relative rotation data to detect the movement segments. Thresholds were computed by calculating the histogram (using 10^4 bins evenly spaced over the data range) of the input data and choosing a value for which data with higher acceleration had a probability lesser than 10%. The output of the algorithm was then filtered using a morphological erosion and dilation process to eliminate the spikes from sensor noise and smooth out any gaps between long movement periods. The algorithm was independently applied on each signal sensory dimension and the results where combined afterwards using a logical disjunction operator. Figure 2 (**C & D**) present a segment of the algorithm's output when applied to a typical accelerometer and gyroscope signal from a single subject's sleep. The shaded regions represent the movement periods and the non-shaded regions represent the non-movement ones.

B. Extraction of Sleep Features

By applying our segmentation algorithm on all data, we extracted the movement regions and evaluated the duration of all stillness periods for each visit, since it has been previously shown that inter-feature durations carry useful information even in very noisy datasets [22]. We then examined the changes in the stillness durations across visits in a principled manner by fitting a multiple parametric probability distributions on each dataset and examining the parameters of the distribution that best fits the data i.e. the one that minimises the Akaike Information Criterion (AIC). We found that in more than 90% of our recordings, the data is best described by a log–normal probability distribution. This fit is shown in Figure 3 where we plot the probability density function (PDF) and cumulative density function (CDF) of stillness durations of a single subject on a logarithmic x-axis along with the cumulative density function (CDF) of the best fitting distribution (log–normal). Note that on a logarithmic x–axis, the probability density function of a log–normal distribution looks like a normal distribution. We then fitted a log-normal distribution each dataset and we extracted the Stillness Interval Markers (SIM): the mean (μ) and standard deviation (σ) of each fit.

C. Stillness Interval Marker Analysis

To determine the relevance of our markers with the progression of the disease, we looked at the relative changes in SARA scores and how they compare to the relative changes of SIM parameters. The changes in SARA scores are presented in Figure 4. All subjects exhibit an increase of

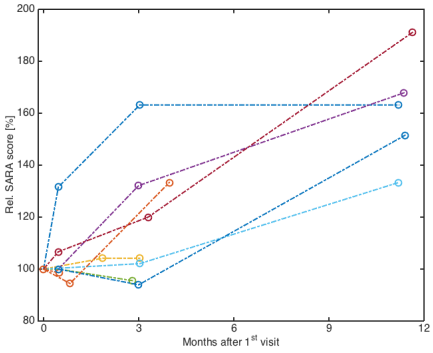

Fig. 4. Relative change in the SARA score for each individual subject with respect to the time since the first visit. Each coloured line represents a different subject. The figure shows a systematic increase in subject's SARA score across time. Note that we used a heterogeneous patient population with different stages of the disease.

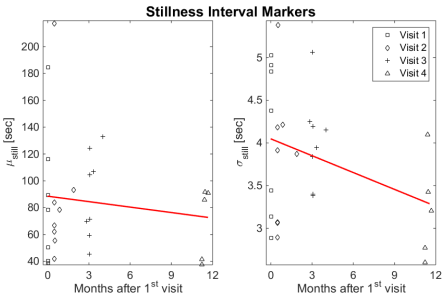

Fig. 5. The μ (**Left**) and σ (**Right**) of the log-normal distribution fitted on the stillness durations across all subjects plotted against the days since the first visit. The red lines represent the regression line fitting the data and highlight the increasing length and decreasing variability of the stillness durations across time.

their SARA score relative to the first visit over the duration of our experiments, consistent with the progressive nature of the FRDA disease. Note that for three of our subjects no data is available at the 12 months time–point as they did not participate in the last stage of the experiments. A similar trend is observed over the same duration for our SIM (Figure 5). While the duration of stillness episodes increases over time in parallel with the SARA scores, the variability in duration decreased, together indicating a consistent decrease in the patient's mobility.

IV. Discussion

We presented a method for objective monitoring and accurate quantification of the progression of FRDA. Current ataxia scales use a score-based system which, although it is efficient in quantifying the ataxic disease, it presents a significant variability due to the subjective nature of the assessment method [12]. We deployed low-cost wireless kinematic BSN technology [10] on FRDA patients and collected kinematic data during sleep over several visits. Using the distribution of inter-movement episodes during sleep, we derive a novel biomarker for monitoring and objectively assessing the progression of FDRA over time. We show that these behavioural biomarkers exhibit trends consistent with clinical assessment of the disease, however, further analysis is required for the quantification of this behaviour.

Our method is another example of our frugal engineering approach to neurotechnology which combines low-cost hardware [23], [24] along with intelligent algorithms [25]–[27] and smart calibration procedures [28] to understand the variability of human behaviour in natural daily life activities.

References

[1] A. H. Koeppen, "Nikolaus friedreich and degenerative atrophy of the dorsal columns of the spinal cord," *J. Neurochem.*, vol. 126, no. s1, pp. 4–10, 2013.

[2] A. H. Koeppen, "Friedreich's ataxia: pathology, pathogenesis, and molecular genetics," *J Neurol Sc.*, vol. 303, no. 1, pp. 1–12, 2011.

[3] A. Dürr *et al.*, "Clinical and genetic abnormalities in patients with friedreich's ataxia," *New England J Med*, vol. 335, no. 16, pp. 1169–1175, 1996.

[4] P. Gibilisco and A. P. Vogel, "Friedreich ataxia," *BMJ*, vol. 347, 2013.

[5] M. Fahey *et al.*, "How is disease progress in friedreich's ataxia best measured? a study of four rating scales," *Journal of Neurology, Neurosurgery & Psychiatry*, vol. 78, no. 4, pp. 411–413, 2007.

[6] T Schmitz-Hübsch *et al.*, "Scale for the assessment and rating of ataxia development of a new clinical scale," *Neurology*, vol. 66, no. 11, pp. 1717–1720, 2006.

[7] S. T. Du Montcel *et al.*, "Composite cerebellar functional severity score: validation of a quantitative score of cerebellar impairment," *Brain*, vol. 131, no. 5, pp. 1352–1361, 2008.

[8] H Jacobi *et al.*, "Inventory of non-ataxia signs (inas): validation of a new clinical assessment instrument," *The Cerebellum*, vol. 12, no. 3, pp. 418–428, 2013.

[9] T Schmitz-Hübsch *et al.*, "Sca functional index: a useful compound performance measure for spinocerebellar ataxia," *Neurology*, vol. 71, no. 7, pp. 486–492, 2008.

[10] C. Gavriel and A. A. Faisal, "Wireless kinematic body sensor network for low-cost neurotechnology applications "in-the-wild"," in *6th Intl IEEE/EMBS Conf. on NER*, IEEE, 2013, pp. 1279–1282.

[11] M. J. Fillyaw *et al.*, "Quantitative measures of neurological function in chronic neuromuscular diseases and ataxia," *J Neurol Sc*, vol. 92, no. 1, pp. 17–36, 1989.

[12] S. Subramony *et al.*, "Measuring friedreich ataxia: interrater reliability of a neurologic rating scale," *Neurology*, vol. 64, no. 7, pp. 1261–1262, 2005.

[13] E. Storey *et al.*, "Inter-rater reliability of the international cooperative ataxia rating scale (icars)," *Movement disorders*, vol. 19, no. 2, pp. 190–192, 2004.

[14] N. A. Di Prospero *et al.*, "Neurological effects of high-dose idebenone in patients with friedreich's ataxia: a randomised, placebo-controlled trial," *The Lancet Neurology*, vol. 6, no. 10, pp. 878–886, 2007.

[15] Á. Jobbágy *et al.*, "Analysis of finger-tapping movement," *J Neurosc Meth*, vol. 141, no. 1, pp. 29–39, 2005.

[16] M. D. McPartland, D. E. Krebs, and C Wall, "Quantifying ataxia: ideal trajectory analysis-a technical note," *J Rehab Res & Dev*, vol. 37, no. 4, pp. 445–454, 2000.

[17] B. Day *et al.*, "Influence of vision on upper limb reaching movements in patients with cerebellar ataxia.," *Brain*, vol. 121, no. 2, pp. 357–372, 1998.

[18] K. Tuisku *et al.*, "Quantitative rest activity in ambulatory monitoring as a physiological marker of restless legs syndrome: a controlled study," *Movement disorders*, vol. 18, no. 4, pp. 442–448, 2003.

[19] K. Tuisku *et al.*, "Actometry in measuring the symptom severity of restless legs syndrome," *European journal of neurology*, vol. 12, no. 5, pp. 385–387, 2005.

[20] V. Libri *et al.*, "Epigenetic and neurological effects and safety of high-dose nicotinamide in patients with friedreich's ataxia: an exploratory, open-label, dose-escalation study," *The Lancet*, 2014.

[21] N. Sim *et al.*, "The head mousehead gaze estimation" in-the-wild" with low-cost inertial sensors for bmi use," in *6th Intl IEEE/EMBS Conf on NER*, IEEE, 2013, pp. 735–738.

[22] G. Tavares and A. Faisal, "Scaling-laws of human broadcast communication enable distinction between human, corporate and robot twitter users," *PloS one*, vol. 8, no. 7, e65774, 2013.

[23] W. W. Abbott and A. A. Faisal, "Ultra-low-cost 3d gaze estimation: an intuitive high information throughput compliment to direct brain-machine interfaces.," *J Neural Eng*, vol. 9, no. 4, p. 046 016, 2012.

[24] S. Fara *et al.*, "Robust, ultra low-cost mmg system with brain-machine-interface applications," in *6th Intl IEEE/EMBS Conf on NER*, IEEE, 2013, pp. 723–726.

[25] A. A. Thomik, D. Haber, and A. A. Faisal, "Real-time movement prediction for improved control of neuroprosthetic devices," in *6th Intl IEEE/EMBS Conf on NER*, IEEE, 2013, pp. 625–628.

[26] D. Haber, A. A. C. Thomik, and A. A. Faisal, "Unsupervised time series segmentation for high-dimensional body sensor network data streams," in *IEEE International Conference on BSN*, IEEE, 2014.

[27] S. Fara *et al.*, "Prediction of arm end-point force using multi-channel mmg," in *IEEE International Conference on BSN*, IEEE, 2014.

[28] A. P. Vicente and A. A. Faisal, "Calibration of kinematic body sensor networks: kinect-based gauging of data gloves in the wild," in *IEEE International Conference on BSN*, IEEE, 2013, pp. 1–6.